

Dissertation

**Development of Laboratory Experiments
and Numerical Modeling Techniques to
Quantify Vadose Zone Water Fluxes in Arid
Regions**

Zur Erlangung des Grades eines Doktors der Naturwissenschaften (Dr.rer.nat)

Vorgelegt von Heike Pfletschinger (M.Sc.) aus Darmstadt

Am Fachbereich Material- und Geowissenschaften

Darmstadt 2012 D17



TECHNISCHE
UNIVERSITÄT
DARMSTADT

Gutachter: 1. Prof. Dr. Christoph Schüth
 2. Prof. Dr. Matthias Hinderer

Tag der Einreichung: 11.01.2012

Tag der Verteidigung: 17.04.2012

Für meine Mutter

Abstract

The quantification of vadose zone water fluxes in arid regions poses many difficulties due to low water input, coupled thermal and isothermal processes, spatial and temporal highly variable meteorological conditions and measurement deficits regarding spatial and temporal resolutions as well as measurement errors. Nevertheless, water flux processes in the vadose zone have to be understood and quantified as they govern rates of direct groundwater recharge.

To quantify vadose zone water fluxes under controlled conditions, laboratory soil column experiments were developed that mimic atmospheric and soil water conditions as they can be expected in arid regions. The experimental setup allowed to measure water content and temperature distribution within a 92 cm deep soil profile in high temporal and spatial resolution. At the top of the column, a head space with controllable air stream, water input and applied temperature accounted for the simulation of changing atmospheric conditions. At the column bottom, temperature and outflow pressure were applied to obtain a temperature gradient within the column and water discharge under controlled pressure conditions. By applying different initial and boundary conditions, soil water dynamics and temperature distributions were studied for two different sands. Water content profiles, that were measured with a TDR “Taupe” cable, showed almost uniform infiltration fronts for steady-state experiments. Subsequent experimental runs indicated the high impact of irrigation amount and intensity on water infiltration, evaporation and redistribution within the sands. Obviously, only single irrigations exceeding potential evaporation and lasting long enough to infiltrate deeper than 20 cm, could account for discharge at the bottom of the column, depending on successively applied irrigations.

According to the experiments, a numerical model was set up in Hydrus-1D, simulating coupled water, vapor and temperature fluxes in variably-saturated media (Šimunek et al., 2009). Hydraulic and thermal soil parameters, which are implemented into the model, were calibrated with experimental data of water content and temperature profiles at different times as well as transient water discharge and evaporation. Amongst the calibrated parameters, those controlling high saturated flow were less sensitive than those controlling evaporation and drainage, whereas highest sensitivities were obtained for the air entry pressure of the retention function of Brooks and Corey (1964). With the calibrated model, predictive scenario modeling was performed representing annual changing soil moisture conditions to identify parameters of primary importance for possible groundwater recharge in arid regions. The predictive modeling emphasized the high importance of single precipitation amounts on deep infiltration and percolation which can induce groundwater recharge. For annually low precipitation amounts, the residual water content of the ambient soil mainly determined percolation processes. Vapor fluxes, induced by temperature gradients, played a major role in total water fluxes under low saturated conditions.

The laboratory experiments were a good tool for first estimates of vadose zone water fluxes under arid conditions and were essential for the model setup and calibration. Based on the calibrated model further predictions upon vertical water fluxes and deep percolation for critical meteorological conditions could be made. By this, the model offers a valuable tool for groundwater management issues, especially regarding smart field observation and measurement schemes and initial predictions on soil water states for expected future hydrological and microclimatological changes.



Zusammenfassung

Die Quantifizierung von Wasserflüssen in der vadosen Bodenzone arider Gebiete ist mit verschiedenen Fehlerquellen behaftet. Schwierigkeiten bestehen aufgrund der generell sehr niedrigen Bodenwassergehalte und Niederschlagsmengen, gekoppelten thermischen und isothermen Prozessen, räumlich und zeitlich hoch variablen meteorologischen Konditionen und Defiziten in Messmethoden für die den Konditionen entsprechenden Messkampagnen. Da Prozesse in der vadosen Bodenzone Raten direkter Grundwasserneubildung bestimmen, ist es jedoch notwendig, diese zu verstehen und zu quantifizieren.

Zur vereinfachten Quantifizierung von vertikalen Wasserflüssen in ungesättigtem Boden unter kontrollierten Bedingungen wurden Labor-Bodensäulenversuche entwickelt, die die Simulation arider klimatischer Bedingungen ermöglichten. Innerhalb des Versuchsaufbaus wurden hochaufgelöste Wassergehalts- und Temperaturprofile in einer 92 cm tiefen Bodensäule gemessen. Über der Bodensäule wurde eine atmosphärische Randbedingung mit kontrollierbarem Luftstrom mit definierter Eingangsfeuchtigkeit, Beregnung und regelbarer Temperatur in einem 5 cm hohen Luftraum vorgegeben. Am Säulenfuß wurde ebenfalls die Temperatur geregelt. Eine Saugplatte mit angelegtem konstantem Unterdruck sorgte für einen kontrollierbaren Wasserfluss aus der Säule. Versuche wurden mit zwei verschiedenen Sanden und ändernden Eingangs- und Randbedingungen durchgeführt. Mehrere Beregnungs- und Trocknungsversuche zeigten den starken Einfluss von Beregnungsmenge und -intensität auf Infiltrationstiefen, Evaporationsmengen und der Wasserredistribution innerhalb des Bodenprofils. Beregnungen führten hierbei nur bei einer Infiltrationstiefe von mindestens 20 cm zu Durchfluss, wobei die Menge des Durchflusses sowohl von der Anfangssättigung als auch von dem weiteren Versuchsverlauf abhing.

Entsprechend des Versuchsaufbaus wurde ein numerisches Modell in Hydrus-1D aufgebaut. Das Programm Hydrus-1D berechnet gekoppelte Wasser-, Wasserdampf- und Temperaturflüsse in variabel gesättigten porösen Medien (Šimunek et al., 2009). Hydraulische und thermische Bodeneigenschaften, die in dem Modell parametrisiert sind, wurden mit Daten der Säulenversuche von Sättigungsprofilen, Temperaturprofilen sowie Evaporations- und Durchflussmengen kalibriert. Innerhalb der kalibrierten Parameter zeigten die hydraulischen Parameter, die Mengen von Evaporation und Durchfluss in niedrig gesättigten Bereichen bestimmen, und insbesondere der Lufteintrittspunkt im hydraulischen Retentionsmodell von Brooks und Corey (1964) die höchsten Sensitivitäten. Mit dem kalibrierten Modell wurden weitere Szenarien modelliert. Hierbei wurden wechselnde Bodenwassergehaltszustände innerhalb typischer Jahregänge arider Gebiete untersucht. Weiterhin wurden Modellläufe zur Bestimmung der Einflussgrößen einzelner Eingangs- und Randparameter auf mögliche Grundwasserneubildungsraten durchgeführt. Als größter Einfluss für tiefe Infiltrationsmengen und mögliche Grundwasserneubildung wurde die Niederschlagsmenge einzelner Regenereignisse bestimmt. Bei geringen jährlichen Niederschlagsmengen beeinflusste hauptsächlich der residuale Bodenwassergehalt die berechneten Perkulationsprozesse. Bei niedrigen Wassersättigungen dominierten thermische Wasserdampf Flüsse die gesamte Wasserflussmenge.

Die Laborexperimente dienten der ersten Untersuchung von Wasserflüssen in der vadosen Bodenzone arider Gebiete. Für die Modellkalibrierung lieferten sie zuverlässige und hochaufgelöste Daten. Mit dem kalibrierten Modell konnten weitere Untersuchungen zu Einflussfaktoren auf Wasserflüsse in der vadosen Zone durchgeführt werden. Das Modell kann

somit für Fragen des Grundwassermanagements in ariden Gebieten eingesetzt werden. Insbesondere kann es als Planungsinstrument für die Durchführung von Messkampagnen entsprechend errechneter Sensitivitäten herangezogen werden. Zusätzlich können weitere Modellläufe Bodensättigungen und Perkulationsraten für zukünftige hydrologische und klimatische Veränderungen oder Extreme abschätzen.

Table of Contents

Abstract	i
Zusammenfassung	iii
Table of Contents	v
List of Figures	ix
List of Tables	xv
List of Equations	xvii
Abbreviations and Variables	xix
Preface	1
1. Introduction	3
1.1. Study Background	3
1.2. Study Concept	4
2. Basic Knowledge and Previous Studies	7
2.1. Arid Zones	7
2.1.1. Soil Water States	7
2.1.2. Groundwater Recharge	8
2.1.3. Soils	9
2.2. Vadose Zone Water Fluxes	10
2.2.1. Soil Hydraulic Parameters	10
2.2.1.1 Retention Curve	11
2.2.1.2 Hydraulic Conductivity	13
2.2.2. Soil Thermal Parameters	13
2.2.3. Vapor Fluxes	14
2.3. Time Domain Reflectometry	14
2.3.1. Theory	15
2.3.2. Sensor Design	15
2.3.3. Effects of Electrical Conductivity, Temperature, Bulk Density and Water Content	16
3. Materials and Methods	17
3.1. Soil Properties	17
3.2. TDR Cable Sensor	18
3.3. Experimental Setup	21
3.4. Experimental Conditions	24
3.4.1. Silica Sand Filling	24
3.4.2. Dune Sand Filling	25
3.4.3. Layered Column Filling	26

3.5. Numerical Modeling	26
3.5.1. Hydrus-1D	26
3.5.2. Inverse Modeling	28
3.5.2.1 PEST	28
3.5.2.2 Model Setup	29
3.5.2.3 Initial and Boundary Conditions	30
3.5.2.4 Observation Data	31
3.5.2.5 Hydraulic and Thermal Properties	32
3.5.2.6 Sensitivity Analysis	32
3.5.3. Predictive Modeling	33
3.5.3.1 Initial and Boundary Conditions	33
3.5.3.2 Monthly Scenarios	34
3.5.3.3 Annual Scenarios	34
4. Results	37
4.1. Soil Properties	37
4.2. TDR Cable Calibration	41
4.3. Experiments	42
4.3.1. Silica Sand Filling	42
4.3.1.1 Steady State Experiment	42
4.3.1.2 Varying Irrigation Amounts	46
4.3.1.3 Varying Irrigation Intensity	48
4.3.1.4 Irrigation and Redistribution	49
4.3.2. Dune Sand Filling	50
4.3.2.1 General Observations	50
4.3.2.2 Two-Stage Irrigation	51
4.3.2.3 Time-Dependant Boundary Conditions	53
4.3.3. Layered Column Filling	57
4.4. Numerical Modeling	60
4.4.1. Inverse Calibration	61
4.4.2. Sensitivity Analysis	67
4.4.2.1 Parameter Sensitivities	67
4.4.2.2 Observation Sensitivities	69
4.4.3. Predictive Modeling	71
4.4.3.1 Initial and Boundary Conditions	71
4.4.3.2 Monthly Scenarios	74
4.4.3.3 Annual Scenarios	77

5. Discussion	87
5.1. Experiments	87
5.2. Modeling	89
5.3. Groundwater Recharge Studies	91
6. Conclusions	93
Literature	95
Acknowledgements	103
Curriculum Vitae	105
Publications and Conference Contributions	107
Erklärung der Urheberschaft	109
Appendix	
A1 Pictures of the experiments	
A1-a Column packing during experimental development and testing phase	
A1-b Final experimental setup before packing	
A1-c Final experimental setup during packing	
A1-d Final experimental setup during experiments (1)	
A1-e Final experimental setup during experiments (2)	
A2 TDR data	
A2-a TDR raw data explanation	
A2-b TDR infiltration curves before processing for the silica sand steady state irrigation	
A2-c TDR infiltration curves before processing for the dune sand irrigation breakthrough	
Supplement Material (CD)	
TDR raw data for the silica steady state irrigation	
TDR raw data for the dune sand calibration irrigation	
Hydrus-1D and PEST input files for the inverse calibration	
Hydrus-1D input files for the basic scenario modeling	



List of Figures

Fig. 1	Study concept with initial and boundary conditions, measured data and analyzed processes for the laboratory experiments and the numerical modeling	5
Fig. 2	TDR “Taupe“ cable design as it was used within the soil column experiments	19
Fig. 3	TDR cable reflection curves for soil profile water content determination	20
Fig. 4	Schematic drawing of the column experiment with controlled and measured parameters	23
Fig. 5	Detail photograph of the top assembly of the experiments during operation	23
Fig. 6	Assembly of TDR and temperature measurement sensors in the experimental column during packing	24
Fig. 7	Conceptual model for the inverse parameter calibration in Hydrus-1D according to the soil column experiments	29
Fig. 8	Annual time-variation curves of temperature and precipitation for high (a), moderate (b) and low precipitation (c) reference scenarios	35
Fig. 9	Grain size distribution of the silica and the dune sand used within the experiments as derived from sieve analysis	37
Fig. 10	SWRC-Fit results for measured retention data of the silica sand to the hydraulic models of van Genuchten, Brooks and Corey, and Durner without (a) and with (b) setting residual water content θ_r to zero	38
Fig. 11	SWRC-Fit results for measured retention data of the dune sand to the hydraulic models of van Genuchten, Brooks and Corey, and Durner without (a) and with (b) setting residual water content θ_r to zero (b)	38
Fig. 12	Thermal conductivity measurements fitted to the thermal conductivity equation of Chung and Horton (1987)	40
Fig. 13	Correlation of TDR cable reflection coefficient measurements with TDR rod sensor volumetric water content measurements and linear regression line for the silica (a) and the dune (b) sand	41
Fig. 14	Temperature profiles in the silica sand after applying boundary temperatures with 50 °C at the soil top and 15 °C at the soil bottom (a) and with a continuous irrigation of 0.55 mm/min (b)	42
Fig. 15	Infiltration front and discharge during wetting with continuous irrigation of 0.55 mm/min measured with the TDR cable (continuous line) and TDR point measurements (circles)	44

Fig. 16	Water content and evaporation during drainage and drying measured with the TDR cable (continuous line) and TDR point measurements (circles)	45
Fig. 17	Water content profiles and cumulative discharge and evaporation during infiltration and redistribution of 12.5 mm (a), 25 mm (b), and 50 mm (c) of irrigation with 6.25 mm/h intensity, measured with the TDR cable (continuous line) and TDR point measurements (circles)	46
Fig. 18	Relative humidity of the effluent air for three different irrigation events of 12.5 mm, lasting 240, 20 and 2 minutes	48
Fig. 19	Volumetric water content changes over time in the sand column for two consecutive irrigation events of 12.5 mm with 72 h of flow interruption between irrigations	49
Fig. 20	TDR cable signal scattering during irrigation within the dune sand packing	50
Fig. 21	Temperature profiles in the dune sand after applying boundary temperatures with 50 °C at the soil top and 15°C at the soil bottom (a) and with irrigation of 0.55 mm/min (b); PT100 temperature measurements are shown in circles	51
Fig. 22	Infiltration front for dune sand irrigation of 0.55 mm/min measured by TDR cable (line) and point (circle) measurements	52
Fig. 23	Discharge and evaporation over time for dune sand irrigation of 0.55 mm/min, lasting 5 h	52
Fig. 24	Cumulative irrigation, evaporation, and bottom discharge over time for changing boundary conditions applied to the experiments with dune sand filling	54
Fig. 25	Water fluxes in different depths over time for the first irrigation cycle (5 x 5 mm) during experiments with dune sand filling, measured with the TDR rod sensors and as integrated water content along the whole soil profile with the TDR cable sensor	54
Fig. 26	Temperature fluxes in different depths over time for the first irrigation cycle (5 x 5 mm) during experiments with dune sand filling	55
Fig. 27	Infiltration fronts measured with the TDR cable for irrigation cycle 2 and 3 of the experiments with dune sand filling	55
Fig. 28	Contour plot compiled from TDR cable measurements for irrigation cycle 2 and 3 of the experiments with dune sand filling	56
Fig. 29	Cumulative irrigation, evaporation, and bottom discharge over time for changing boundary conditions applied to the experiments with layered sand filling	58
Fig. 30	TDR cable signals for consecutive irrigation events during experiments with the layered sand packing given as reflection coefficient changes and adapted volumetric water content as calculated from a mixed calibration equation	58

Fig. 31	TDR cable signals for the 50 mm irrigation during experiments with the layered sand packing given as reflection coefficient changes and adapted volumetric water content as calculated from a mixed calibration equation	59
Fig. 32	Temperature calibration for the silica (a) and the dune sand (b) from steady-state temperature gradient application; measured values are shown in circles, model fit in straight lines	60
Fig. 33	Fitting results of the inverse calibration to cumulative discharge, cumulative evaporation, and soil water storage over time for the silica sand experiments	62
Fig. 34	Fitting results of the inverse calibration to water content measurements over time in eight different depths for the silica sand experiments	63
Fig. 35	Fitting results of the inverse calibration to cumulative discharge, cumulative evaporation, and soil water storage over time for the dune sand experiments	64
Fig. 36	Fitting results of the inverse calibration to water content measurements over time in eight different depths for the dune sand experiments	65
Fig. 37	Hydraulic conductivity – water content relationship for the silica and the dune sand with values obtained from the inverse model calibration	67
Fig. 38	Parameter sensitivities during dune sand calibration for observation groups of cumulative boundary fluxes (a), water contents in different depths (b), and temperature in different depths (c)	68
Fig. 39	Composite parameter sensitivities during dune sand calibration for all observation groups	69
Fig. 40	Observation sensitivities during dune sand calibration for water content in different depths over time	70
Fig. 41	Observation sensitivities during dune sand calibration for cumulative evaporation (a) and cumulative discharge (b) over time	71
Fig. 42	Comparison of infiltration fronts for changed scenario boundary conditions – 92 cm with suction plate and seepage face (experimental) versus 92 cm with suction plate and free drainage, versus 200 cm with free drainage without suction plate; water contents were taken after infiltration (a) and 10 h redistribution (b) for the dune sand calibration experiment	72
Fig. 43	Comparison of cumulative discharge (a) and cumulative evaporation (b) for experimental boundary conditions and changed boundary conditions with a 200 cm profile for predictive modeling	73
Fig. 44	Initial water content and temperature distribution conditions for the predictive modeling as obtained from a 90 days model pre-run	73

Fig. 45	Cumulative discharge (a) and cumulative evaporation (b) compared for 50 mm precipitations as of 50 mm within one day and 50 mm within 25 days with 5 times 10 mm precipitation and 5 days drying between each event	74
Fig. 46	Infiltration fronts compared for 50 mm precipitations of different monthly patterns with 50 mm in one day, 50 mm in 10 consecutive days, 50 mm with alternating 1 day of 10 mm precipitation and 1 day of drying, and 50 mm with alternating 1 day of 10 mm precipitation and 4 days of drying	75
Fig. 47	Water content profiles with initial homogenous water content for 1 day drying, 10 mm precipitation, and drying after precipitation with top temperature of 8 °C (a) and 30 °C (b) and bottom temperature of 20 °C	76
Fig. 48	Cumulative evaporation (a) and soil water storage (b) for 10 mm precipitation compared for a top temperature of 8 °C and 30 °C with a bottom temperature of 20°C for both	76
Fig. 49	Cumulative bottom fluxes and cumulative evaporation fluxes for three tested sand properties for high flux scenarios with initial gradient water content (a), and compared for the dune sand with initial dry water contents (b)	77
Fig. 50	Cumulative bottom fluxes for dune sand properties during moderate flux annual reference scenario with dry initial conditions	78
Fig. 51	Water contents for initial scenario modeling conditions after the 90 days model pre-run and after an annual scenario run with moderate precipitation amounts with initially dry conditions	78
Fig. 52	Water contents for annual scenario runs with low precipitation reference scenario (30 mm/a); initial water contents was set to residual for the first year, each following annual run continued with the final water content of the former year	79
Fig. 53	Cumulative bottom fluxes for different sand properties during moderate flux annual reference scenario (a) and low flux reference scenario (b) with initial gradient water content conditions	80
Fig. 54	Composite parameter sensitivities during annual low precipitation scenario for cumulative bottom flux, cumulative evaporation and water content profiles	80
Fig. 55	Simulated soil water storages for decreasing precipitation intensity (one day, 10 days, 30 days) for the moderate flux reference scenario	81
Fig. 56	Cumulative evaporation during the low (a) and high (b) flux annual reference scenario with sands of different hydraulic properties; evaporation during dry times was driven by water vapor uptake from the air	82
Fig. 57	Precipitation and cumulative precipitation and evaporation for running the model with diurnal temperature changes, without diurnal temperature changes and without vapor fluxes	82

Fig. 58	Water and vapor fluxes during a high flux period (a) and according temperature and water content profiles with and without considering vapor fluxes (b) in the model	83
Fig. 59	Water and vapor fluxes during a low flux period (a) and according temperature and water content profiles with and without considering vapor fluxes (b) in the model	84
Fig. 60	Water and vapor fluxes during a no flux period (a) and according temperature and water content profiles with and without considering vapor fluxes (b) in the model	84



List of Tables

Tab. 1	Climate zone classification according to the ratio of annual precipitation to potential evapotranspiration (UNEP, 1992)	7
Tab. 2	Time-variable boundary conditions (irrigation and temperature) as applied to the experiments with dune sand filling	25
Tab. 3	Time-variable single irrigations (amount and intensity) as applied to the experiments with layered sand filling	26
Tab. 4	Time-variable boundary conditions for the inverse model calibration of the silica sand experiments	30
Tab. 5	Time-variable boundary conditions for the inverse model calibration of the dune sand experiments	31
Tab. 6	Physical properties of the silica and the dune sand used within the experiments	38
Tab. 7	Hydraulic model parameters for silica sand and dune sand obtained from retention data, and reference data for 100 % pure sand obtained from pedotransfer functions and Rawls et al., 1982	39
Tab. 8	Thermal conductivity parameters derived and fitted according to Chung and Horton (1987) for silica sand and dune sand measurements	40
Tab. 9	Summarized water balance results for 12.5, 25 and 50 mm irrigation of the same intensity of 6.25 mm/h with cumulative values 7 days after irrigation	45
Tab. 10	Summarized results for amounts of evaporation for three 12.5 mm irrigations with intensities of 0.052 mm/min (240 min), 0.625 mm/min (20 min), and 6.25 mm/min (2 min)	47
Tab. 11	Water balance calculations of irrigation and drying cycles applied to the experiments with dune sand filling	53
Tab. 12	Water balance calculations of irrigation and drying cycles applied to the experiments with layered sand filling	57
Tab. 13	Thermal conductivity parameters according to Chung and Horton optimized for silica and dune sand by inverse calibration	61
Tab. 14	Hydraulic parameters from inverse parameter estimation compared to measured values for silica and dune sand	66



List of Equations

Eq. 1	Penman-Monteith equation	8
Eq. 2	Richards equation for 1-dimensional vertical water flow in unsaturated porous media	10
Eq. 3	van Genuchten hydraulic model equation for retention curve fitting	11
Eq. 4	Brooks-Corey hydraulic model equation for retention curve fitting	11
Eq. 5	Durner bimodal hydraulic model equation for retention curve fitting	12
Eq. 6	Effective saturation calculation for all hydraulic models	12
Eq. 7	Hydraulic conductivity function according to Mualem-van Genuchten	13
Eq. 8	Hydraulic conductivity function according to Brooks and Corey	13
Eq. 9	Thermal diffusivity equation	13
Eq. 10	Thermal conductivity function according to Chung and Horton	14
Eq. 11	Relation of relative dielectric permittivity to the reflection length of a reflected electromagnetic pulse along a TDR sensor	15
Eq. 12	Topp equation for converting dielectric permittivity to water content in variably saturated soils	15
Eq. 13	Calculation of absolute humidity from temperature and relative humidity measurements	21
Eq. 14	Modified Richards equation for nonisothermal water and vapor flux as implemented in Hydrus-1D	26
Eq. 15	Thermal hydraulic conductivity function as implemented in Hydrus-1D	27
Eq. 16	Isothermal vapor conductivity function as implemented in Hydrus-1D	27
Eq. 17	Thermal vapor conductivity function as implemented in Hydrus-1D	27
Eq. 18	One-dimensional heat transport with vapor transport as implemented in Hydrus-1D	27
Eq. 19	Correlation coefficient R for measuring the goodness of the model fit	28
Eq. 20	Diurnal temperature changes as implemented in Hydrus-1D	33
Eq. 21	TDR volumetric water content calculation from cable reflection coefficient measurements for the silica sand	41

Eq. 22	TDR volumetric water content calculation from cable reflection coefficient measurements for the dune sand	41
Eq. 23	Mixed TDR volumetric water content calculation from cable reflection coefficient measurements for the layered column setting derived from the single calibration curves of the silica and the dune sand	57

Abbreviations and Variables

A	Temperature amplitude at the soil surface during diurnal temperature changes, as implemented in Hydrus-1D (-)
AH	Absolute humidity (g/m ³)
b1, b2, b3	Fitting parameters in the Chung and Horton thermal conductivity function (-)
c _a	Specific heat capacity of air (J/kgK)
c _{vp}	Volumetric heat capacity (J/cm ³ K)
c _{vv}	Volumetric heat capacity of vapor (J/cm ³ K)
c _{vw}	Volumetric heat capacity of water (J/cm ³ K)
D _v	Vapor diffusivity (cm ² /min)
e _a	Vapor pressure air (kPa)
e _s	Vapor pressure soil (kPa)
g	Gravitational acceleration (9.81 m/s ²)
G	Soil heat flux (J/cm ² d)
G _{wT}	Gain factor for temperature dependence of the soil water retention function, as implemented in Hydrus-1D (-)
h	Hydraulic pressure head (cm)
h _b	Fitting parameter in the Brooks and Corey retention function, physically related to the hydraulic pressure head at air entry pressure (cm)
k	Thermal conductivity (W/mK)
K _a	Relative dielectric permittivity (-)
K _{Lh}	Isothermal liquid hydraulic conductivity (cm/h)
K _{LT}	Thermal liquid hydraulic conductivity (cm/h)
K _s	Saturated hydraulic conductivity (cm/h)
K _{vh}	Isothermal vapor hydraulic conductivity (cm/h)
K _{vT}	Thermal vapor hydraulic conductivity (cm/h)
l	Tortuosity factor in the hydraulic conductivity function (-)
L	Latent heat of vaporization (MJ/kg)
L	TDR pulse reflection length in air, real sensor length (m)
L _a	TDR pulse reflection length, apparent signal length (m)
m	Fitting parameter in the van Genuchten soil water retention function (-)
M	Molecular weight of water (0.018015 kg/mol)
n	Fitting parameter in the van Genuchten soil water retention function (-)

PET	Potential Evapotranspiration (cm)
P	Precipitation (cm)
q_v	Vapor flux density (cm/h)
Q	Water flux (cm/h)
r_a	Aerodynamic resistance (s/m)
r_s	Surface resistance (s/m)
R	Correlation coefficient (-)
R_n	Net radiation (MJ/m ² d)
R_u	Universal gas constant (8.314 J/mol K)
RC	TDR reflection coefficient (-)
RH	Relative humidity (%)
S_e	Effective saturation (-)
t	Time (h)
T	Temperature (°C)
TDR	Time Domain Reflectometry
w	Fitting parameter in the Durner dual domain retention function – domain fraction (-)
α	Fitting parameter in the van Genuchten soil water retention function (-)
Δ	Slope of the saturation vapor pressure temperature relationship (kPa/°C)
η_e	Enhancement factor in the thermal vapor conductivity function (-)
γ_c	Psychrometric constant (kPa/°C)
γ	Soil water surface tension (J/cm ²)
γ_0	Soil water surface tension at 25°C (J/cm ²)
λ	Fitting parameter in the Brooks and Corey soil water retention function (-)
ρ_a	Dry air density (g/cm ³)
ρ_{vs}	Saturated vapor density (g/cm ³)
ρ_w	Water density (g/cm ³)
θ	Volumetric water content (cm ³ /cm ³)
θ_r	Residual water content (cm ³ /cm ³)
θ_s	Saturated water content (cm ³ /cm ³)





Preface

This study was performed under the framework of the “International Water Research Alliance Saxony” (IWAS) initiative. IWAS aims at developing and implementing contributions to an integrated water resources management in hydrological sensitive regions (IWAS, 2011). IWAS model regions for research studies are Eastern Europe, Central Asia, South-East Asia, Latin America and the Middle East. In the Middle East, the study focus is on developing appropriate methodologies to investigate groundwater recharge for quantifying available renewable groundwater resources in water scarce areas. Project areas are in Oman and in the Kingdom of Saudi Arabia. Studies include laboratory work, field campaigns as well as different-scale modeling.

The laboratory soil column and numerical modeling studies presented in this work are part of the projects in Saudi Arabia. Nevertheless, this work did not consider a specific areal context but was designed to study typical and general patterns in arid regions.

Besides the analysis of vadose zone water fluxes, the laboratory column experiments also aimed at evaluating water content measurements with a Time Domain Reflectometry (TDR) “Taupe” cable. The measurement method and evaluation was conducted in close cooperation with the Competence Centre for Material Moisture (CMM) at the Karlsruhe Institute of Technology, where the sensor was developed.

Part of this work, including the experimental setup and silica sand experiments, was published in Pflöschinger et al. (2012), where copyrights are held by Springer Publishing.



1. Introduction

The introduction combines the study background and the study concept which resulted from the overall aim of quantifying vadose zone water fluxes under arid conditions.

1.1. Study Background

Over the past five decades, in many parts of the world groundwater resources have been overexploited. Especially in arid regions, where large amounts of water are needed for irrigation, and the water demand increases due to increasing population and industry, water scarcity is a demanding problem (FAO, 2003). As surface water resources in arid regions are mostly limited and unreliable, groundwater is the primary water source in these areas (Scanlon et al., 2006). To minimize declining groundwater levels, a sound integrated water resources management (IWRM) has to be set up. For sustainability, it is important to quantify potential groundwater recharge in contrast to groundwater extraction. Even if large parts of the exploited groundwater are fossil aquifers and as such non-renewable, infiltrating water can contribute to groundwater recharge and renew especially shallow water resources. If infiltrating water can reach the groundwater highly depends on processes in the vadose zone, which can exceed several hundreds of meters in arid regions (Scanlon et al., 1997). As in these areas annual potential evaporation by far exceeds annual rates of precipitation, vadose zone water fluxes are naturally very low and rates of percolation and redistribution patterns within the vadose zone are hard to quantify. Thus, there is a high uncertainty in vadose zone water fluxes, as well as overall water balance calculations, and in groundwater recharge predictions (Scanlon et al., 1997; Walvoord et al., 2002).

Recently, efforts have been made to better understand and quantify vadose zone processes and water fluxes by improved measurement techniques of water content (e.g. Dahan et al., 2003; Jones et al., 2005), observation of different scale phenomena (e.g. Hendrickx and Flury, 2001; Hopmans and Schoups, 2006; Mattson et al., 2004) and enhanced numerical modeling (e.g. Dong et al., 2003; Saito et al., 2006; Sakai et al., 2009). Nevertheless, especially for arid regions there are still many uncertainties due to difficult field conditions, highly variable and unpredictable meteorological conditions and coupled processes, influenced, amongst others, by pressure and temperature gradients. Obtained values for groundwater recharge are highly dependent upon the applied measurement and calculation methods as well as upon considered scales of time and space (Gee and Hillel, 1988; Scanlon et al., 2002a). The most common methods for arid regions are lysimeter studies, tracer studies and numerical modeling (Scanlon et al., 2002a). Nevertheless, the lack of reliable and continuous data of water fluxes under pressing boundary conditions enlarge errors in recharge calculations, model verification and the overall understanding of the complex processes within the variably saturated vadose zone.

Bench-scale laboratory experiments can greatly support the understanding and quantification of fluxes in the vadose zone by simulating and investigating processes that occur in the field under controlled initial and boundary conditions (Oostrom et al., 2007). In the past, several soil column experiments have been developed, mainly for the determination of soil hydraulic properties, rates of infiltration and evaporation, and contaminant transport studies. Specific aims of these experiments include:

-
- the determination of water saturation and retention functions as introduced by Brooks and Corey (1964) and van Genuchten (1980),
 - the testing of water content and matrix potential measurement probes (Heimovaara et al., 1993; Mattson et al., 2006; Mori et al., 2005)
 - the investigation of preferential flow processes (Mooney and Morris, 2004; Silio and Tellam, 2000), and
 - water infiltration and redistribution studies for homogenous and heterogeneous unsaturated media (Yang et al., 2004).

However, when studying vadose zone water fluxes under arid conditions, there is still a lack in bench-scale experimental work, as most experiments focus on single parameter vadose zone studies rather than on complex overall flux studies under multiple gradients. For the verification and calibration of unsaturated zone models the high spatial and temporal resolution measurements of all gradients influencing the systems behavior, are of crucial importance. With adequate laboratory experiments, readily available numerical models can be inversely calibrated against experimental data and analyzed regarding system specific behavior (Benson, 2007; Finsterle, 2004). Based on the calibrated model further model predictions that simulate recharge for critical precipitation rates or extreme temperature events are feasible without any further experimental investigations. Therefore, well defined laboratory experiments and subsequent appropriate numerical modeling can be a valuable tool for groundwater management issues.

1.2. Study Concept

This study aimed at quantifying water and temperature fluxes in unsaturated porous media in dependence of transient soil water contents and meteorological conditions as they can be expected in arid regions. For this purpose, laboratory experiments with well defined and adjustable boundary conditions as well as spatial and temporal high resolution measurements of water content and temperature were developed. With the experimental setup and data, a numerical model was set up and calibrated in Hydrus-1D (Šimůnek et al., 2009). With the calibrated model, predictive modeling to analyze the significance of varying initial and boundary conditions on possible groundwater recharge was performed.

Special focus of the work was the analysis of water infiltration, evaporation, redistribution and percolation. The work intended to identify primary parameters of importance for groundwater recharge in arid regions. Therefore, the study was not conducted with a fixed regional context but rather with a climatic context to reflect regions of arid climate as such. Nevertheless, study results can improve regional groundwater recharge studies by optimizing observation and measurement schemes according to the model sensitivity and scenario studies.

The study concept included the main tasks of the development of laboratory soil column experiments and the subsequent 1-dimensional numerical modeling based on the experiments (Fig. 1).

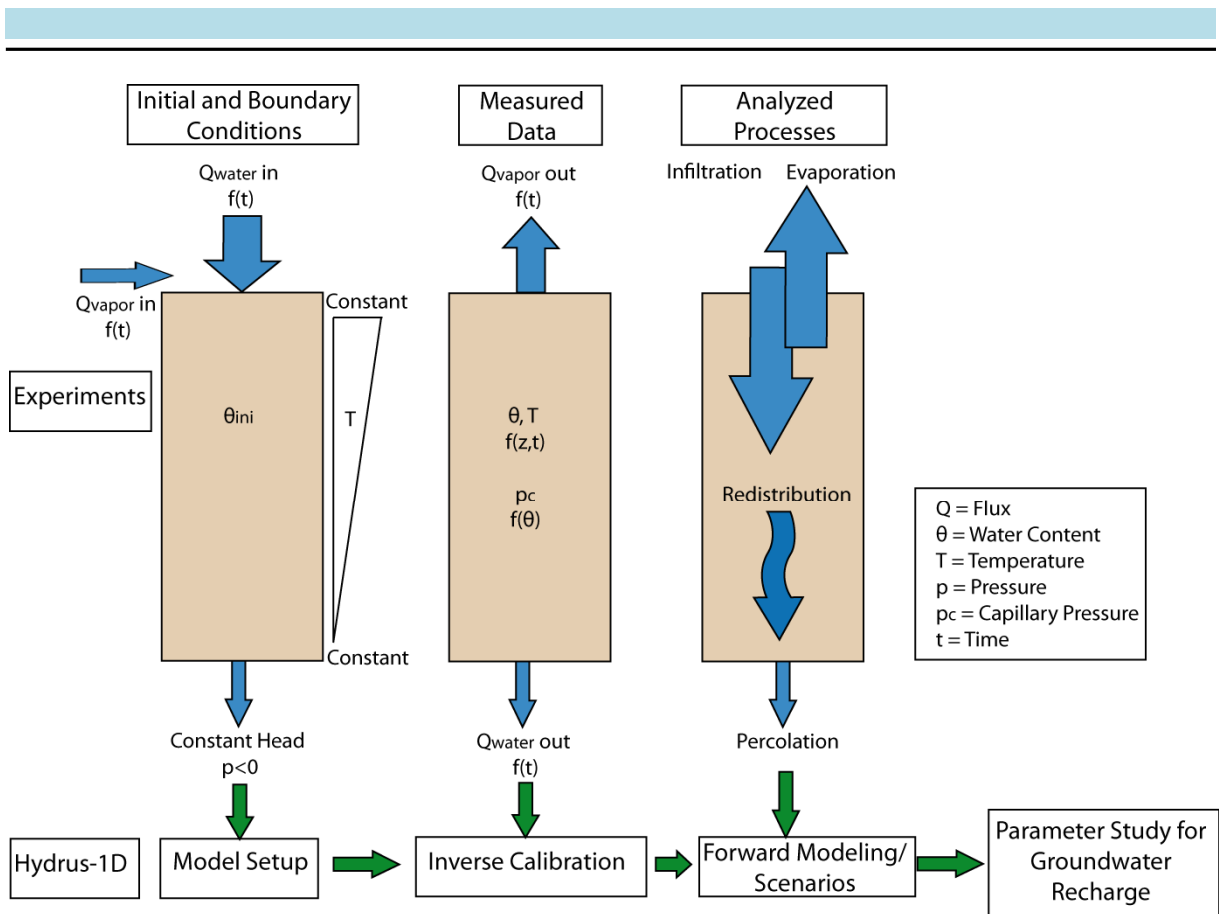


Fig. 1 - Study concept with initial and boundary conditions, measured data and analyzed processes for the laboratory experiments and the numerical modeling

The research concept included the following tasks:

- Develop a closed soil column system to measure 1-dimensional water and temperature fluxes in unsaturated soil under defined initial and boundary conditions as they can be expected under arid climate.
- Test and evaluate a cable sensor for the measurement of water content changes within a whole soil profile by time domain reflectometry. The sensor is to be tested in the soil column experiments and evaluated for the usage in field studies.
- Conduct experiments under different initial and boundary conditions, as they can be expected in arid regions, and analyze their influences on water infiltration, evaporation and redistribution.
- Set up a model for unsaturated zone flow according to the experimental setup and calibrate the model with data of water content, water fluxes and temperature obtained from the experiments.
- Identify parameters of primary importance for possible groundwater recharge under arid conditions by conducting predictive scenario modeling.



2. Basic Knowledge and Previous Studies

In this chapter, general hydrological characteristics of arid regions and their influences on vadose zone water fluxes are introduced. Controlling equations that are important for vadose zone characteristics as well as the modeling of vadose zone water fluxes and heat transport are listed and explained. Additionally, one main methodological feature of the experiments, which is the measurement of water content by time domain reflectometry, is presented. Details on the application of these methods and equations in the experiments and numerical modeling are given in chapter 3.

2.1. Arid Zones

Around 30 % of the global terrestrial surface area are within an arid or semi-arid climate (Scanlon et al., 2006). As population tend to grow, water scarcity in this already water scarce areas will presumably increase. In general, arid regions are not only characterized by water scarcity but also by a high spatial and temporal variability in precipitation and temperature. Thus, precipitation as the main soil water input component is mostly unpredictable in arid zone hydrology and water balance calculations (Noy-Meir, 1973).

In general, arid regions are characterized by a negative water balance, where potential evapotranspiration exceeds precipitation for 8 - 10 months within the year (Littmann and Berkowicz, 2008). Depending on the annual exceedance of potential evapotranspiration over precipitation, arid regions can be subdivided into semi-arid, arid and hyper-arid zones (Tab. 1).

Tab. 1 – Climate zone classification according to the ratio of annual precipitation to potential evapotranspiration (UNEP, 1992)

	UNEP (1992) Annual P/PET
Hyper-Arid Zone	< 0.05
Arid Zone	0.05 – 0.2
Semi-Arid Zone	0.2 – 0.5

2.1.1. Soil Water States

Varying seasonal as well as regional climate patterns can highly influence ambient soil water states. Seasonal patterns are often described as summer dry period, transitional fall wetting period, winter low flux period, spring high flux period and transitional late-spring drying period (Bazuhair and Wood, 1996; McNamara et al., 2005; Seyfried et al., 2005). High flux periods contribute to almost 100 % of total annual precipitation. Depending on the occurrence and intensity of the wetting and low flux periods, the change from dry to wet conditions can be very abrupt whereas the drying process lasts over several months (Seyfried et al., 2005). Drying rates are induced by actual evapotranspiration, whereas the time-scales for drying depend on the soil properties, on atmospheric conditions and, if present, on the vegetation cover (Pan and Mahrt, 1987).

Overall, 70 – 80 % of annual precipitation may evaporate under arid climate (Sorman and Abdulrazzak, 1995). When excluding effects of vegetation cover, drying by evaporation can be divided into three different stages. During the constant-rate stage, evaporation is only limited by the energy supply to the soil surface. During the falling-rate stage, it is restricted by the available water supply at the surface which is controlled by the soil moisture conditions and the soil hydraulic properties (Suleiman and Ritchie, 2003). The final low-rate state is only determined by soil physical characteristics and water flow only occurs in the vapor phase (Qiu and Ben-Asher, 2010). The constant-rate stage evaporation, describing the maximum evaporation under non-limiting soil water conditions, resembles the potential evaporation and can, amongst others, be calculated by the Penman-Monteith equation (Eq. 1):

$$PET = \frac{1}{L} \frac{\Delta(R_n - G) + \rho_a c_a \frac{(e_s - e)}{r_a}}{\Delta + \gamma_c \left(1 + \frac{r_s}{r_a}\right)}$$

Eq. 1 – Penman-Monteith equation (Allen et al., 1998; Monteith and Unsworth, 1990)

where L is the latent heat of vaporization (MJ/kg), R_n is the net radiation (MJ/m²d), G is the soil heat flux (MJ/m²d), $(e_s - e_a)$ is the vapor pressure deficit in the air (kPa), Δ is the slope of the saturation vapor pressure temperature relationship (kPa/°C), γ_c is the psychrometric constant (kPa/°C), ρ_a is the dry air density (kg/m³), c_a is the specific heat capacity of air (MJ/kg°C), r_a is the aerodynamic resistance and r_s is the surface resistance (s/m).

Infiltrated water that does not escape by evaporation, can have long storage times in the vadose soil zone of arid regions, whereas redistribution patterns, including the vertical percolation, strongly depend on the physical properties and the wetting history. Additionally, temperature gradients and heat fluxes, underlying seasonal and diurnal fluctuations, can influence water fluxes, especially in the low saturation range. In the late-spring drying and summer dry period, air temperatures can reach values up to 50 °C and soil temperatures generally decrease with depth. In the autumn and winter periods, air temperatures can fall below 0 °C and soil temperatures increase with depth (Scanlon and Milly, 1994). Diurnal temperature fluctuations can make up to differences in 20 °C during day-time and night-time temperatures.

2.1.2. Groundwater Recharge

Desert regions are largely known as regions where no groundwater recharge can occur. Nevertheless, during high flux periods, which are short in time but periodically with intensive precipitation, infiltration depths can reach beyond depths of evaporation and eventually contribute to recharge. Thus, in arid regions, most of the recharge results from episodic and single precipitation events (Gee and Hillel, 1988).

On a global synthesis, Scanlon et al. (2006) estimated recharge in arid regions of 0.1 – 5 % of long-term average annual precipitation, when totaled over large areas. For Saudi Arabia, estimates for recharge of 3 - 4 % of annual precipitation are given (Bazuhair and Wood, 1996). Some regional groundwater recharge studies conclude that it can be directly calculated as fraction of annual precipitation, with threshold values, below which no infiltration water

reaches the groundwater table (Lerner et al., 1990). Altogether, data on regional groundwater recharge rates are still rare and estimates strongly depend on the methods used.

When studying groundwater recharge in arid regions, mainly three different mechanisms can be distinguished (de Vries and Simmers, 2002; Lerner et al., 1990):

- direct recharge, where water directly percolates vertically through the vadose zone
- indirect recharge, where water percolates through beds of surface-water
- localized recharge, where water first travels above-surface and most of the times is collected in depressions, before vertically percolating through the vadose zone.

Within this work, only direct recharge is considered. Direct recharge is often neglected when looking at total groundwater recharge in a catchment area. Nevertheless, especially in sandy regions, where water can infiltrate quickly into the ground, direct recharge can play a significant role and might be underestimated in many cases (Dincer et al., 1974).

2.1.3. Soils

Groundwater recharge highly depends on the overlying soils, its hydraulic and thermal properties and thus its infiltration capacities and water holding capacities. Additionally, depth and stratigraphy of the soils determine vadose zone storage time of infiltrated precipitation water (Aba-Husayn and Sayegh, 1977).

Soils in arid regions show differences to those in humid regions, mostly owing to low moisture availability. They are generally less weathered resulting in coarse textures and low soil formation (Cooke et al., 1993). Sandy soils occur throughout all arid regions, forming planes and dunes. As these sands have low water holding capacities and seedlings can hardly settle, they are often not vegetated and have low to zero organic content (Balba, 1995). Especially in the sandy desert regions, the soils are generally undeveloped, occasionally deep, only weakly structured and have little horizon differentiation (Singer, 1995).

Some soils in arid regions are known to form water-repellent films at their surfaces, resulting in lower infiltration rates. As these hydrophobic films consist of organic matter, water repellency occurs mainly in vegetated regions. Nevertheless, even in soils with low organic matter, temporary water repellency for up to 45 seconds was reported before the soil was wetted (Dregne, 1976). Thus, water repellency can highly influence infiltration rates, especially for low precipitation and infiltrations that are disrupted by frequent drying.

2.2. Vadose Zone Water Fluxes

“Vadose zone” refers to the soil region between the land surface and the groundwater, excluding the capillary fringe (Scanlon et al., 1997). As such, the vadose zone is differently saturated and water flow is generally induced by pressure and temperature gradients, distinguishing isothermal and thermal water flow. Compared to saturated soils, the water phase in unsaturated soil is bound partially by solid surfaces and partially by the air interface (Jury and Horton, 2004). Pressure gradients are caused by differences in soil water potential as a sum of pressure in the liquid phase due to water elevation, the attraction to solid surfaces, and the tension of the air-water interface (Jury and Horton, 2004). Generally, decreasing water content leads to decreasing liquid pressure and water flows from regions of higher to lower water pressure heads. Temperature gradients induce water flow from warmer to colder regions. Thermal water flow is lower than isothermal water flow but can occur even without pressure gradients. As thermally induced water flow changes water potential gradients, and isothermal water flow can change temperature gradients, isothermal and thermal water fluxes are closely coupled (Cary, 1965). The importance of coupled isothermal and thermal water transport increases with increasing temperature gradients (Constantz et al., 2003; Scanlon and Milly, 1994). A first theory for describing non-isothermal moisture movement in porous media was provided by Philip and de Vries (1957), consisting of a water transport equation considering liquid and vapor phases, as well as an energy equation (Griffoll et al., 2005). The theoretical model of Philip and de Vries is widely used and modified, especially regarding vapor flux mechanisms. Today, for the numerical simulation of vadose zone water fluxes, several modeling tools are readily available, as for example compared in Scanlon et al. (2002b). The models mainly vary in the possibilities to include heat and vapor fluxes as well as the internal coupling approaches of these fluxes.

2.2.1. Soil Hydraulic Parameters

The amount of isothermal water flow is controlled by two basic soil specific hydraulic characteristics. The retention characteristics specify the relationship of water content and pressure head, $\theta(h)$. The conductivity characteristics specify the relationship of unsaturated hydraulic conductivity to pressure head, $K(h)$ (Wildenschild et al., 2001). Both can be described by analytical functions and are commonly measured under steady-state conditions. Soil hydraulic functions of water retention and hydraulic conductivity are generally temperature dependant due to the influence of temperature on surface tension (Šimůnek et al., 2009).

When knowing the soil specific retention and conductivity relationship of water content, vertical isothermal moisture movement can be expressed by the Richards' equation (Richards, 1931) (Eq. 2).

$$\frac{\partial \theta}{\partial t} = - \frac{\partial}{\partial z} \left[K_{hz}(\theta) \frac{\partial h}{\partial z} \right]$$

Eq. 2 – Richards equation for 1-dimensional vertical water flow in unsaturated porous media

where θ is the volumetric water content (cm^3/cm^3), h is the pressure head (cm), t is the time (s) z is the flow direction and K_{hz} is the hydraulic conductivity in flow direction (cm/s).

If soil hydraulic parameters are not available from measurements, so-called pedotransfer functions can estimate unsaturated hydraulic properties from soil texture and bulk density data. One of the most common computer programs implementing pedotransfer functions is ROSETTA. The accuracy of the hydraulic parameters obtained from pedotransfer functions strongly depends on the available input information and the soil texture, whereas generally fine textured soils give better results (Schaap et al., 2001).

2.2.1.1 Retention Curve

The retention curve of a soil describes the relationship between soil water saturation and the soil water tension. For a saturation where only gravity acts as driving force for flow, the soil water tension equals zero as the water is completely unbound to the soil matrix. As soon as the soil drains to a saturation where no continuous water film is abundant in the matrix, capillary pressures define the further drainage and water retention. The pressure at this specific saturation is called air-entry pressure and is an important, soil specific retention parameter. Water retention data are commonly shown in water retention curves where single measurements of soil water tension, which correspond to a specific saturation, are fitted to analytical models. The shape of the retention curve mainly depends on the bulk density, the grain size distribution, the grain shapes and the mineral composition of the soil (Hillel, 2004).

The most common analytical models for describing the retention characteristics of a soil are the van Genuchten model (Eq. 3) (van Genuchten, 1980) and the Brooks and Corey model (Eq. 4) (Brooks and Corey, 1964). Corresponding equations include fitting parameters. The goodness of fit can largely differ between different hydraulic models. Generally, the van Genuchten model better describes finer-textured soils, whereas the Brooks and Corey model better describes coarse textured soils (Valiantzas, 2011).

$$S_e = \left[\frac{1}{1 + (\alpha h)^n} \right]^m$$

Eq. 3 – van Genuchten hydraulic model equation for retention curve fitting

where S_e is the effective saturation (-), and $\alpha(\text{cm}^{-1})$, n (-) and m (-) are fitting parameters. The parameter n can be physically related to the grain size distribution, and m is normally constrained by the relation $m=1-l/n$, where l (-) is the tortuosity (Bitterlich et al., 2004).

$$S_e = \begin{cases} \left(\frac{h}{h_b} \right)^{-\lambda} & (h > h_b) \\ 1 & (h \leq h_b) \end{cases}$$

Eq. 4 – Brooks-Corey hydraulic model equation for retention curve fitting

where h_b (cm) is a fitting parameter that can be physically related to the air-entry pressure, and λ (-) is a fitting parameter that can be physically related to the pore size distribution (Hillel, 2004).

Especially in heterogeneous soils, water retention can be better described by dual domain models, where one domain resembles large pores, and one domain resembles the soil matrix. In the large pores, only negligible amounts of water are retained and water flow is fast, whereas in the soil matrix, water retention is much higher, resulting in low water fluxes. Even in homogenous soils dual domain models can be applicable. In this context, infiltrating water accounts for pore water flow that does eventually not mix and equilibrate with slower moving resident water captured in the soil matrix. The amount of equilibration is assumed to depend on the amount and intensity of the infiltration water (Jarvis, 2007). Comparing single and dual domain hydraulic flow models can be useful when fitting and modeling transient water flux data in unsaturated soils. The combined retention characteristics can be described for example by the model of Durner (Eq. 5) (Durner, 1994):

$$S_e = \left[\frac{1}{1 + (\alpha_1 h)^{n_1}} \right]^{m_1} + w_2 \left[\frac{1}{1 + (\alpha_2 h)^{n_2}} \right]^{m_2}$$

Eq. 5 – Durner dual domain hydraulic model equation for retention curve fitting

where the single parameters correspond to the van Genuchten parameters (Eq. 3), w (-) is the fraction amount of the corresponding domain, and indices 1 and 2 indicate macropore and matrix characteristics.

For all hydraulic models the effective saturation S_e is assigned as

$$S_e = \frac{\theta - \theta_r}{\theta_s - \theta_r}, \quad \text{i. e., } \theta = \theta_r + (\theta_s - \theta_r)S_e$$

Eq. 6 – Effective saturation calculation for all hydraulic models

where θ is the measured water content (cm^3/cm^3), θ_r is the residual water content (cm^3/cm^3), and θ_s is the saturated water content (cm^3/cm^3).

The residual water content is defined as the water content where only adsorptive forces act on the water. At this state, the hydraulic head is rapidly decreasing with almost no change in water content (Jury and Horton, 2004). The saturated water content is defined as the maximum water content that a soil can collect. Under ideal conditions it equals the soil porosity. However, as soon as air is trapped in soil micropores, the saturated water content decreases, as it does during drying and wetting cycles. Another aspect of drying and wetting cycles is the effect of hysteresis. In general, hysteresis describes the differences of the retention relationship for drying and wetting conditions due to air entrapment. Several drying and wetting cycles can enhance hysteresis effects making it hard to measure it in advance. Hysteresis effects in soils show that a drying soil tends to retain a greater amount of water than a wetting soil for the same pressure head (Zeng et al., 2009). Thus, retention curves are not unique for a single soil but their shape and inclination strongly depend on the wetting history and accordingly the obtaining method.

2.2.1.2 Hydraulic Conductivity

Especially for coarse grained soils, hydraulic conductivity rapidly decreases with decreasing saturation. The unsaturated hydraulic conductivity is a nonlinear function of water content (Jury and Horton, 2004) and can be described by analytical functions, e.g. by Mualem and van Genuchten (Eq. 7) (van Genuchten, 1980) or Brooks and Corey (Eq. 8) (Brooks and Corey, 1966).

$$K(h) = K_s S_e^l \left[1 - \left(1 - S_e^{\frac{1}{m}} \right)^m \right]^2$$

Eq. 7 – Hydraulic conductivity function according to Mualem-van Genuchten

$$K(h) = K_s S_e^{\frac{2}{\lambda} + 1 + 2}$$

Eq. 8 – Hydraulic conductivity function according to Brooks and Corey

where K_s is the saturated hydraulic conductivity (cm/s) and l is the tortuosity parameter (-). The variables m and λ are the retention curve parameters of the corresponding retention model (Eq. 3 and Eq. 4).

Out of 47 soil samples of different grain size distributions, Mualem estimated the tortuosity factor l to be 0.5 (Mualem, 1976), which is a common value used. Nevertheless, the appropriateness of this value is to be verified. Especially for arid regions, much higher values of up to 8 were suggested (Sakai et al., 2009).

2.2.2. Soil Thermal Parameters

Thermal water fluxes are governed by thermal gradients which develop according to the ambient temperatures and the thermal diffusion. The thermal diffusivity α (cm²/s), which is the transmission of heat into a material with a defined rate of change in temperature, is given by (Venkanna, 2010)

$$\alpha = \frac{k}{\rho c}$$

Eq. 9 – Thermal diffusivity equation

where k is the material specific thermal conductivity (W/cmK), ρ is the materials density (g/cm³), and c is its specific heat capacity (J/gK), resulting in $\rho \cdot c$ as the volumetric heat capacity c_{vp} (J/cm³K).

The soil thermal conductivity mainly depends on the soil density, its moisture content, salt concentrations and organic matter. It can be measured in dependence of water saturation and described with thermal property functions, like for example from Chung and Horton (Chung and Horton, 1987).

$$k(\theta) = b_1 + b_2 * \theta + b_3 * \theta^{0.5}$$

Eq. 10 – Thermal conductivity function according to Chung and Horton (1987)

where b_1 , b_2 and b_3 are curve shape fitting parameters (-). The parameter b_1 can be physically related to the unsaturated thermal conductivity (W/mK).

The soil heat capacity c_p (J/cm³K) is the change in heat content per unit change in temperature (Hillel, 2004). The ambient heat capacity in a soil can be calculated by a simple mixing equation according to the fractions of soil, water and air. Volumetric heat capacities are known with 4.17 J/cm³K for liquid water, 0.0012 J/cm³K for air, and 1.9 J/cm³K for silica sand (Abu-Hamdeh, 2001; Hillel, 2004).

2.2.3. Vapor Fluxes

Vadose zone water fluxes not only include liquid water, but also vapor fluxes, which can also be distinguished between isothermal and thermal vapor fluxes. Especially in arid regions, where high temperature gradients might exist in the soil and soil water contents are mostly very low, vapor fluxes can highly exceed liquid water fluxes, playing a significant role in total flux calculations (Parlange et al., 1998). Vapor flow is induced by differences in vapor density resulting from temperature (thermal) and pressure (isothermal) gradients. Isothermal vapor fluxes can often be neglected whereas the importance to consider thermal vapor fluxes increases with increasing temperature gradients and dryness (Walvoord et al., 2002).

As vapor density decreases with increasing temperatures, vapor flows from colder to warmer temperatures. Some studies reported on vapor diffusion under temperature gradients, which exceed expected diffusion values (Lu et al., 2011; Walvoord et al., 2002; Zeng et al., 2011). This phenomenon can be described by a fixed enhancement factor, whereas mechanisms driving this enhanced vapor diffusion are not fully understood. One explanation, already stated by Philip and de Vries (1957) is the diffusion through liquid islands, where vapor condenses at one end of trapped liquid islands and evaporates at the other end. Nevertheless, this theory could not be underpinned by recent studies (Lu et al., 2011).

2.3. Time Domain Reflectometry

One main analytical aspect of the soil column experiments was the water content measurement by Time Domain Reflectometry (TDR). TDR is a common method to indirectly determine the water content by measuring dielectric properties of material surrounding a sensor. Generally, an electromagnetic pulse is generated and propagates through a system, consisting of a sensor and a coaxial cable, connecting the sensor and the pulse generator. The short rise time electromagnetic pulse is partly reflected at the coaxial cable and totally reflected at the end of the sensor (Huebner and Kupfer, 2007). The reflections can be viewed by an oscilloscope, whereas nowadays, the pulse generator and the oscilloscope are installed within one reflectometer.

2.3.1. Theory

Time Domain Reflectometry indirectly measures the water content by measuring the travel time of an electromagnetic pulse propagating from a TDR device along a transmission line of known length and back. From the pulse travelling time, or the pulse reflection length, the relative dielectric permittivity of the material surrounding the sensor can be calculated according to equation 11 (Noborio, 2001).

$$K_a = \left(\frac{L_a}{L}\right)^2$$

Eq. 11 – Relation of relative dielectric permittivity to the reflection length of a reflected electromagnetic pulse along a TDR sensor

where K_a is the relative dielectric permittivity (-), L_a is the pulse reflection length along the TDR sensor, also called apparent sensor length (m), and L as the pulse reflection length measured in air, resembling the real length of the sensor (m).

In unsaturated soil, dielectric constants of the single phases are known as 1 for the air phase, 4-10 for the solid matrix, depending on its mineral composition, and around 80 for the liquid water phase. Thus, changes in water content strongly influence the total permittivity measured (Robinson et al., 2003).

Several equations for the relationship of the measured dielectric permittivity to the volumetric water content of a medium are available. The most common equation for converting dielectric permittivity to volumetric water content was developed by Topp et al. (1980) (Eq. 12).

$$\theta = -5.3 * 10^{-2} + 2.92 * 10^{-2}K_a - 5.5 * 10^{-4}K_a^2 + 4.3 * 10^{-6}K_a^3$$

Eq. 12 – Topp equation for converting dielectric permittivity to water content in variably saturated soils

The reliability of the Topp equation depends on the soil texture, the water content range, and the sensor design. It is mostly applicable for coarse textured soils and uncoated rod sensors.

2.3.2. Sensor design

Most TDR sensors are designed to measure the average water content along the sensor line. Common waveguides for these measurements are unshielded metallic 2- or 3-rod sensors with length between 5 cm and 100 cm (Worsching et al., 2006). The shorter the sensors the easier is the installation, whereas measurement accuracy decreases with decreasing sensor length, especially for low water range measurements.

Within the last years, TDR sensor development intensified for the measurement of water contents along deep soil profiles. Sensor designs include flexible probes that are attached to flexible sleeves for single measurements along the sleeve (Dahan et al., 2003), and variable constructions of enlarged three rod probes (Stacheder et al., 2009). To prevent signal losses along long transmission lines, enlarged probes are isolated and sensors are designed as cables

or tubes. One of these cables, the so-called “Taupe” cable, was developed and patented at the Soil Moisture Group (now IFG at KIT) (Brandelik et al., 1998; Huebner et al., 2005; Koeniger et al., 2005; Stacheder et al., 2009). The name “Taupe” is given by the French word for “mole”, indicating that the sensor can be buried into the soil. The “Taupe” cable can measure changes in water content along the whole sensor transmission line by analyzing changes in the course of the reflected electromagnetic signal. The analysis of the TDR cable signals is still under development, as especially under field conditions, changing environmental factors including temperature, soil heterogeneities and conductivities can influence the signal. Within the last 5 years, algorithms were developed to inversely calculate the water content from TDR signal output reflection coefficient analysis by developing models of the electrical properties of the sensors (Schlaeger, 2005; Todoroff and Luk, 2001). These approaches are still under development and very laborious, especially when working in changing environmental conditions.

2.3.3. Effects of Electrical Conductivity, Temperature, Bulk Density and Water Content

TDR measurements can be influenced by changing environmental conditions, like electrical conductivity, temperature and bulk density of the surrounding medium. Increased electrical conductivity causes energy losses of the electromagnetic signal, which can be seen in a flattening of the reflected signal with increasing conductivity and increasing depth (Robinson et al., 2003). Temperature effects on TDR measurements occur due to changes of the dielectrical properties of water with changing temperature. For example, the dielectric constant of water at 45 °C is 60, water of 20 °C has a dielectric constant of 80 (Or and Wraith, 1999). Thus, temperature effects on TDR measurements are mainly detectable for high water contents. Changes in the soil bulk density results in changes of the volume ratio of the solid particles to the pores. Thus, if density changes, the ratio of the solid part of the measured total dielectric permittivity changes accordingly and same volumetric water contents can result in different total dielectric permittivities (Gong et al., 2003). The reliable measurement of low water contents also can pose errors due to the different dielectric constant values for free (78-86), capillary (78-86) and bound water (35) (Scheuermann et al., 2002). Thus, measurement in low water content ranges might not appropriately account for bound water when converting the measured dielectric permittivity to volumetric water content. All these possible effects challenge the correct determination of water content by time domain reflectometry under transient and non-controllable environmental conditions.

3. Materials and Methods

Prior to the main study focus, physical properties of the soils that were used in the experiments and for the modeling, were determined (chapter 3.1.) and the TDR sensors were calibrated (chapter 3.2.). The core study included the soil column experiments with different settings (chapter 3.3.) and the inverse and predictive modeling (chapter 3.4.).

3.1. Soil Properties

The experiments were performed with two different homogenized sands,

- a middle to coarse grained pre-washed and dried well sorted silica sand (Dorsilit® 0.4 – 0.8 mm), and
- a fine grained red dune sand.

The dune sand was sampled in Saudi Arabia, close to the Wasia Wellfield, which is located northwest of Riyadh with the geographic coordinates 25°13'N and 47°61'E. The sampling location was chosen close to groundwater recharge field studies, conducted under the IWAS framework. Nevertheless, within this study, the dune sands did not represent site-specific recharge studies but were chosen to represent arid region dunes sands as such for comparison to pure and coarser grained silica sand.

Physical soil properties of both sands were determined prior to the column experiments. Grain-size distribution was obtained by sieve analysis. Saturated hydraulic conductivity was measured with a constant head permeability test (Wietsma et al., 2009). As the determination of field capacity is not standardized, it was defined as the amount of remaining water of a pre-saturated soil volume after three days of free drainage, and determined in a separate single drainage experiment within the experimental column. Nevertheless, this drainage approach could only give a rough estimate (Hillel, 2004). Water repellency of the soils was determined by the “Water Drop Penetration Time” test, measuring the penetration time of a water drop placed on top of the soil (Letey et al., 2000).

Water retention of the silica sand was measured with a Tempe-cell-like pressure cell as described in Engelhardt et al. (2003). The 80 ml measurement cell was filled with saturated sand lying above a water-permeable membrane with a bubbling point of 1 bar. The sand was filled with a dry density of 1.65 g/cm³, corresponding to experimental conditions (chapter 3.4.1.). By inducing air pressure, a water pressure adjusted below the membrane. Capillary pressure inside the soil resulted from subtracting the outflowing water pressure from the induced air pressure, describing the remaining water pressure inside the measurement cell. By also measuring the amount of outflowing water, the established water saturation was determined. Retention was measured within 15 steps between 0 and 200 mbar. Water retention of the dune sand was measured by a hanging column apparatus at the Environmental Molecular Sciences Laboratory EMSL (Richland, USA). A saturated soil sample with a volume of 100 ml was risen up to 2 m within 15 levels and the bottom outflow to a reservoir, installed at 0 cm height, corresponding to the sample rise level was measured. The water retention measurements were fitted to the soil hydraulic models of van Genuchten (1980) (Eq. 3), Brooks and Corey (1964) (Eq. 4) and Durner (1994) (Eq. 5) with the open

source program SWRC Fit (Seki, 2007), version 1.2. SWRC Fit includes the option of setting residual water content to zero, which can significantly change the obtained hydraulic parameter values. As under the partially dry conditions and high surface temperatures of the experiments residual water contents close to zero can be expected, one separate calculation was performed with this option. Additionally, retention data from the pedotransfer functions program ROSETTA (Schaap et al., 2001) was obtained for 100 % pure sand.

Thermal conductivity for the dune sand was measured by a transient line heat source method with a KD2 thermal analyzer (Decagon Devices, Pullman, WA), also at the EMSL (Richland, USA). Measurements were made for increasing saturations from dry to fully saturated within 5 steps. Measurements were fitted to the thermal conductivity model equation of Chung and Horton (1987) (Eq. 10). For the silica sand, values for pure silica sand were derived from measurements made by Chung and Horton (1987).

3.2. TDR Cable Sensor

To track water content changes along the soil profile, a TDR “Taupe” cable sensor was installed in the experimental column. The cable was produced by Promet^h in Frankfurt (Germany) with a length of 100 cm, a RG58 coaxial cable length of 5 m and a BNC adapter for connection to the TDR reflectometer. The sensor itself consisted of three copper wires acting as electromagnetic transmission lines. The copper wires were soldered to the coaxial cable which transmitted the electromagnetic signal from the generator to the sensor cable. The junction of the coaxial cable to the sensor transmission lines and the sensor end were sealed with two-part resin (Fig. 2). To prevent transmission losses along the sensor lines, the wires were coated with polyethylene, resulting in a flat-ribbon cable. The sensor was 6 cm wide and had a sensitive area of 3 to 5 cm around the wires, depending on the permittivity of the surrounding material (Schlaeger et al., 2006). The sensor length was adjusted to the soil column length by cutting and resealing the end. Figure 2 shows the TDR cable at the transition from the signal input line (RG58 coaxial cable) to the sensor cable.

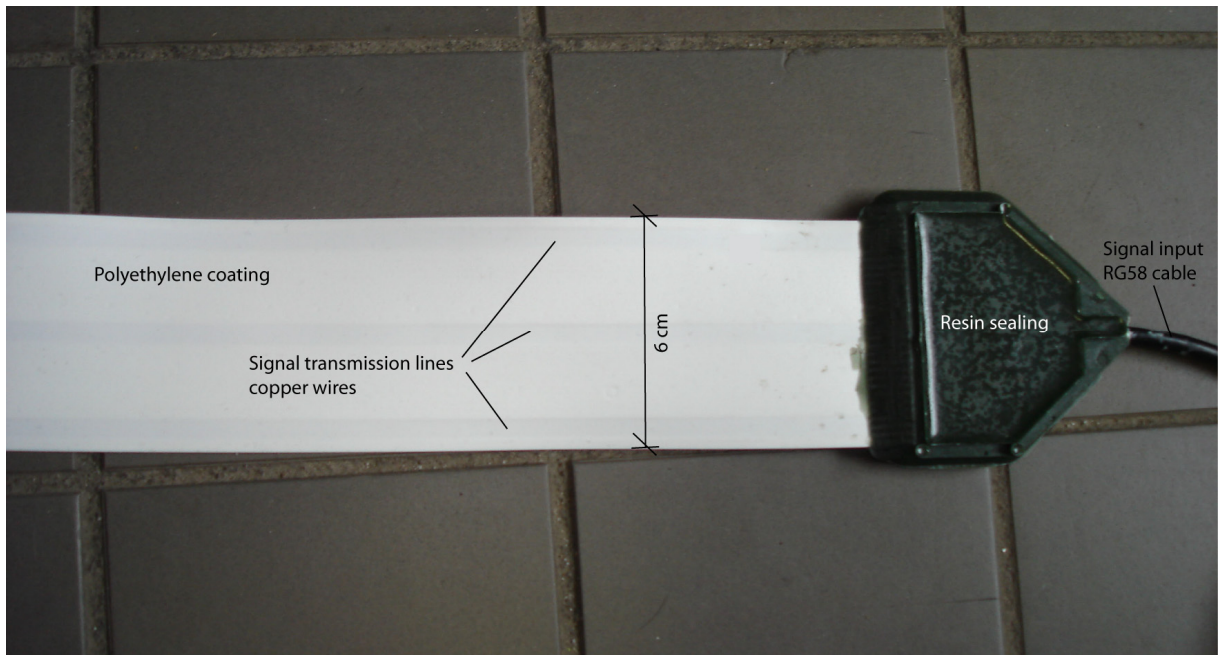


Fig. 2 - TDR "Taupe" cable design as it was used within the soil column experiments

The TDR "Taupe" cable sensor is capable of resolving local changes in water content by analyzing the amplitude of the reflected input signal, which is the reflection coefficient. The reflection coefficient can be directly correlated to volumetric water content. For this correlation, calibration measurements were done with point measurements of water content from commercial TDR rod sensors (Campbell Scientific CS640). The cable sensor was installed into a soil column with changing water content. Rod sensors were installed at different depths of the column. By taking the volumetric water contents of the point measurements and relating them to the reflection coefficient of the cable in the same depth, a calibration curve and a linear calibration function was determined for both sands used for the experiments.

As increased water contents enlarge the reflected signal length ("apparent sensor length" or L_a), the recorded signal length had to be recalculated to an identical total length for the correct spatial location of reflection amplitudes. This was done by referring the signal length of sections with different moisture content linearly to the physical length of the sensor. Parts of higher water content in a curve had to be shortened while sections with no change kept the same physical length. A signal measured in a material with an initial homogenous moisture distribution acted as a reference for the total length (Fig. 3). All subsequent measurements were related to the length of the reference signal, which could be transferred to the real sensor length. When transferring reflection coefficient values to water contents, restrictions were given for the beginning of the sensor line. As the virtual transition from the coaxial cable, which connected the pulse generator and the sensor, to the sensor line was part of the reflected signal, the real start of the measurements along the sensor line could not be clearly defined (Fig. 3). Thus, the reflection coefficients at the beginning of the analyzed signal might not have accounted for the real sensor head. This was more pronounced during drying since changes in reflection coefficient were less abrupt than during infiltration.

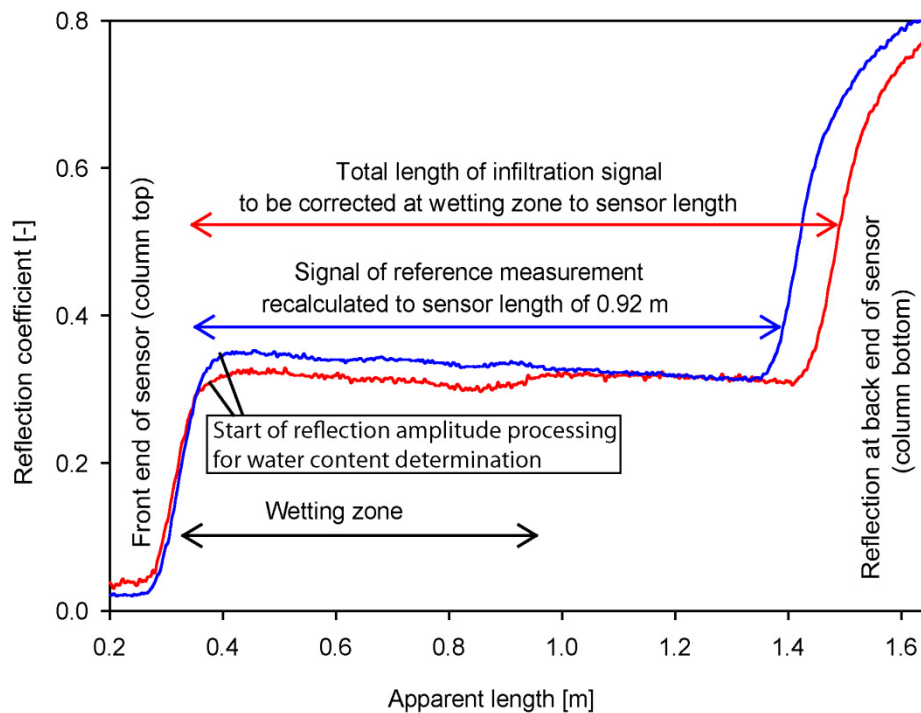


Fig. 3 - TDR cable reflection curves for soil profile water content determination. Signals show reflection transition from pulse input line (coaxial cable) to sensor top, signal reflection along the sensor which is to be analyzed and transition from analyzed first reflection signal to scattered multiple reflections. The analyzed signals are adapted in length from apparent signal length to real sensor length.

Algorithms for the inverse calibration of water content from reflection coefficient were not applied within this study. The focus of analysis was set on the correlation of the reflection signals according to known changes in initial and boundary conditions. By using the cable within controlled experimental conditions, the signal analysis could be simplified and its usage be tested for measurement accuracies and its usability in the field.

To test the influence of the applied experimental temperature boundaries within the experiments on the TDR measurements, prior to the experiments, measurements with the TDR cable and rod probes were made in the column with saturations ranging from 0.05 – 0.25 cm³/cm³ for a stepwise increasing temperature from 20 °C to 50 °C.

3.3. Experimental Setup

The experimental setup covered the column itself, the attached measurement and control units and the data acquisition system (Fig. 4). The acrylic column had a height of 100 cm and an inner diameter of 19 cm. The dimensions were chosen for the ability to analyze water redistribution depths beyond expected infiltration and drying fronts and to minimize column wall effects. Inside the column, the soil could be packed up to a height of 92 cm, with an air layer above the soil packing of 5 cm. The remaining 3 cm contributed to the bottom and top assembly. The whole column was insulated with a flexible 10 mm thick mat of expanded polyethylene.

A temperature gradient over the lengths of the soil column was maintained by circulating water with different temperatures through stainless steel capillary tubes at the top and the bottom of the column packing. Water was heated between 25 °C and 100 °C in a laboratory water bath and pumped through the capillary tubes with a 12 V immersion pump. To account for imprecision of the water bath temperature regulation of 1 – 5 °C, temperature was monitored inside the column. Increased water evaporation in the heated water bath was prevented by a cover of floating spheres made of polypropylene. For water cooling between 5 °C and 25 °C a Van der Heijden Cool-Care® was installed. The circulating cooler worked with a regulation precision of +/- 1°C.

The temperature in the column was measured by 7 platinum resistance sensors (PT-100 FS International) at depths of 4, 14, 24, 34, 44, 70 and 84 cm. One additional sensor measured the air temperature above the column packing. The cable probes with a measurement range of -100 °C to +250 °C were adapted to the column wall with Swagelok nylon tube fittings. Temperature data was logged with an 8-channel OctRTD MadgeTech datalogger with a temperature resolution of 0.01 °C and a calibrated accuracy of +/- 0.1 °C.

Rainfall was simulated with an Ismatec MCP Process peristaltic pump and two mounted MS/CA 8-channel pumping heads. Tygon tubing was used for the water pumping through the 16 pumping channels. The tubes were mounted to stainless steel capillaries with an inner diameter of 1 mm, distributed uniformly over the top cover of the column (Fig. 5).

Air flow into the column was controlled by a Bronkhorst El-Flow gas mass flow controller with a flow range of 0.5 to 5 l/min. To adjust relative humidity, the air was passed over a saturated magnesium chloride solution which defined the ambient water vapor pressure before entering the column resulting in a relative humidity between 25 % and 35 %, depending on the temperature (Wernecke, 2005). Relative humidity of the in- and effluent air was measured using Vernier RH-BTA sensors. Sensor measurement stability was tested with mean measurement deviations of 0.7 % and maximum deviations of 1.3 %. The temperature of the inflowing air was measured with a Vernier surface temperature sensor STA with a resolution of 0.03 °C and maximum measurement deviations of +/- 0.5 °C. All Vernier sensors were connected to a Vernier LabQuest datalogger for continuous data monitoring. Absolute humidity was calculated with the measured air temperatures and relative humidity according to (BSL, 2009):

$$AH = (0.000002T^4 + 0.0002T^3 + 0.0095T^2 + 0.337T + 4.9034) * RH$$

Eq. 13 – Calculation of absolute humidity from temperature and relative humidity measurements

where AH is the absolute humidity (g/cm^3), RH (%) is the measured relative humidity, and T is the measured temperature ($^{\circ}\text{C}$). The difference between inflowing- and outflowing air absolute humidity accounted for soil water uptake and, accordingly, evaporation.

At the column bottom, a water saturated porous ceramic plate (Soilmoisture Equipment Corporation) was installed and connected to a Vacuubrand MD 4C Vario vacuum-pump to obtain constant suction. The ceramic plate with a thickness of 1 cm was manufactured for a bubbling pressure of 500 mbar and the applied suctions ranged between 60 and 100 mbar. Water outflow was recorded using an Ohaus Scout-Pro balance with a measurement precision of 0.01 g.

The volumetric water content in the sand was measured with two different TDR sensor systems (Fig. 6).

(1) Three rod sensors (Campbell Scientific 640) with sensor lengths of 7.5 cm each, and a resolution of $0.01 \text{ cm}^3/\text{cm}^3$ volumetric water content, were mounted in the column at depths of 4 cm, 44 cm and 84 cm for local point measurements, and

(2) a TDR Taupe cable was mounted in the center of the column to measure the water content continuously over the whole column length. To avoid cable measurements in the air, the length of the cable was adapted to the soil profile depth. The sensor offset was buried in the top 2 cm of the sand.

Both sensor systems were connected to a Campbell Scientific TDR reflectometer (TDR100) with a multiplexer for up to eight sensors (SDMX50) and a datalogger (CR800). To keep the dielectric loss for the laboratory measurements constant and as low as possible, de-ionized water was used for the pre-saturation of the sand, the irrigation water and the incoming relative humidity.

Data of all parameters were collected automatically in specified time intervals, ranging from 1 minute during overhead irrigation to 30 minutes during soil moisture redistribution.

Homogenous initial soil water distribution, as well as homogenous material density within the column was assured by stepwise packing. For each 3 cm of column height, a defined amount of sand and water was weighted, mixed, filled into the column, and compressed. For a smooth transition, the top of each packing step was loosened with a fork before filling in the next layer. The TDR-cable was installed by fixing it to the bottom heat spiral and holding it vertically tight and straight during sand filling. All other sensors were installed during filling (Fig. 6).

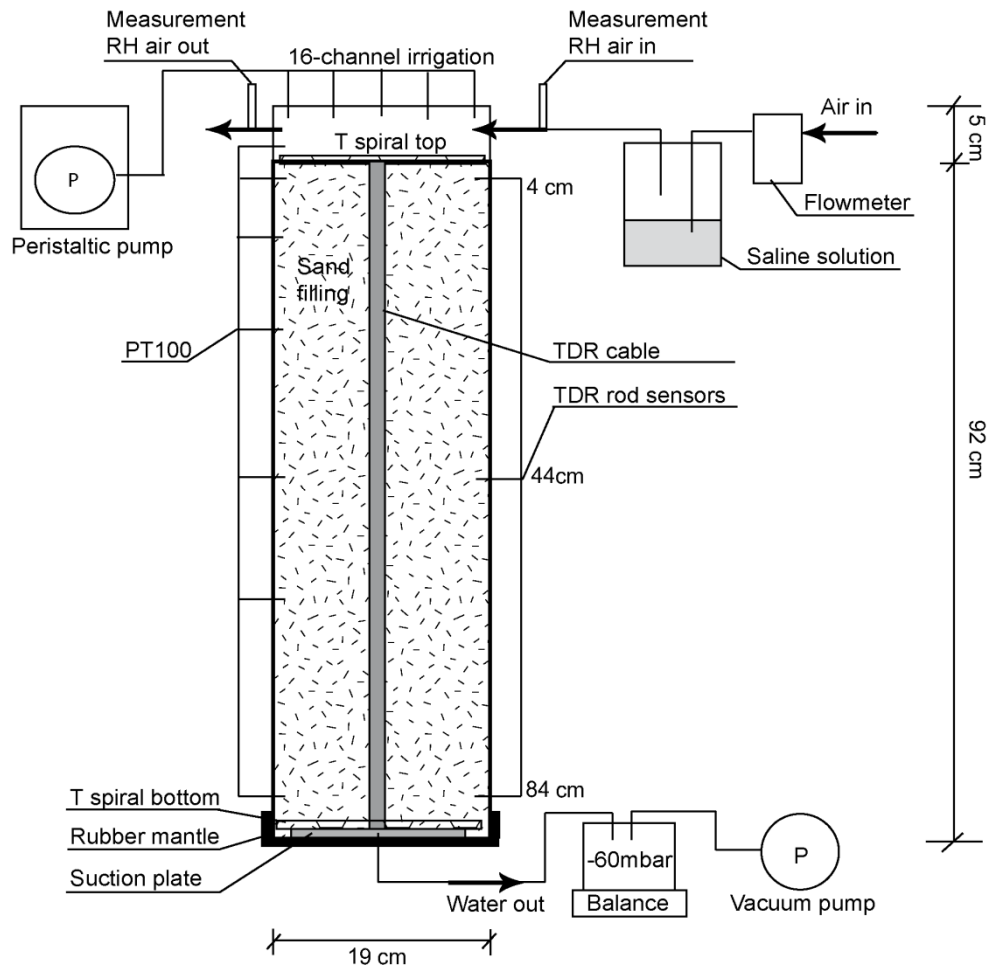


Fig. 4 - Schematic drawing of the column experiment with controlled and measured parameters

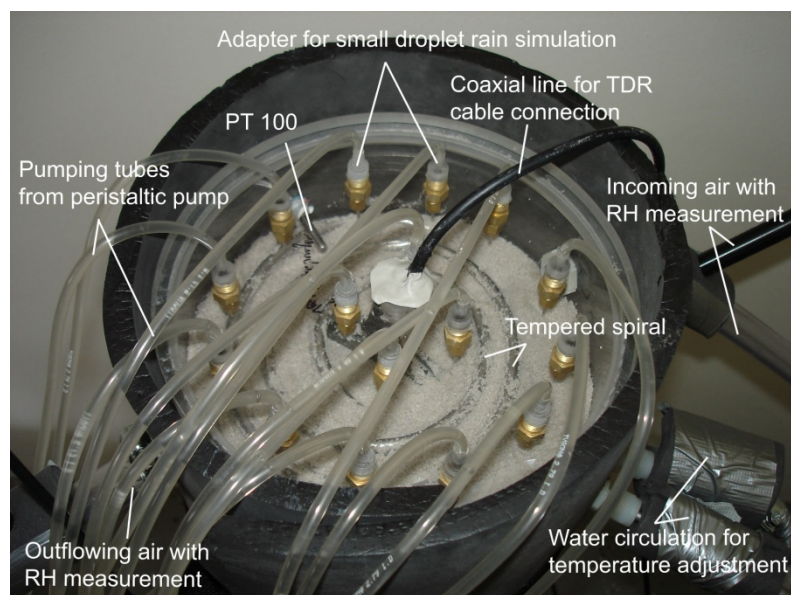


Fig. 5 - Detail photograph of the top assembly of the experiments during operation

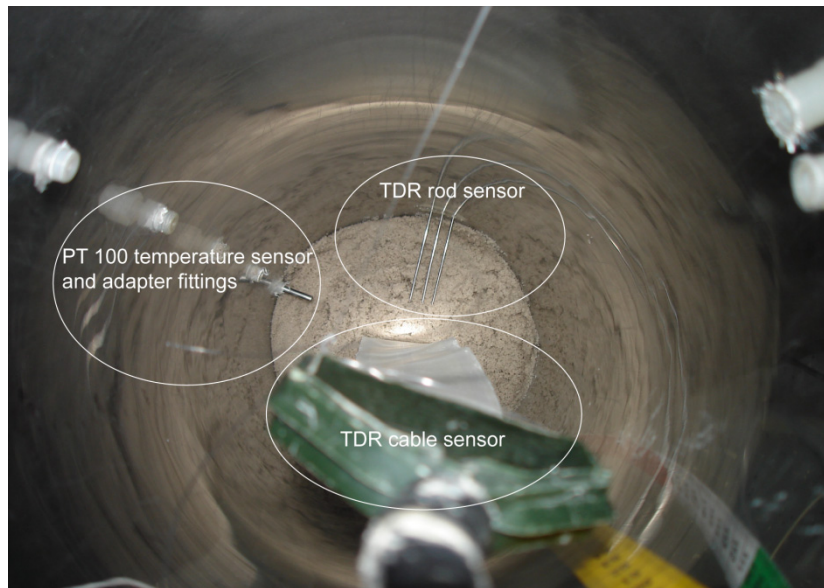


Fig. 6 - Assembly of TDR and temperature measurement sensors in the experimental column during packing

3.4. Experimental Conditions

Experiments were performed with three different sand fillings. For a first set of experiments, aiming at evaluating the experimental performance, the column was filled homogeneously with the silica sand. The second set of experiments was performed with homogeneous dune sand filling and time-varying boundary conditions were applied to simulate changing soil moisture states as they can be expected under arid conditions. The third setting was packed with alternating layers of the silica and the red dune sand, to specifically investigate wetting fronts in soil profiles of different hydraulic characteristics and their behavior for different irrigation patterns.

3.4.1. Silica Sand Filling

The setup with the TDR sensor systems was tested in a steady-state experiment. The column was filled with the silica sand with a density of 1.65 g/cm^3 , having a volumetric water content of $0.07 \text{ cm}^3/\text{cm}^3$. The temperature was fixed with $50 \text{ }^\circ\text{C}$ at the column top and $15 \text{ }^\circ\text{C}$ at the column bottom. The inflowing air stream was applied with a constant flow of 5 l/min and a relative humidity between 25% and 35% . The suction at the bottom was held constant at 60 mbar . First, a uniform overhead irrigation of 0.55 mm/min was applied until steady-state conditions were reached for column water content, temperature distribution, water outflow and evaporation. After stopping overhead irrigation, measurements continued until again steady-state was reached for the aforementioned parameters.

Within the next experimental runs, the effects of irrigation amount, irrigation intensity and sequenced low amount irrigations on infiltration, redistribution and evaporation were evaluated. Temperature boundary conditions were fixed with $40 \text{ }^\circ\text{C}$ at the top and $15 \text{ }^\circ\text{C}$ at the bottom. Air flow and air relative humidity were adjusted to 5 l/min and 25% and 35% ,

respectively. Experiments started with an initial water content of $0.07 \text{ cm}^3/\text{cm}^3$. To evaluate the effect of irrigation amounts, single irrigation events with the same intensity of 6.25 mm/h (0.104 mm/min) but with different total irrigation amounts of 50 mm , 25 mm , and 12.5 mm were applied. To evaluate irrigation intensities, overhead irrigation intensity was varied for single 12.5 mm events from 0.052 mm/min (240 min) to 0.625 mm/min (20 min) and 6.25 mm/min (2 min). To evaluate the influence of sequenced low amount irrigations on water flow in the column, two 12.5 mm irrigations were applied with an intensity of 6.25 mm/min each. Between these two irrigations, 72 hours were allowed for water redistribution.

3.4.2. Dune Sand Filling

The dune sand was packed with a density of 1.7 g/cm^3 , and an initial water content of $0.07 \text{ cm}^3/\text{cm}^3$. First, a two-stage irrigation experiment was performed. The temperature was fixed with $50 \text{ }^\circ\text{C}$ at the top and $15 \text{ }^\circ\text{C}$ at the bottom. The inflowing air stream was applied with a constant flow of 5 l/min and a relative humidity between 25% and 35% . The suction at the bottom was held constant at 60 mbar . A first irrigation was applied with 0.55 mm/min until bottom drainage breakthrough was reached. After 120 h of drying, a second irrigation with 0.2 mm/min was applied for 2 hours . Measurements continued for altogether 270 h .

Within the following experimental run, water flux and temperature boundary conditions were changed time-dependant according to table 2. Bottom temperature was held constant at $18 \text{ }^\circ\text{C}$. The inflowing air stream was held constant at 5 l/min , with a relative humidity between 25 and 35% . The suction at the bottom was also held constant at 60 mbar . Initial soil water content corresponded to the water content distribution after the previous two-stage irrigation.

Tab. 2 - Time-variable column top boundary conditions (irrigation and temperature) as applied to the experiments with dune sand filling

Time (d)	Description	Irrigation amount (intensity)	Temperature
1	Irrigation cycle # 1	5 mm (1mm/min)	40 °C
2		5 mm (1mm/min)	40 °C
3		5 mm (1mm/min)	40 °C
4		5 mm (1mm/min)	40 °C
5		5 mm (1mm/min)	40 °C
6 - 30	Redistribution	-	Gradually decreasing
31	Irrigation cycle # 2	5 mm (1mm/min)	26 °C
32		5 mm (1mm/min)	26 °C
33-34	Redistribution	-	26 °C
36	Irrigation cycle # 3	10 mm (1mm/min)	26 °C
37		10 mm (1mm/min)	26 °C
38 - 70	Redistribution	-	Gradually decreasing
71	Irrigation cycle # 4	25 mm (1.25mm/min)	20 °C
75		25 mm (1.25mm/min)	20 °C
76 - 95	Redistribution	-	Gradually increasing
96 - 100	Redistribution	-	50 °C

3.4.3. Layered Column Filling

The layering consisted of a 10 cm silica sand layer at the bottom, a 30 cm dune sand layer, a 30 cm silica layer, a 15 cm dune sand layer and a 7 cm silica sand layer at the top. Initial water content was 0.04 cm³/cm³ for each layer. The temperature was fixed with 25 °C at the top and 15 °C at the bottom. The inflowing air stream was applied with a constant flow of 5 l/min and a relative humidity between 25 % and 35 %. The suction at the bottom was held constant at 60 mbar. Single irrigations were applied according to table 3.

Tab. 3 - Time-variable single irrigations (amount and intensity) as applied to the experiments with layered sand filling

Time (d)	Irrigation amount (intensity)
1	25 mm (0.835 mm/min)
8	12.5 mm (0.835 mm/min)
22	12.5 mm (0.835 mm/min)
27	25 mm (1.67 mm/min)
84	50 mm (1.67 mm/min)

3.5. Numerical Modeling

For the numerical simulation of water and heat fluxes in variably saturated porous media, several modeling tools are readily available, as for example compared in Scanlon et al., 2002b. Most of the models are using an approach according to the Richards equation (Eq. 2) for calculating water fluxes (Richards 1931). One common model for simulating water, vapor and heat fluxes under different saturations is Hydrus which is available as 1D, 2D and 3D. Hydrus was, amongst others, tested for applicability under semi-arid (Scanlon et al., 2003) and arid field conditions (e.g. Twarakavi et al., 2008; Zeng et al., 2009).

3.5.1. Hydrus-1D

The numerical modeling was performed using the Hydrus-1D software Version 4.14. Hydrus-1D simulates the one-dimensional coupled movement of water, vapor and heat, as well as solute transport in variably saturated porous media (Šimůnek et al., 2009). It numerically solves a modified Richards equation for unsaturated water and vapor flow by employing a finite element method (Eq. 14) (Benson, 2007; Saito et al., 2006). The equation includes the gravitational liquid flow, isothermal liquid flow, isothermal vapor flow, thermal liquid flow and thermal vapor flow. Heat transport is calculated by Fickian-based advection-dispersion equations (Eq. 18). The coupling of the water and heat transport is ensured by the simultaneous solving of the corresponding equations (Šimůnek et al., 2009).

$$\frac{\partial \theta(h)}{\partial t} = \frac{\partial}{\partial x} \left[(K + K_{vh}) \left(\frac{\partial h}{\partial x} \right) + (K_{LT} + K_{vT}) \frac{\partial T}{\partial x} \right]$$

Eq. 14 - Modified Richards equation for nonisothermal water and vapor flux as implemented in Hydrus-1D

The unsaturated hydraulic conductivity K is calculated according to the specified hydraulic conductivity function (e.g. Eq. 7 or Eq. 8).

The thermal liquid conductivity function K_{LT} includes a gain factor G_{wT} , quantifying the temperature dependence of the soil water retention curve (Nimmo and Miller, 1986; Šimůnek et al., 2009) and is calculated by:

$$K_{LT}(T) = K_{Lh}(h) \left(h G_{wT} \frac{1}{\gamma_0} \frac{\partial \gamma}{\partial T} \right)$$

Eq. 15 - Thermal hydraulic conductivity function as implemented in Hydrus-1D

where γ is the surface tension of the soil water (J/cm²) and γ_0 is the surface tension of the soil water at 25 °C (J/cm²).

The isothermal vapor hydraulic conductivity K_{vh} (Eq. 16) and the thermal vapor hydraulic conductivity K_{vT} (Eq. 17) are calculated according to (Nassar and Horton, 1989; Šimůnek et al., 2009):

$$K_{vh} = \frac{D_v}{\rho_w} \rho_{vs} \frac{Mg}{R_u T} RH$$

Eq. 16 - Isothermal vapor conductivity function as implemented in Hydrus-1D

$$K_{vT} = \frac{D_v}{\rho_w} \eta_e H_f \frac{\partial \rho_{vs}}{\partial T}$$

Eq. 17 - Thermal vapor conductivity function as implemented in Hydrus-1D

where D_v is vapor diffusivity (cm²/min), ρ_{vs} is saturated vapor density (g/cm³), M is the molecular weight of water (0.018015 kg/mol), g is the gravitational acceleration (9.81 m/s²), R_u is the universal gas constant (8.314 J/molK), and η_e is an enhancement factor for enhanced vapor movement (-) (Cass et al., 1984; Šimůnek et al., 2009).

$$C_{vp}(\theta) \frac{\partial T}{\partial t} + L \frac{\partial \theta_v}{\partial t} = \frac{\partial}{\partial x} \left(\lambda(\theta) \frac{\partial T}{\partial x} \right) - C_{vw} q \frac{\partial T}{\partial x} - C_{vv} \frac{\partial q_v T}{\partial x} - L \frac{\partial q_v}{\partial x}$$

Eq. 18 - One-dimensional heat transport with vapor transport as implemented in Hydrus-1D

where L is the latent heat of vaporization of liquid water (J/m³) and q_v is the vapor flux density (cm/s) (Šimůnek et al., 2009).

The 1-dimensional flow direction in Hydrus-1D is read with negative values for downward and positive values for upward flow. Units for fluxes and water contents are generally given 1-dimensional, according to the chosen time and space units of the model set-up.

3.5.2. Inverse Modeling

Inverse modeling is the process of estimating model parameters by fitting numerical model calculation results to measured experimental or field data (Finsterle, 2004). In this study, inverse modeling was performed on the two-stage irrigation experiment for the dune sand and a comparable two-stage experiment for the silica sand to calibrate hydraulic and thermal model parameters. The two-stage experiments were chosen to include wetting and drying cycles into the calibration.

3.5.2.1 PEST

The “Model-Independent Parameter Estimation” program PEST (Doherty, 2010) can adjust pre-defined parameters of a model by matching model results with measurement data. In vadose zone modeling, the adjustable parameters are commonly hydraulic and thermal properties of the soil material. PEST uses a weighted least squares Marquardt-Levenberg type optimization method (Marquardt, 1963). Calibration is performed along the optimization of an “objective function” which is defined as the sum of the squared deviations between given observations (measured data) and model outputs, weighted according to user-defined weights. PEST reduces the objective function until the best available fit is obtained.

The goodness of the overall model fit is provided by the correlation coefficient R which is calculated as (Doherty, 2010):

$$R = \frac{\sum(w_i c_i - m)(w_i c_{oi} - m_o)}{[\sum(w_i c_i - m)(w_i c_i - m) \sum(w_i c_{oi} - m_o)(w_i c_{oi} - m_o)]^{1/2}}$$

Eq. 19 - Correlation coefficient R for measuring the goodness of the model fit

where c_i is the i ’th observation value, c_{oi} is the model-generated counterpart to the i ’th observation value, m is the mean value of weighted observations, m_o is the mean of weights model-generated counterparts to the observations and w_i is the weight associated with the i ’th observation. For a good fit, R should be above 0.9 (Doherty, 2010; Hill, 1998).

PEST was coupled to Hydrus-1D. By user-defined input files, it automatically varied model parameters, ran the model, and evaluated the model output. Three types of input files had to be prepared to properly run PEST (Doherty and Hunt, 2010):

- template files to insert PEST-estimated parameter values into the corresponding model input files,
- instruction files to give the demand on where simulated equivalents of the observations are found in the model output files, and
- a control file to provide parameter optimization, regularization, and algorithm operation constraints, as well as values and weights for observation data.

Parameter optimization was performed on hydraulic and thermal model parameters. After the first optimization run, parameters of low sensitivity were identified from internal sensitivity calculations (see chapter 3.5.2.6). As low sensitivity parameters slow down the optimization

process, they were excluded from the following optimization runs. Additionally, highly correlated parameters were identified from the parameter correlation matrix. For the following optimization runs, one of the correlated parameters had to be excluded. The simultaneous optimization of two correlated parameters enhances the possibility of a non-unique solution as in PEST the parameters are adjusted independently, but in reality the parameters are highly connected to each other. If required, multiple optimizations were started with decreasing the parameter optimization ranges for obtaining a final good fit of the results.

3.5.2.2 Model Setup

The model was set up according to the experiments (Fig. 7).

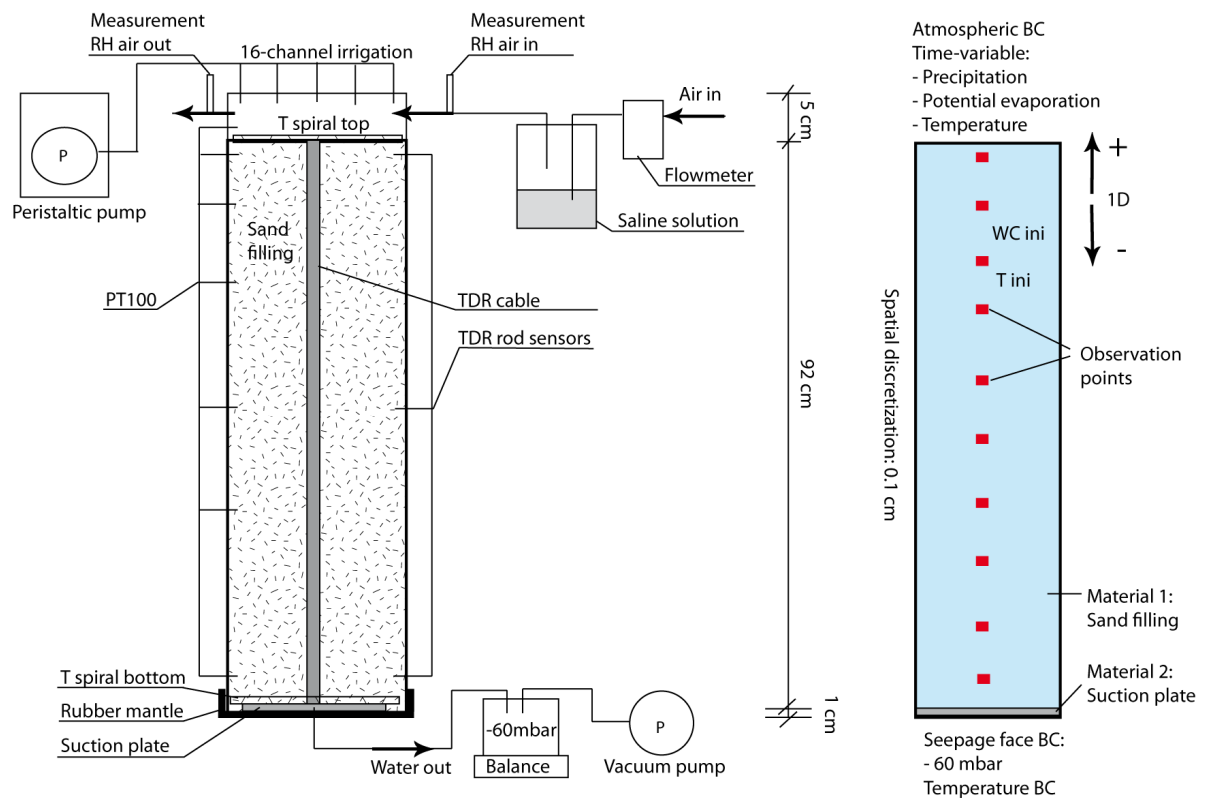


Fig. 7 - Conceptual model for the inverse parameter calibration in Hydrus-1D according to the soil column experiments

The model length of 93 cm was divided into two materials with 92 cm of material one, resembling the soil filling, and 1 cm at the bottom of material two, resembling the suction plate. The soil profile was discretized with 931 nodes, equally spaced with 0.1 cm. Observation points, where data for water content, pressure head and temperature were extracted separately for each time step, were inserted at depths 4, 14, 24, 34, 44, 60, 70, and 84 cm. The observation points were chosen to correspond to the measurement depths of temperature and the TDR rod sensors in the experiments. Additional observation points were

inserted for the retrieval of water content measurements from the TDR cable sensor. For the inverse calibration, a uniform time discretization of 0.001 h was applied to ensure consistent model output files for the inverse model automatization.

3.5.2.3 Initial and Boundary Conditions

Initial conditions for the calibrations were set according to the initial conditions of the corresponding two-stage irrigation experiments, which were a homogenous volumetric water content of $0.07 \text{ cm}^3/\text{cm}^3$ for the soil material and a homogenous temperature distribution of $20 \text{ }^\circ\text{C}$. The water content of the suction plate was set to $0.5 \text{ cm}^3/\text{cm}^3$, according to the saturated installation.

Top boundary conditions were implemented with an atmospheric layer for water flow and defined time-variable temperature for heat transport. The atmospheric boundary condition implied time-variable changes in precipitation and potential evaporation at the soil air interface. Precipitation and temperatures were set according to the experiments (Tab. 4 and 5). Potential evaporation was calculated as the maximum intake capacity of the streaming air according to the experimental measurements of the relative humidity and air temperature of the air flowing into the column. Generally, the atmospheric boundary condition is system-dependant. As such, the potential fluid flux is only controlled by external conditions, whereas the actual fluid flux also depends on the soil moisture conditions near the soil surface. The system switches between a flux and a head condition, constrained by the maximum head at the soil top, until which potential evaporation equals actual evaporation. As soon as this maximum head is exceeded, the actual evaporation rate is decreased and constrained by the availability of water in the soil profile. The value of the maximum soil surface head for potential evaporation rates was set to 200 cm, according to recommendations for sandy materials (Šimůnek et al., 2009).

Bottom boundary conditions were implemented with a fixed seepage face of -60 mbar for water flow, according to the applied bottom pressure of the experiments, and the applied temperature for heat transport. The seepage face boundary implies that a zero-flux boundary condition applies as long as the local pressure head at the bottom of the profile is below the fixed seepage face pressure value. A pressure head boundary condition applies as soon as the local pressure head at the bottom of the profile reaches the fixed seepage face pressure head value.

Tab. 4 - Time-variable boundary conditions for the inverse model calibration of the silica sand experiments

Time (h)	Irrigation (cm/h)	Evaporation (cm/h)	Temperature top ($^\circ\text{C}$)	Temperature bottom ($^\circ\text{C}$)
0 - 24	0	0.018	43	18
25 - 32	0.625	0.018	43	18
33 - 123	0	0.018	43	18
124 - 166	0	0.015	35	18
167 - 170	0.625	0.015	35	18
171 - 260	0	0.015	35	18
261 - 300	0	0.01	20	18

Tab. 5 - Time-variable boundary conditions for the inverse model calibration of the dune sand experiments

Time (h)	Irrigation (cm/h)	Evaporation (cm/h)	Temperature top (°C)	Temperature bottom (°C)
0 - 2	0	0.018	43	18
3 - 7	3.42	0.018	43	18
8 - 50	0	0.018	43	18
51 - 122	0	0.015	35	18
123 - 124	1.26	0.015	35	18
125 - 200	0	0.015	35	18
201 - 270	0	0.01	20	18

3.5.2.4 Observation Data

The inverse model calibration was based on observation data for transient water contents and temperature in different profile depths and boundary water fluxes, measured as water discharge at the column bottom and evaporation at the column top.

Water discharge and evaporation were inserted with cumulative values for every 0.5 h to 2 h. Water contents data were assembled for 4, 14, 24, 34, 44, 60, 70 and 84 cm depths, according to the inserted model observation points. Data were obtained from the TDR rod and cable measurements. Time intervals for data on water contents were chosen depending on infiltration patterns with every 0.5 h during and shortly after irrigation and up to 5 h during redistribution. Temperature profiles were emerged from the temperature measurements at 4, 14, 24, 44, 60, 70 and 84 cm depths and time intervals were chosen according to the water content measurements.

For composite parameter sensitivity analysis (see chapter 3.5.2.6), observation data were grouped in observation groups. These were water content measurements within each depth (8 groups), cumulative evaporation (1 group), cumulative discharge (1 group) and temperature measurements within each depth (7 groups).

Each observation point was prescribed with an observation weight. Normally, all observations can carry equal weights in the parameter estimation process (e.g. 1). Only if observations are known to be prone to experimental errors their weights should be decreased (Doherty, 2010). Nevertheless, when running PEST with observation data of different type, care must be given regarding the data magnitudes. If one type of data has significant higher magnitudes than the others, it will highly define the objective function compared to the other observations. Thus, observation weights of the temperature data were decreased by a factor of 10, whereas the water content weights were increased by a factor of 10. Additionally, during some of the optimization runs, the observation weights were changed regarding their importance upon fit. If, after an optimization run, a specific system behavior of the measured observations was not simulated accordingly by the model, another optimization run was performed. Within this run, weights were increased for the poorly displayed observations to increase their influence upon parameter optimization.

3.5.2.5 Hydraulic and Thermal Properties

Within calibration, the hydraulic models of van Genuchten-Mualem (1980) (Eq. 3), Brooks and Corey (1964) (Eq. 4) and the dual domain model of Durner et al. (1994) (Eq. 5) were tested for the applicability to the experimental conditions.

The parameters of the hydraulic retention models, residual and saturated water contents, and the hydraulic conductivity functions parameters (Eq. 7 and Eq. 8) were calibrated within the inverse modeling process. Initial parameter values were chosen according to the measured hydraulic conductivities and the SWRC-Fit results (Seki, 2007), whereas the results of the fitting options for setting residual water content to zero were tested separately. The tortuosity factor, used in the hydraulic conductivity function, was initially set to 0.5, according to Mualem (1976). Hysteresis was not taken into account for the models, as retention data was not obtained for drying and wetting curves and thus too many unknowns would have been included in the optimization process.

Thermal conductivity was calculated for the model of Chung and Horton (1987) (Eq. 10). Calibration was performed on the model parameters and the volumetric heat capacity of the sands.

Thus, altogether, up to 13 parameters, depending on the hydraulic model, were to be optimized by inverse calibration.

For the suction plate, hydraulic properties were fixed according to manufacturing information with $\theta_r = 0.1$, $\theta_s = 0.5$, $h_b = 500$ cm and $K_s = 0.0000311$ cm/s. Thermal properties of the suction plate were not considered as the heating element in the experiments was placed above the suction plate.

3.5.2.6 Sensitivity Analysis

Within PEST optimization, two different sensitivities are calculated. The composite parameter sensitivity measures the sensitivity of each calibrated parameter regarding its importance upon model fit. It is calculated for all observations together, and for each predefined observation group separately (Doherty, 2010). As such, it defines the relevance of each parameter on the modeled processes and observations and identifies parameters of primary importance.

The composite observation sensitivity measures the sensitivity of each single observation to all parameters that are optimized during the final optimization step (Doherty, 2010). By knowing observation sensitivities, future measurement setups can be optimized with increased data collection for high observation sensitivities and less data collection for times, depths, or type of data with lower sensitivities.

3.5.3. Predictive Modeling

The predictive modeling was performed with the calibrated data and real as well as modified meteorological datasets. It aimed at identifying factors of primary importance upon possible groundwater recharge in arid regions. To point out the significance of single factors, the predictive modeling scenarios were partly hypothesized and simplified.

3.5.3.1 Initial and Boundary Conditions

For the predictive modeling, the model set-up was adjusted to better reflect field conditions. Every change on the model conditions was tested upon changes to the overall system behavior by adapting them to the calibrated model.

Changed boundary conditions were:

- Bottom water flow boundary: the suction plate was virtually removed and a free drainage boundary was applied, supposing the groundwater level to be deep beyond the model boundary
- Bottom heat transport boundary: the fixed temperature boundary was changed to a temperature gradient boundary induced by the top boundary temperature
- Top time-variable atmospheric boundary: meteorological data for the calculation of potential evaporation according to the Penman-Monteith equation (Eq. 1) were introduced
- Top temperature boundary: diurnal temperature changes according to equation 20 were tested upon their effects on water and vapor fluxes

$$T = T_0 + A \sin\left(\frac{2t}{p} - \frac{7}{12}\right)$$

Eq. 20 - Diurnal temperature changes as implemented in Hydrus-1D

where A (-) is the temperature amplitude at the soil surface, p is the time interval for completion of one sine wave temperature (usually 1 day) and T_0 is the average temperature (°C) at the soil surface during time period p. The maximum temperature is set at 1 p.m. (Šim nek et al., 2009).

Additionally, the profile depth was enlarged to 200 cm and the nodal distances were increased to 0.2 cm.

Initial conditions for the annual scenarios were obtained from running the model with a homogenous initial profile water content of 0.06 cm³/cm³ and temperature distribution of 20 °C for a 90 days pre-scenario with no irrigation, a top temperature of 14 °C and a potential evaporation rate of 0.25 mm/d, accounting for low flux period conditions. Initials for the pre-run were chosen to be below field capacity. The temperature boundary accounted for the scenario start in the winter period. For the monthly scenarios no pre-run was performed, as these scenarios only should outline extremely hypothesized conditions. The monthly scenarios

started with a homogenous initial water content of $0.07 \text{ cm}^3/\text{cm}^3$ and initial temperature of $20 \text{ }^\circ\text{C}$.

Time-discretization was implemented variable to adapt simulation time to the time-dependant boundary conditions. Initial time step was set to 0.0001 h and minimum time step was set to 0.000001 h . This low minimum time step was chosen to minimize truncation failure during precipitation, as large and abrupt decreases in pressure head can occur for wetting after complete drying.

3.5.3.2 Monthly Scenarios

Monthly scenarios were run to indicate the influence of rainfall distribution patterns within one month, as well as temperature effects on soil water contents and fluxes. The monthly scenarios were run with the calibrated hydraulic and thermal properties of the dune sand.

One scenario set was run with a total monthly precipitation amount of 50 mm , distributed among 30 days in different patterns:

- one single 50 mm precipitation event
- 50 mm within 10 consecutive days (5 mm/d)
- 50 mm within 10 days with alternating 1 day of 10 mm/d precipitation and one day without precipitation
- 50 mm within 25 days with alternating 1 day of 10 mm/d precipitation and 4 days without precipitation

The effects of reversed temperature gradients during single precipitation events and the subsequent drying process were tested with $20 \text{ }^\circ\text{C}$ bottom temperature and:

- 10 mm precipitation with $30 \text{ }^\circ\text{C}$ top temperature
- 10 mm precipitation with $8 \text{ }^\circ\text{C}$ top temperature

3.5.3.3 Annual Scenarios

The modified model was run for annual scenarios with daily values of precipitation, mean, maximum and minimum temperature, relative air humidity and wind velocity. The scenario inputs were adapted from real data of selected meteorological stations in Saudi Arabia, obtained from the Satellite and Information Service of the National Climatic Data Centre of the National Oceanic and Atmospheric Administration (NOAA, 2010). Solar radiation values were available from 13 stations in Saudi Arabia as monthly averages from the “Solar Radiation Atlas for the Kingdom of Saudi Arabia” (Energy Research Institute, 1998).

The predictive modeling was based on three reference scenarios (NOAA station number 403560; NOAA, 2010): one year with total annual precipitation of 600 mm (Fig. 8a; year

1980) mainly due to one extreme storm event of 480 mm/d, one year with total annual precipitation of 250 mm with a high precipitation event of around 80 mm (Fig. 8b; year 1982) and one year with total annual precipitation of 30 mm (Fig. 8c; year 1983) to account for high, moderate and low precipitation scenarios.

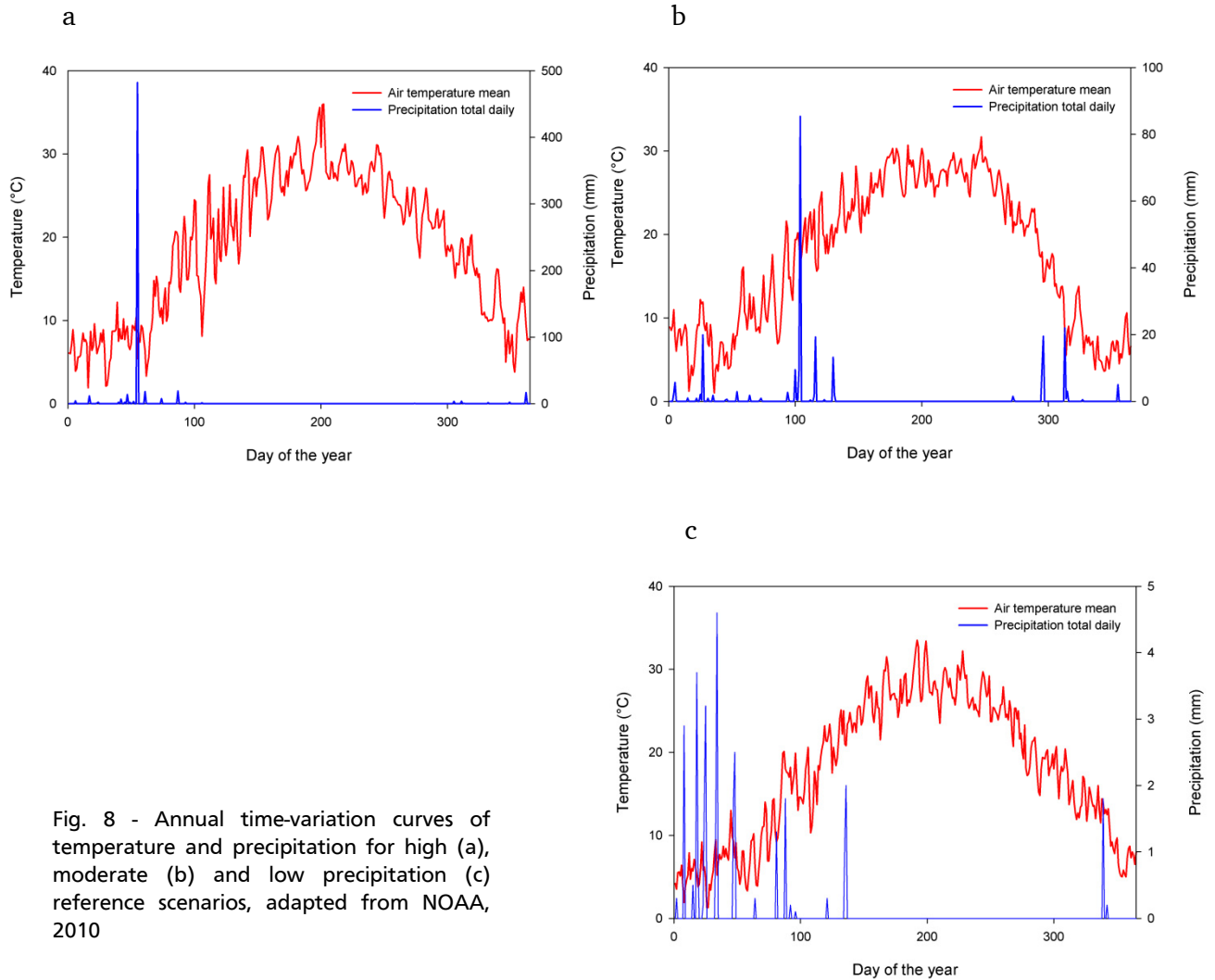


Fig. 8 - Annual time-variation curves of temperature and precipitation for high (a), moderate (b) and low precipitation (c) reference scenarios, adapted from NOAA, 2010

Each of the three reference scenarios was run with

- hydraulic and thermal parameter values as calibrated with the silica sand
- hydraulic and thermal parameter values as calibrated with the dune sand
- hydraulic and thermal parameters as derived from pedotransfer functions for pure sand

Within further model runs, the reference scenarios were configured to evaluate single parameter changes on water fluxes and analyze groundwater recharge predictions for different model settings:

- The high irrigation events of the high and moderate precipitation years were splitted into several irrigations within one month
- The high irrigation amount of 480 mm was decreased stepwise to 20 mm
- Temperatures were increased and decreased by up to 10 °C
- Relative humidity was increased and decreased by up to 10 %
- Solar radiation was increased and decreased by up to 10 %
- Initial water contents were set to residual water content
- Water vapor simulations were excluded and heat flux simulations were excluded

The single model runs were evaluated for infiltration depths, evaporation, discharge and the relevance of isothermal and thermal water and vapor fluxes. The relevance of single model input parameters on model output was additionally evaluated by a PEST sensitivity analysis.

4. Results

Results are ordered according to chapter 3. All results on water content are given in volumetric water content (cm^3/cm^3), rather than in saturation. The saturation, covering 0 for none and 1 for complete saturation does only describe the water filling of the soil pores, whereas the saturation of 1 equals the soil porosity. Nevertheless, as already stated, under drying and wetting conditions, not 100 % of the pores will ever get fully saturated. Thus, the so-called saturated water content does not equal a saturation of 1, nor the soil pores, but the wettable pores under transient conditions. As such, the water content gives more information, additionally to porosity, than the saturation. The modeling results for water and vapor fluxes are given in 1-dimensional flow units, as of the units for the model set-up, which was cm and h for the model calibration or d for the predictive modeling. The flow direction of the modeled water and vapor fluxes are given in – for downwards and + for upward flow.

4.1. Soil properties

Both sands were well sorted with a homogenous grain size distribution in the range of middle to coarse grained (silica sand) and fine to middle grained sand (dune sand) (Fig. 9).

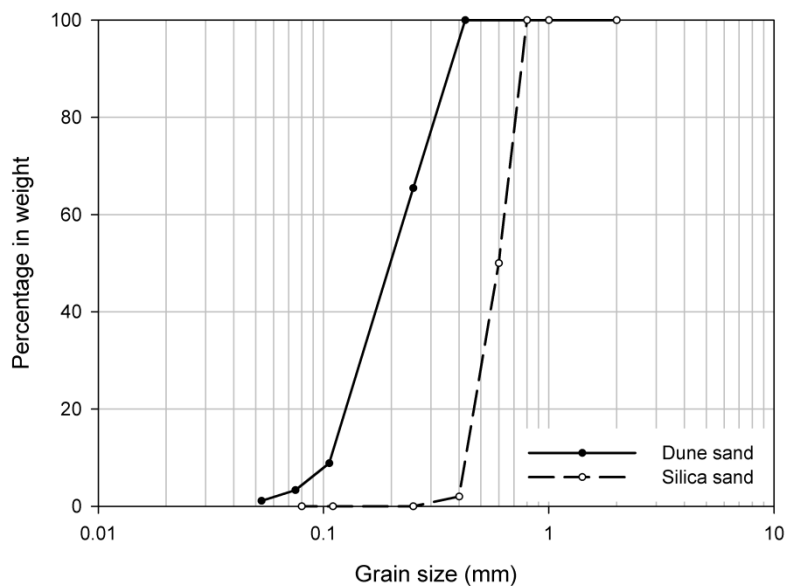


Fig. 9 - Grain size distribution of the silica and the dune sand used within the experiments as derived from sieve analysis

Measured physical soil properties were in good agreement with common values for pure sand, indicating high infiltration and low retention capacities (

Tab. 6). Field capacity values represented the measured water content range in the upper 50 cm of the soil column after the drainage experiment.

Tab. 6 - Physical properties of the silica and the dune sand used within the experiments

	Bulk density (g/cm ³)	Porosity (-)	K _s (cm/s)	Field capacity (cm ³ /cm ³)
Silica sand	1.65	0.42	1.3*10 ⁻²	0.08 – 0.1
Dune sand	1.7	0.39	7.3 *10 ⁻³	0.075 – 0.1

Water drop penetration times were below 1 second for both sands, classifying the sands as non-water repellent. Both sands had 0 % organic content and thus, no water repellency was expected.

Water retention measurements and their fitting to the hydraulic models of van Genuchten (1980), Brooks and Corey (1964), and Durner (1994), all with and without setting residual water content θ_r to zero, are shown in figures 10 and 11. Setting the residual water content to 0 showed worse fitting results for the retention curve models. Nevertheless, it was expected to show better results for the inverse modeling due to the different boundary conditions applied during the retention curve measurements in contrast to the transient non-isothermal experiments.

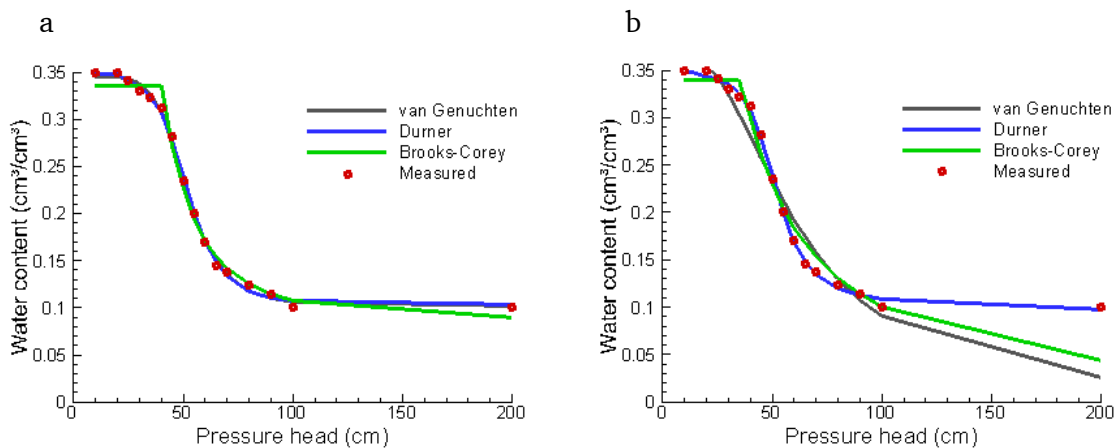


Fig. 10 - SWRC-Fit results for measured retention data of the silica sand to the hydraulic models of van Genuchten (1980), Brooks and Corey (1964), and Durner (1994) without (a) and with (b) setting residual water content θ_r to zero

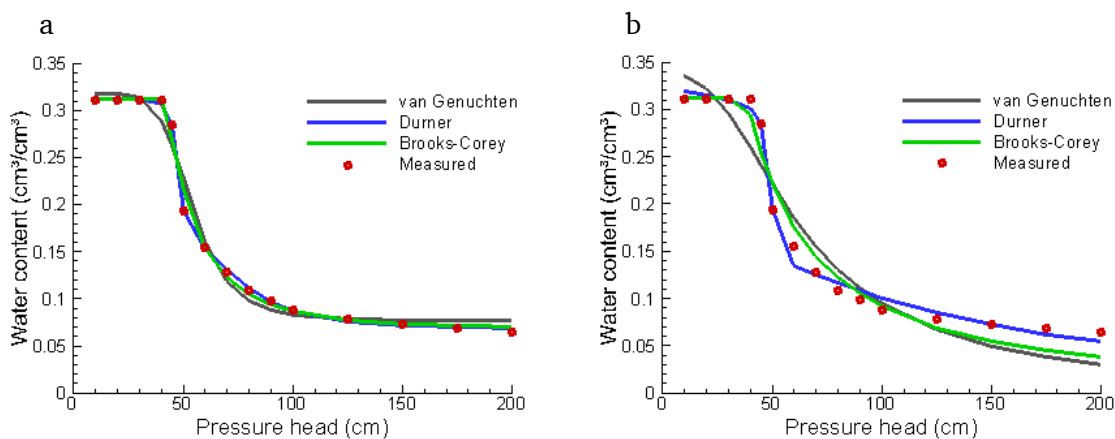


Fig. 11 – SWRC-Fit results for measured retention data of the dune sand to the hydraulic models of van Genuchten (1980), Brooks and Corey (1964), and Durner (1994) without (a) and with (b) setting residual water content θ_r to zero

Results of the model parameters are listed in table 7. Additionally to the parameter values of the fitted retention data, also hydraulic parameters according to ROSETTA pedotransfer function calculations for pure sand are listed for comparison. For the Brooks and Corey model, values for comparison were taken from pure sand hydraulic function data as estimated by Rawls et al. (1982). For the Durner model no such estimates were available.

Tab. 7 - Hydraulic model parameters for silica sand and dune sand obtained from retention data, and reference data for 100 % pure sand obtained from pedotransfer functions and Rawls et al., 1982

θ_r = residual water content; θ_s = saturated water content; h_b , λ = Brooks-Corey parameter; α , n = van Genuchten parameter; w_1 = fraction of porosity 1 upon total porosity; R^2 = correlation coefficient

Model	Parameter	Silica sand	Silica sand	Dune sand	Dune sand	100% sand
Brooks-Corey	θ_r	0.086	0	0.067	0	0.02
	θ_s	0.336	0.34	0.312	0.312	0.417
	h_b	40.304	36.074	42.102	38.222	7.25
	λ	2.701	1.201	2.912	1.273	0.592
	R^2	0.98	0.98	0.99	0.97	-
van Genuchten	θ_r	0.101	0	0.077	0	0.051
	θ_s	0.345	0.372	0.318	0.337	0.376
	α	0.0199	0.0201	0.019	0.019	0.034
	n	6.71	2.907	6.664	2.757	4.425
	R^2	0.99	0.94	0.98	0.92	-
Durner	θ_r	0.103	0	0.068	0	-
	θ_s	0.35	0.365	0.313	0.32	-
	w_1	0.047	0.409	0.521	0.466	-
	α_1	0.04	0.121	0.021	0.021	-
	n_1	48.778	1.132	31.054	28.637	-
	α_2	0.0197	0.0197	0.015	0.013	-
	n_2	7.15	7.726	5.49	2.152	-
R^2	0.99	0.99	0.99	0.99	-	

The parameter results showed the clear difference between the fitting of the retention data with and without setting the residual water content θ_r to zero, especially for the model parameters that can be physically related to the pore size distribution (n and λ), which decreased by more than 50 %. As already seen in the graphs, the correlation of the measured data to the hydraulic models, given by the correlation coefficient R^2 , decreased when setting θ_r to zero. Best fittings were given for the Durner dual-porosity model. Nevertheless, the increased number of parameters in the dual-porosity model also increased the non-uniqueness of the solution and values should be handled with care.

Fitting of the thermal conductivity measurements of the dune sand to the equation of Chung and Horton (1987) are shown in figure 12 and table 8. Reference values for pure silica sand, as measured by Chung and Horton (1987) are listed for the silica sand and included in figure 12.

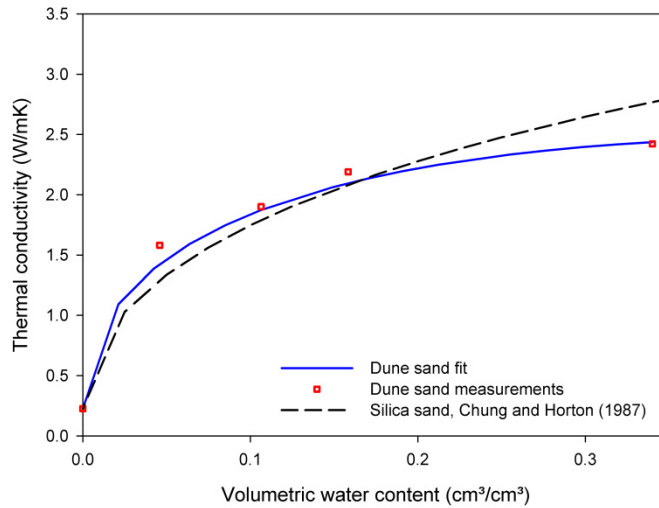


Fig. 12 - Thermal conductivity measurements fitted to the thermal conductivity equation of Chung and Horton (1987)

Tab. 8 - Thermal conductivity parameters derived and fitted according to Chung and Horton (1987) for silica sand and dune sand measurements

Model parameter	Silica sand	Dune sand
b1	0.23	0.23
b2	-2.1	-5.6
b3	5.97	6.58

In the model, b1, b2 and b3 are fitting parameters and thus are given without units. Nevertheless, as b1 physically equals the unsaturated thermal conductivity, its unit resembles W/mK.

Especially in the higher water content ranges, thermal conductivity of silica sand was higher than measured for the dune sand, and the thermal conductivity curve had a steeper inclination. For lower water contents, the dune sand measurements had higher thermal conductivity values than compared silica sand values.

4.2. TDR Cable Calibration

Figure 13 a and b show the cable calibration measurements and linear regression curves of the TDR cable reflection coefficient values to the TDR rod measurements of volumetric water content.

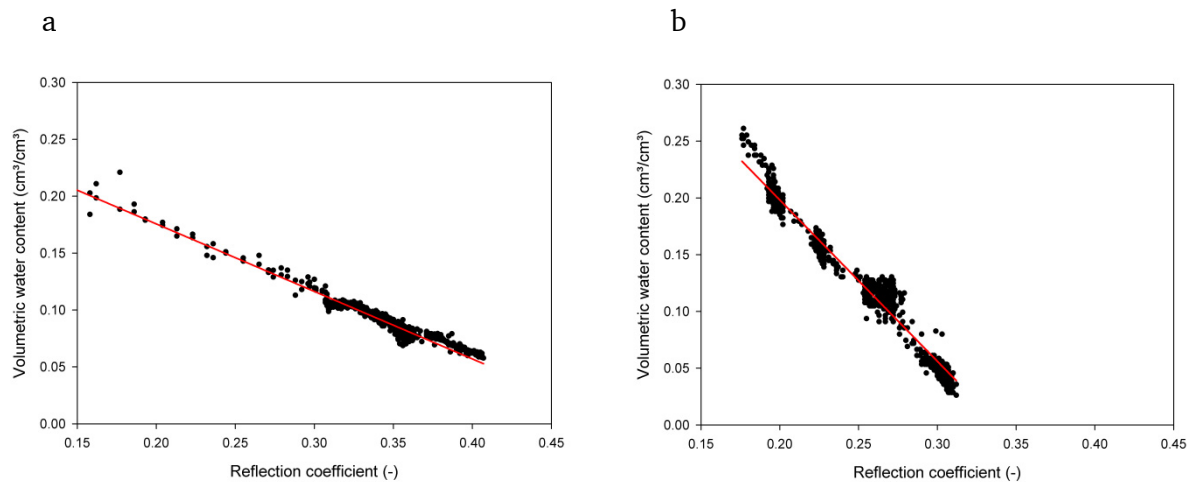


Fig. 13 - Correlation of TDR cable reflection coefficient measurements with TDR rod sensor volumetric water content measurements and linear regression line for the silica (a) and the dune (b) sand

In the silica sand, measurements above a water content of $0.13 \text{ cm}^3/\text{cm}^3$ were hardly adjustable due to the fast drainage in the column. Thus, for higher water contents, much fewer measurements were available. For the dune sand measurements, equal reflection coefficients were measured for water contents with differences of up to $0.02 \text{ cm}^3/\text{cm}^3$, resembled in measurement points that are stacked in lines. It was caused by measurement scattering of the TDR point measurements, as several measurements were taken within short time.

Calibration functions were obtained by linear regression:

Silica sand ($R^2=0.96$)

$$\theta = -0.593 * RC + 0.294$$

Eq. 21 - TDR volumetric water content calculation from cable reflection coefficient measurements for the silica sand

Dune sand ($R^2=0.97$)

$$\theta = -1.421 * RC + 0.482$$

Eq. 22 - TDR volumetric water content calculation from cable reflection coefficient measurements for the dune sand where RC is the reflection coefficient (-).

Comparing both calibration curves and functions revealed large differences for the two sands in electromagnetic reflection properties. The dune sand measurements had lower resolutions within reflection coefficients, shown in the steeper calibration curve, whereas higher water contents were better correlated than within the silica sand calibration. The obvious differences in the calibration functions revealed probable trouble for the water

content correlation of measured reflection coefficients in heterogeneous soil profiles. Especially for layered stratigraphies, the calibration results suggested that single calibrations are required for each layer, whereas the applicability of mixing functions should be considered. For both sands the data scattering was relatively high. Thus, volumetric water content values for the TDR cable measurements were reassured by water balance calculations during the experiments.

Temperature influences on the TDR cable as well as on the TDR rod sensor measurements were not detected. Recorded reflection curves did not show differences for measurements at 20 °C, 35 °C or 50 °C in the water content ranges of 0.05 cm³/cm³ up to 0.25 cm³/cm³ and were thus not considered for the further experiments.

4.3. Experiments

Experiments were performed with three different sand fillings, one homogenous silica sand filling, one homogenous dune sand filling, and a layered filling with both sands. Changing boundary conditions aimed at analyzing the influences of irrigation patterns and temperature on water infiltration and redistribution. The detailed experimental initial and boundary conditions are listed in chapter 3.4.

4.3.1. Silica Sand Filling

The experiments with the silica sand aimed at evaluating the experimental setup, as well as different irrigation patterns on water infiltration, redistribution and evaporation. The silica sand was used to provide a homogenous grain size distribution and exclude influences of organic content or mineralogy.

4.3.1.1 Steady State Experiment

After column packing and before starting irrigation, the temperatures at the top and the bottom of the column were applied. A stable temperature gradient maintained within 10 h (

Fig. 14 a). After temperature in the upper 4 cm reached maximum values (5 h), measured temperature in this depth slightly decreased again for around 2 °C due to evaporative cooling. Temperatures in the deeper profile still increased. In the non-irrigated soil, only temperatures of up to 38 °C were measured in a depth of 4 cm, even with an applied top temperature of 50 °C. When starting irrigation, convective heat transport with the infiltrating water, as well as an increase in thermal conductivity of the soil due to higher water contents increased the temperatures in the soil profile (Fig. 14 b). The irrigation front could well be traced with the temperature measurements.

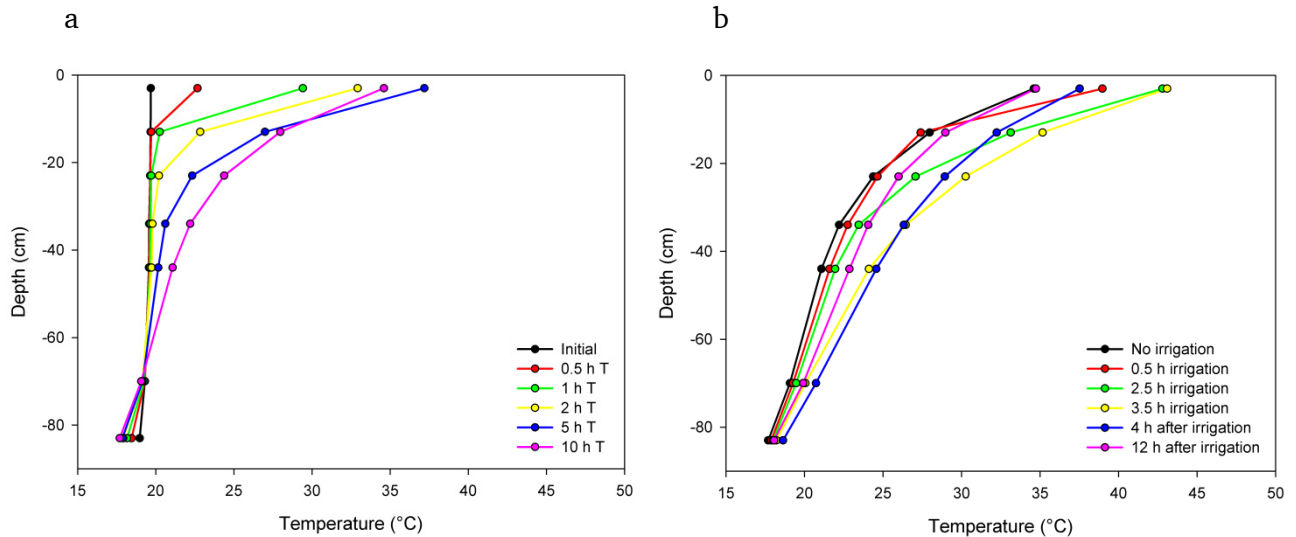


Fig. 14 - Temperature profiles in the silica sand after applying boundary temperatures with 50 °C at the soil top and 15 °C at the soil bottom (a) and with a continuous irrigation of 0.55 mm/min (b); PT100 temperature measurements (T) are shown in circles

The infiltration front was also clearly detectable with the TDR cable sensor (Fig. 15). Initially, the volumetric water content in the upper part of the column increased to a maximum of 0.13 cm³/cm³, indicating the unsaturated downward flow of water. Discharge at the bottom of the column started about 3 hours after irrigation started. At this time, the volumetric water content within the column was almost evenly distributed at 0.13 cm³/cm³. Discharge reached maximum values between 0.5 and 0.6 mm/min about 1 h after breakthrough and persisted as long as irrigation continued, accounting for the irrigation input of 0.55 mm/min. The delayed maximum discharge resulted from a delayed saturation accounting for an increased hydraulic conductivity. The persistent fluctuations of the discharge were probably due to the suction of the vacuum pump, which regularly adjusted itself to the predefined suction of 60 mbar. Relative humidity of the effluent air reached 100 % during irrigation, which accounted for an evaporation rate of around 0.007 mm/min, or about 1.2 % of the irrigation flow. The TDR rod probes measured similar water contents as the TDR cable sensor at their specific locations, indicating the capability of the TDR flat cable to trace water infiltration in high vertical resolution.

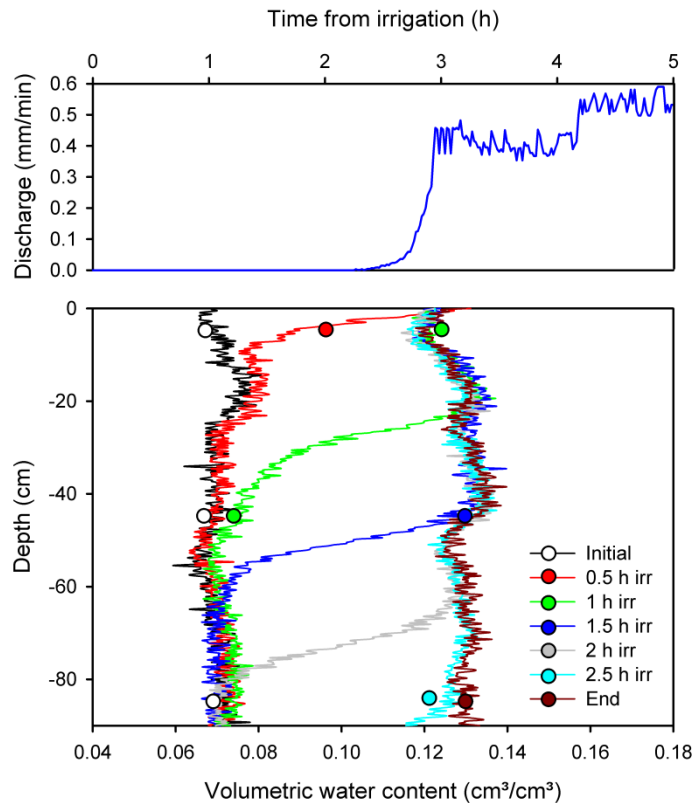


Fig. 15 - Infiltration front and discharge during wetting with continuous irrigation of 0.55 mm/min ("irr") measured with the TDR cable (continuous line) and TDR point measurements (circles)

After overhead irrigation stopped, the sand drained within about 4 hours to a homogenous water content of 0.09 cm³/cm³. In the first hour of drainage, water content in the upper profile part rapidly decreased inducing a significant lowering of the unsaturated hydraulic conductivity. Due to higher water contents at the bottom of the column, water moved faster to the lower end until equilibrium was reached throughout the whole column. Thus, drainage appeared to be almost homogenous in the entire column (Fig. 16). During the drying period, the upper parts of the sand column dried to a volumetric water content of 0.06 cm³/cm³ by evaporation (Fig. 16). Evaporation depth was measured to be around 20 cm after 72 hours. Evaporation, as well as discharge, linearly decreased and converged to zero after 6 days.

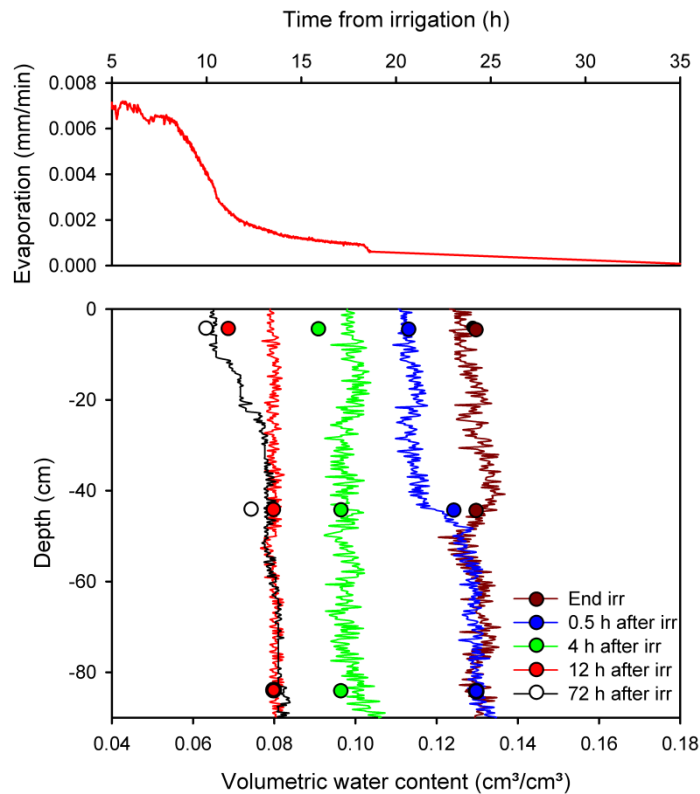


Fig. 16 - Water content and evaporation during drainage and drying measured with the TDR cable (continuous line) and TDR point measurements (circles); irr = irrigation

The drying front could not be traced with the TDR cable until a drying depth of around 10 cm was reached. Thus, the cable measurements did not match the TDR point measurements at the beginning of the drying period. In addition, as the measurement curves for irrigation stop in Figures 15 and 16 were taken from two consecutive measurements, they apparently did not completely match at the top end of the profile measurements. This illustrated the problem of the reflection curve interpretation of the cable measurements when defining the sensor start within the signal. As infiltration curves were clearly detectable, measurements also suggested a lower sensitivity of the reflection amplitude measurements at the drier ends. Thus, the TDR point measurements were necessary to complement the cable measurements at the column top, especially during drying.

4.3.1.2 Varying Irrigation Amounts

Water balance results for the evaluation of changing irrigation amounts with the same irrigation intensity of 6.25 mm/h are compiled in table 9.

Tab. 9 - Summarized water balance results for 12.5, 25 and 50 mm irrigation with the same intensity of 6.25 mm/h with cumulative values 7 days after irrigation

Irrigation			7 days after irrigation					
Irrigation amount (mm)	Irrigation time (h)	Infiltration depth (cm)	Evaporation (mm)	Evaporation (%)	Discharge (mm)	Discharge (%)	Water storage increase, calculated (mm)	Water content change, calculated (Vol%)
12.5	2	19 cm	4.85	38.8	0	0	7.65	0.008
25	4	35 cm	4.80	19.2	3.52	14.1	16.68	0.018
50	8	85 cm	5.83	11.7	23.38	46.8	20.79	0.022

For the lowest irrigation amount of 12.5 mm, no further downward water movement occurred after irrigation stopped. As a result, only in the top few cm of the column water contents well above the estimated field capacity were reached (Fig 17 a). During the next days, evaporation caused water contents to significantly decrease. For an overhead irrigation of 25 mm, a uniform water content of around 0.14 cm³/cm³ was reached within the upper 35 cm directly after irrigation stopped. 24 h after irrigation, water redistributed to a uniform water content of about 0.11 cm³/cm³ within a depth of 65 cm (Fig. 17 b). Discharge started 36 h after irrigation stopped and the highest evaporation rates were measured during the first 24 h within and after irrigation. Total evaporation after 7 days was slightly lower compared to the 12.5 mm irrigation. The 50 mm overhead irrigation showed a homogeneously distributed wetting front with a volumetric water content of about 0.13 cm³/cm³ over the whole column length (Fig. 17 c). Discharge at the column end was observed 2 hours after irrigation stopped. One week after irrigation, drainage and redistribution of the water content within the sand resulted in a uniform volumetric water content at around field capacity. Similar to the 25 mm overhead irrigation, the highest evaporation rates were measured during the first 24 h after irrigation.

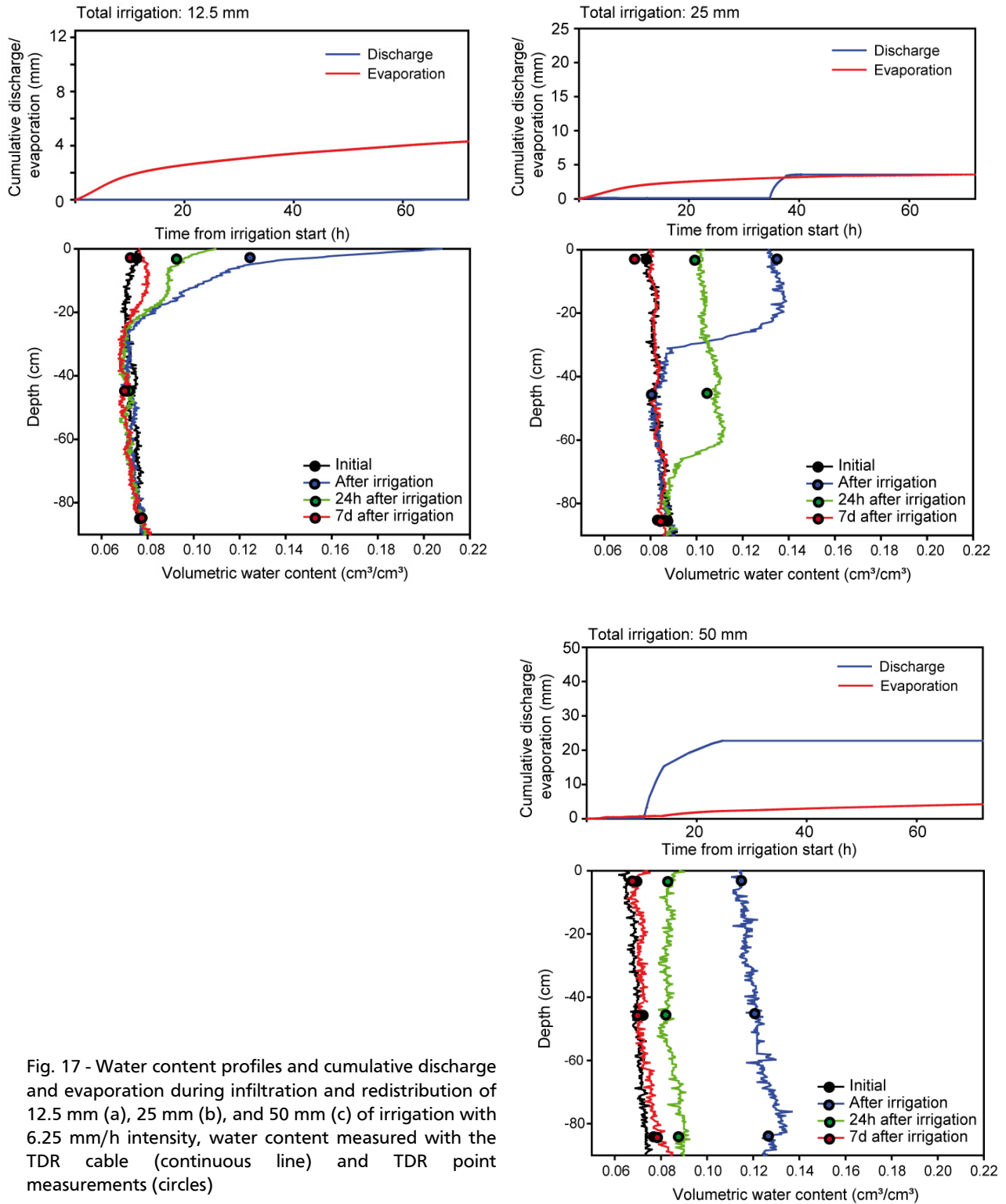


Fig. 17 - Water content profiles and cumulative discharge and evaporation during infiltration and redistribution of 12.5 mm (a), 25 mm (b), and 50 mm (c) of irrigation with 6.25 mm/h intensity, water content measured with the TDR cable (continuous line) and TDR point measurements (circles)

Overall, the experiments showed the large impact of irrigation amount on redistribution patterns within the column and on discharge rates. Drainage started when irrigation amounts were high enough to form a homogenous wetting front with a water content well above field capacity through at least the upper 30 cm of the column. With low irrigation amounts, as in the 12.5 mm experiment, the irrigated water was held within the upper centimeters of the sand, resulting in a high percentage of water loss due to evaporation.

Comparable to the steady-state experiments, the TDR cable was not capable of detecting an evaporation front in the upper few cm of sand. Additionally, calculated water balances 7 days after irrigation showed overall increases in soil water storage compared to initial conditions, whereas, especially for the 25 mm irrigation, the cable measurements indicate almost initial conditions. A small water content increase within the upper centimeters was detected only for the 12.5 mm irrigation.

4.3.1.3 Varying Irrigation Intensity

As in the former experiments discharge was not measured for any of the 12.5 mm irrigations. Changing irrigation intensity had no significant effect on infiltration depths and redistribution, but mainly showed an effect on evaporation. The overall results are presented in Table 10.

Tab. 10 - Summarized results for amounts of evaporation for three 12.5-mm irrigations with intensities of 0.052 mm/min (240 min), 0.625 mm/min (20 min) and 6.25 mm/min (2 min); values are given for direct evaporation loss during irrigation and cumulative evaporation 7 days after irrigation

Irrigation amount (mm)	Irrigation time (min)	Infiltration depth (cm)	Evaporation during irrigation (mm)	Evaporation during irrigation (%)	Evaporation 7 days after irrigation (mm)	Evaporation 7 days after irrigation (%)
12.5	240	18 cm	1.42	11.4	4.93	39.4
12.5	20	19 cm	0.13	1.0	3.68	29.4
12.5	2	18 cm	0.01	0.1	3.6	28.8

As the effluent air reached a relative humidity of about 100 % during overhead irrigation, direct evaporation losses were increasing with decreasing irrigation intensity. When overhead irrigation ended, the relative humidity of the effluent air decreased exponentially in all three experiments and values converged after 24 h (Fig. 18). Direct evaporation losses of the 2 minutes and 20 minutes irrigation events differed by a factor of 10. Nevertheless, cumulative evaporation losses after 7 days were almost equal for both (Tab. 10). This indicated that for short irrigation events evaporation losses are dominated by evaporation of the infiltrated water after irrigation ends. For the irrigation with the lowest intensity, direct evaporation losses were substantial and accounted for more than 10% of the total irrigation.

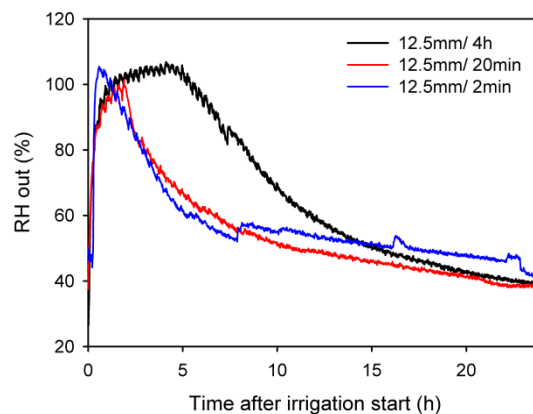


Fig. 18 - Relative humidity (RH) of the effluent air for three different irrigation events of 12.5 mm, lasting 240, 20 and 2 minutes

4.3.1.4 Irrigation and Redistribution

Two 12.5 mm irrigations were applied with a redistribution time of 72 hours in between. After the first irrigation, water infiltrated to a depth of about 30 cm and water redistribution was completed in about 10 hours. Thereafter, evaporation processes led to a loss of 3.6 mm of water. When the second irrigation event was applied, the former wetting front was pushed downward to a depth of 52 cm (Fig. 19). No discharge was monitored at the column end. At the end of the observation time (150 h) there was a zone with a homogeneously increased water content in a depth between 10 cm and 55 cm. The two irrigation events were not distinguishable within the profile but composed one wetting front; however, the total amount of infiltrated water of the separate irrigation events was less compared to one single irrigation event of the same amount, due to evaporation losses.

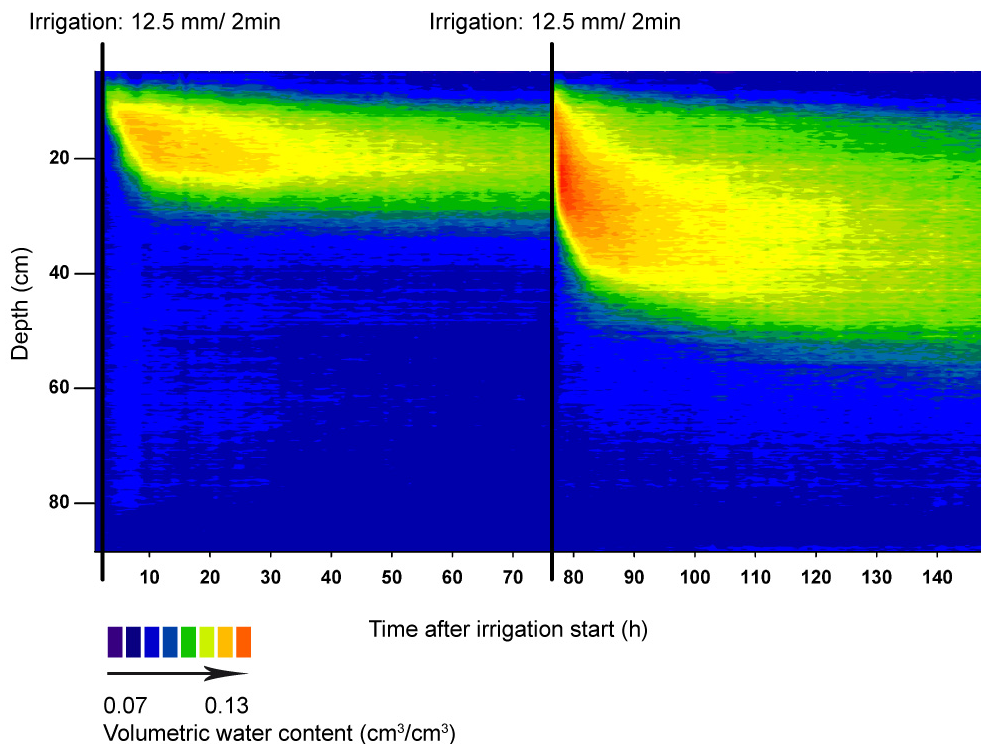


Fig. 19 - Volumetric water content changes over time in the sand column for two consecutive irrigation events of 12.5 mm with 72 h of flow interruption between irrigations

The results showed, that, under the given experimental conditions, for homogeneous sediments in the unsaturated zone, a homogeneous water content at field capacity could be expected below the zone influenced by evaporation. Single precipitation events therefore could not be distinguished by different water contents in the vertical soil profile.

4.3.2. Dune Sand Filling

The experiments with the dune sand filling aimed at analyzing effects of transient changes in top boundary conditions as they can be expected in arid regions, on infiltration, redistribution and evaporation patterns.

4.3.2.1 General Observations

During almost all experimental conditions, water retention at the bottom of the column above the suction plate was measurable, as the induced suction at the suction plate was too low to account for free water outflow. Nevertheless, infiltration, wetting and drying fronts could well be traced with the TDR cable measurements.

For low intensity irrigation, irrigation droplets formed small depressions on the soil surface until the whole surface was wetted. This resulted from a thin surface crust that built up during drying. As the surface was wetted evenly 1-2 minutes after irrigation started, no effects of water retention on the soil surface were measurable.

With the TDR cable, enhanced signal scattering was detected during the dune sand experiments, especially during irrigation (Fig. 20). These scattering effects did not occur during the silica sand experiments.

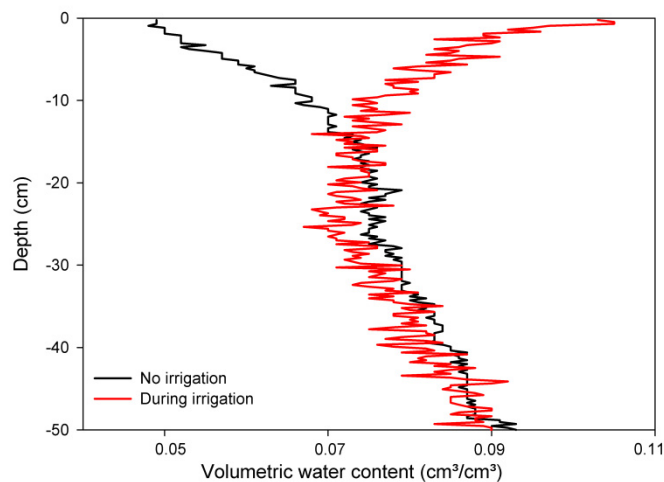


Fig. 20 - TDR cable signal scattering during irrigation within the dune sand experiments

The definite source for the scattering could not be detected. Generally, TDR signals can be disturbed by any electromagnetic signal in the sensors vicinity. The magnitude of influence depends on the frequency and distance of the interference factor to the sensor. Thus, any electrical device that was used in the vicinity of the experiments could have caused signal scattering.

4.3.2.2 Two-Stage Irrigation

After packing, the top and bottom temperatures were applied and a steady temperature gradient developed within 10 h (Fig. 21 a). With 16°C, the initial temperature was close to the applied bottom temperature of 15°C and thus, no decrease in the bottom soil temperature was measured after the 10 h. During irrigation, convective heat transport and the increase in thermal conductivity increased the temperatures in the soil profile (Fig. 21 b). Compared to the silica sand, the temperature in the dune sand showed higher increases due to higher thermal conductivities in wetted conditions, as measured in the thermal conductivity curve (Fig. 12). After irrigation stopped, temperature decreased in the upper layers below the initial temperatures, caused by evaporative cooling and decreased thermal conductivity under dry conditions.

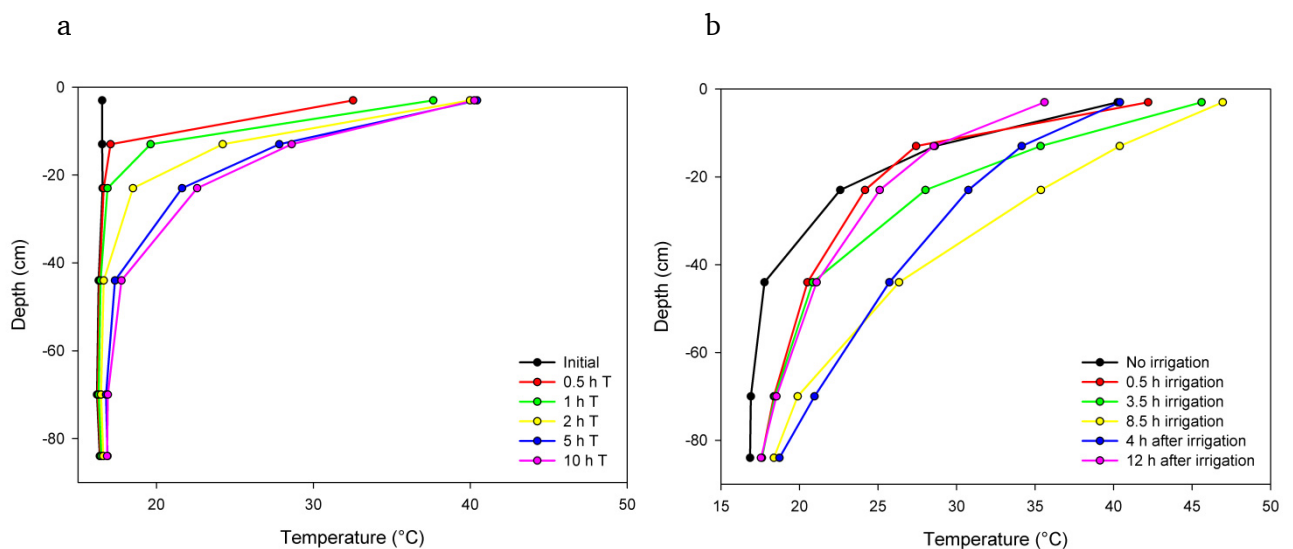


Fig. 21 – Temperature profiles in the dune sand after applying boundary temperatures with 50°C at the soil top and 15 °C at the soil bottom (a) and with irrigation of 0.55 mm/min (b); PT100 temperature measurements are shown in circles

The infiltration front of the first irrigation could well be traced with the TDR cable sensors (Fig. 22). The infiltration front was not as homogenous as within the silica sand steady-state irrigation. During the dune sand experiments, the infiltration front formed a wetting front with wetter conditions at the top of the front and thus in depths. Discharge was reached after approximately 4.5 h of irrigation (Fig. 23) and irrigation was stopped half an hour later. Altogether, approximately 75 % of the infiltrated water discharged.

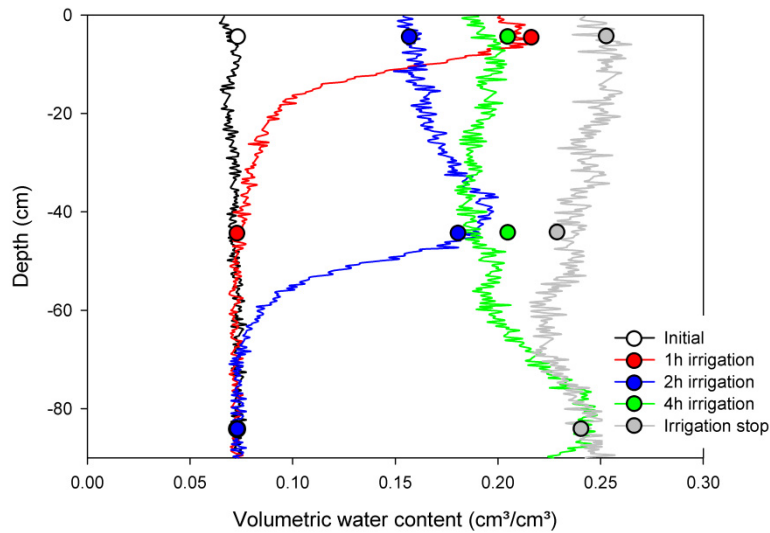


Fig. 22 - Infiltration front for dune sand irrigation of 0.55 mm/min measured by TDR cable (line) and point (circle) measurements

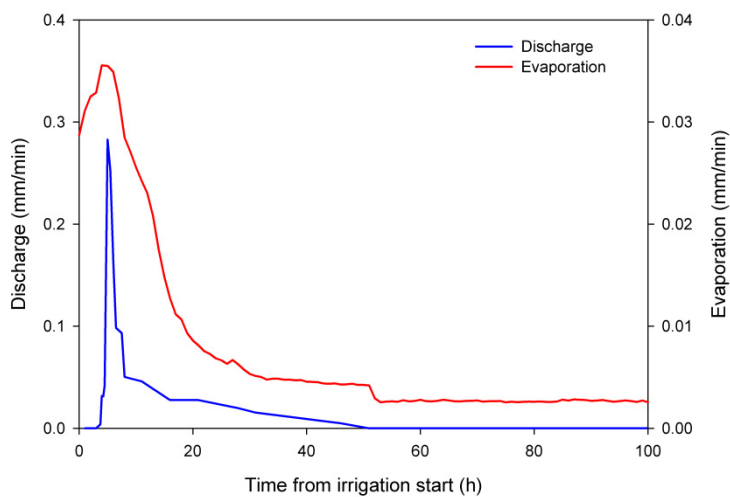


Fig. 23 - Discharge and evaporation over time for dune sand irrigation of 0.55 mm/min, lasting 5 h

The infiltration front of the second irrigation reached down to a depth of around 30 cm. After 5 h of redistribution, discharge started again and altogether around half of the infiltrated water discharged. After the two-stage irrigation, water content throughout the whole column profile did not equilibrate homogeneously as within the silica sand experiments, but a water content gradient built up with around 0.18 cm³/cm³ water content at the bottom and, depending on the drying state, down to 0.03 cm³/cm³ water content at the top of the column. This was, as already stated, partly due to the retention of the suction plate. As the data of the two-stage experiment was provided for the model calibration, water contents, cumulative discharge and cumulative evaporation over time are displayed in chapter 4.4.1 (Fig. 35 - 36).

4.3.2.3 Time-Dependant Boundary Conditions

Water balances for all irrigation and drying cycles showed the high influence of irrigation amount and intensity on discharge and evaporation (Tab. 11).

Tab. 11 - Water balance calculations of irrigation and drying cycles applied to the experiments with dune sand filling

Time (d)	Irrigation cycle #	Cumulative irrigation in (mm)	Cumulative evaporation out (mm)	Cumulative discharge out (mm)	Soil water storage change (mm)
1	1	5	3.34	0	+ 1.66
2		10	6.78	0	+ 3.22
3		15	10.5	0	+ 4.5
4		20	14.39	0	+ 5.61
5		25	18.01	0	+ 6.99
6 - 17			23.96	0	+ 1.04
18	2	30	26.18	0	+ 3.82
19		35	29.11	0	+ 5.89
20-22			30.93	0	+ 4.07
23	3	45	34.47	0	+ 10.53
24		55	37.49	0	+ 17.51
25-58			49.06	19.8	-13.86
59	4	80	52.25	19.8	+7.95
64		105	58.75	20.0	+26.25
65-90				67.6	49.6

For the first irrigation cycle, soil water storages were very low. For all 5 mm irrigations, more than 50 % of the irrigation water was directly lost by evaporation. After drying, less than 10 % of the altogether 25 mm irrigated water was stored in the soil due to this continuously high water loss by evaporation.

Only after the two 10 mm irrigations (irrigation cycle 3), water could infiltrate deep enough to escape from evaporation and percolate through the whole column. Discharge started about 36 h after the third irrigation cycle stopped. Altogether, almost all 20 mm of the irrigation water of this irrigation cycle discharged during the following 24 days. Together with the high evaporation amounts, soil water storage decreased to less than initial experimental conditions. The high discharge amount indicated that, as soon as a continuous water film throughout the soil pores was maintained, water that might had been trapped within the soil pores, was caught and contributed to overall discharge. Especially in soils with large pores, water contents that lead to continuous water films throughout the pores highly increase the unsaturated hydraulic conductivity and thus temporarily increase vertical water fluxes. Similar effects were observed after the fourth irrigation cycle. Altogether, evaporation outreached discharge, due to the low irrigation intensities and correspondingly high evaporation losses directly during irrigation (Fig. 24).

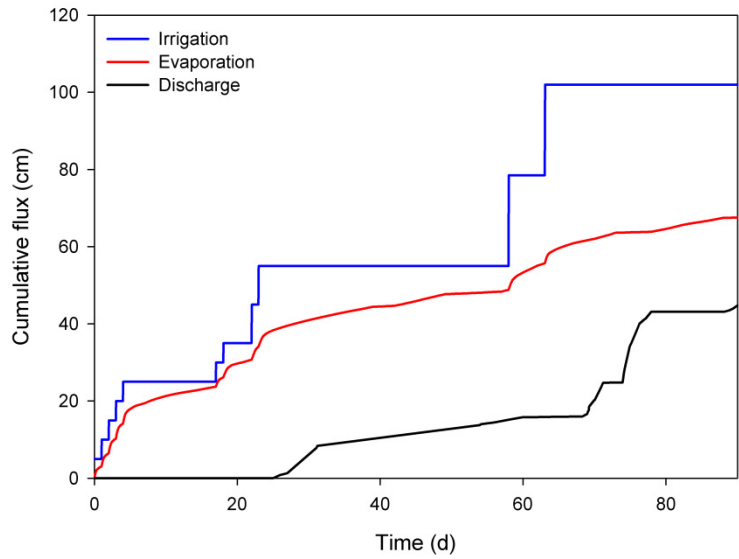


Fig. 24 - Cumulative irrigation, evaporation, and bottom discharge over time for changing boundary conditions applied to the experiments with dune sand filling

When looking at the TDR cable measurements, infiltration fronts for the first irrigation cycle were not detectable. Total water contents, as obtained from the cable measurement, increased by approximately $0.001 \text{ cm}^3/\text{cm}^3$ per irrigation. For the three TDR rod sensors, irrigation was only measurable at the uppermost sensor at 4 cm. Here, water content increased to around $0.075 \text{ cm}^3/\text{cm}^3$ and decreased again to $0.03 \text{ cm}^3/\text{cm}^3$ within the following 24 h (Fig. 25). Regarding the quality of the TDR measurements, the low water content measurements of the uppermost TDR rod sensor showed highest noise compared to the other two rod sensors.

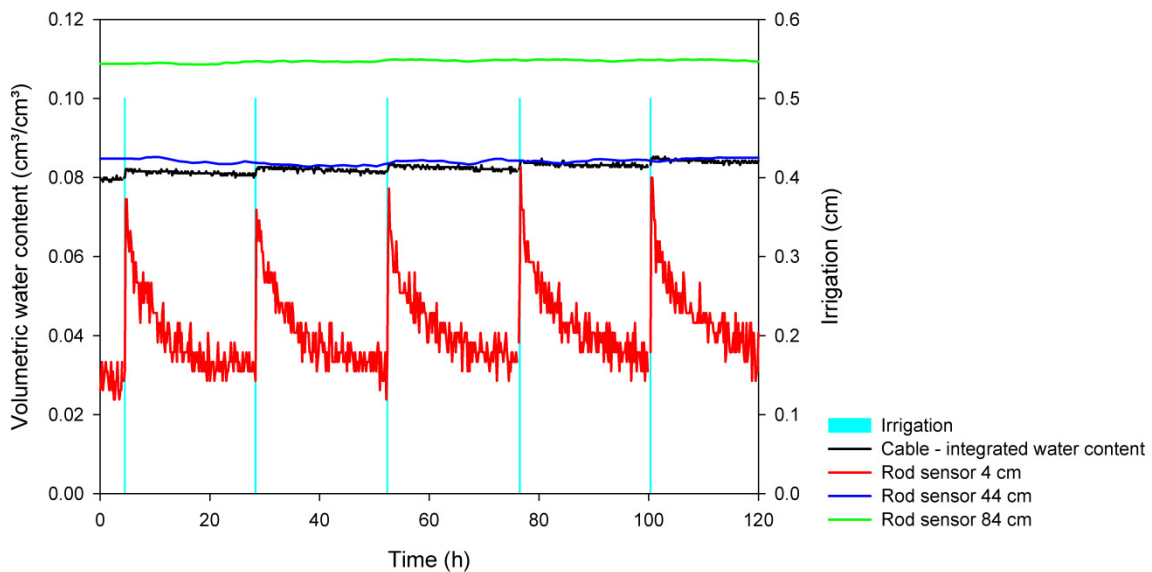


Fig. 25 - Water fluxes in different depths over time for the first irrigation cycle (5 x 5 mm) during experiments with dune sand filling, measured with the TDR rod sensors and as integrated water content along the whole soil profile with the TDR cable sensor

Heat fluxes during the first irrigation cycle were traced down to a depth of 44 cm (Fig. 26). On the one hand, convective heat transport with the infiltrating water and higher thermal conductivity due to higher water contents increased the temperature in the upper 4 cm. With the ambient thermal conductivities in the deeper profile the heat was transported further downward. As soon as the soil surface dried, temperatures decreased again.

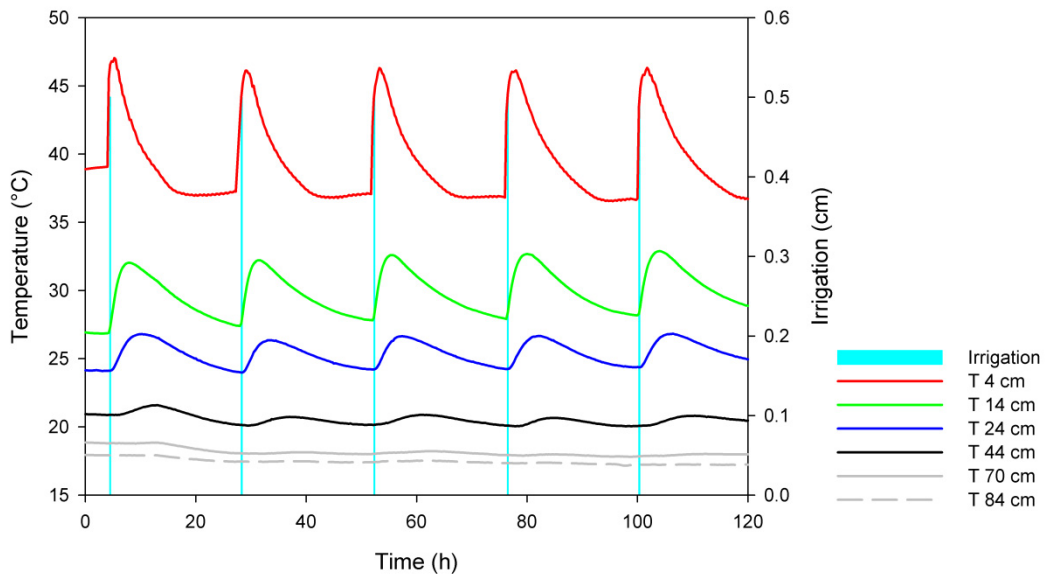


Fig. 26 - Temperature fluxes in different depths over time for the first irrigation cycle (5 x 5 mm) during experiments with dune sand filling

The two 5 mm and two 10 mm irrigations of the second irrigation cycle were detectable with the TDR cable (Fig. 27). Due to lower top temperatures, direct evaporation losses were lower than during the former irrigations. Compiling the TDR cable measurements to a contour plot visualized the downward percolation of the water after the second 10 mm irrigation (Fig. 28).

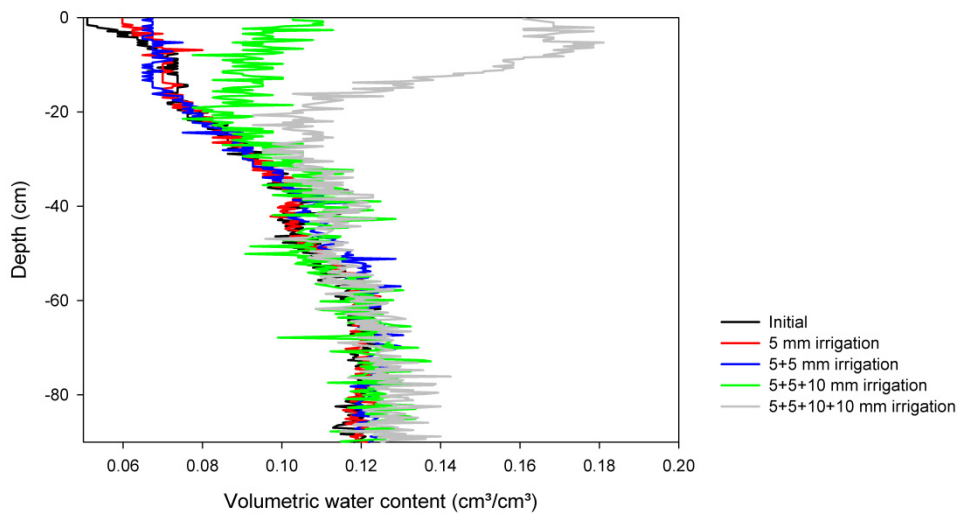


Fig. 27 - Infiltration fronts measured with the TDR cable for irrigation cycle 2 and 3 of the experiments with dune sand filling

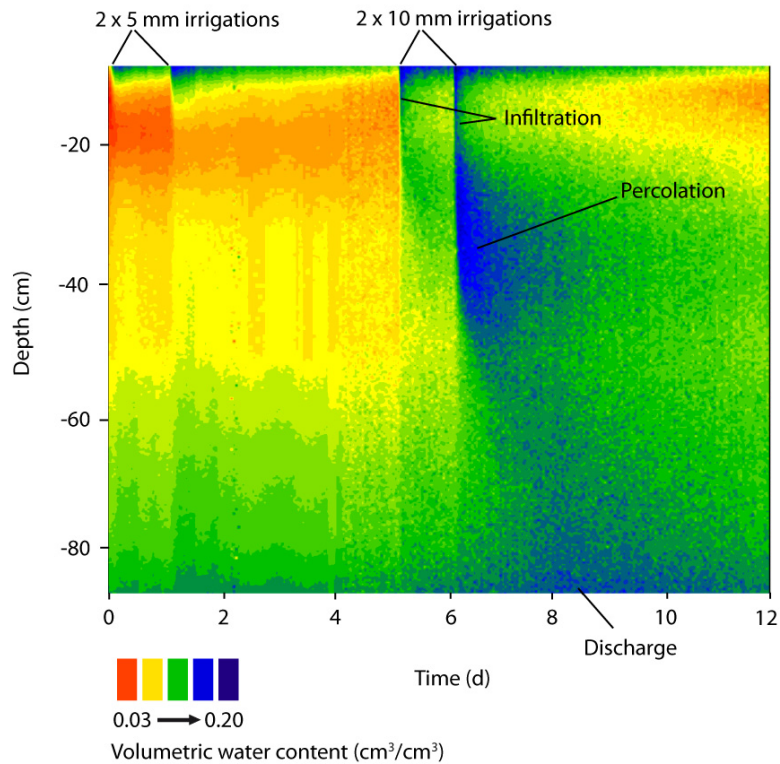


Fig. 28 - Contour plot compiled from TDR cable measurements for irrigation cycle 2 and 3 of the experiments with dune sand filling

During the final irrigation cycle, infiltration fronts reached down to depths of approximately 25 cm with maximum water contents of $0.2 \text{ cm}^3/\text{cm}^3$. Slightly increased irrigation intensity, high irrigation amounts, and low top temperatures decreased water losses by direct evaporation. Discharge was measured for both 25 mm irrigations (Fig. 24) and final soil water storages were lower than initial values (Tab. 11).

Similar to the silica sand experiments, the dune sand experiments showed the high influence of irrigation amount and irrigation intensity on infiltration, evaporation and redistribution patterns. Applying different irrigation and redistribution cycles demonstrated that under high temperatures, low irrigation amounts evaporated very fast and almost completely. Only after irrigations of 25 mm or consecutive 10 mm irrigations within a short time, the sand was wetted sufficiently for drainage at the bottom of the column. Compared to the silica sand experiments, the dune sand had higher retention capacities and thus higher water contents under similar pressure gradients.

When unpacking the column, the uppermost 10 cm of the soil were dry and some cracks were visible on the soil surface. Dried parts of the sand formed blocks, indicating soil aggregation. Soil aggregation can enhance preferential flow by enlarged pores between single aggregates. Especially during high intensity irrigations, water distributes faster through these macropores until the whole aggregates are wetted. It could not be determined, if this was the case during the experiments. Nevertheless, when wetting the aggregates that had formed in the column, with intensities as applied during the former experiments, water distributed immediately throughout the whole aggregate and the soil loosened again.

4.3.3. Layered Column Filling

The layers of the two different sands were clearly distinguishable with the TDR cable, especially during irrigation (Fig. 30). The measured TDR signals displayed the difficulties of interpreting and converting the data into absolute water contents when installing the sensor into layered or heterogenous soil. As both sands had different calibration functions for the conversion of the reflection coefficient to water content, and also slightly different porosities, the TDR signal after column packing appeared heterogenous, even at initially homogenous water contents for both sands. Additionally, the transitions zones between the two layers were not clearly distinguishable and convertible to water content values. Thus, the TDR signals for the layered column filling were evaluated regarding relative changes in water content by means of changes in reflection coefficient rather than directly correlated to absolute water content values. By this, infiltration fronts could be tracked and water flow patterns within the layered system could be qualified. Nevertheless, a conversion of the TDR reflection curve measurements was performed by applying a mixed equation of the silica and the dune sand calibration (Eq. 23). More reliable quantifications were made by means of water balance calculations throughout the whole soil column (Tab. 12).

$$\theta = -1.025 * RC + 0.394$$

Eq. 23 - Mixed TDR volumetric water content calculation from cable reflection coefficient measurements for the layered column settings derived from the single calibration curves of the silica and the dune sand (Eq. 21 and Eq. 22)

Tab. 12 - Water balance calculations of irrigation and drying cycles applied to the experiments with layered sand filling

Time (d)	Cumulative irrigation in (mm)	Cumulative evaporation out (mm)	Cumulative discharge out (mm)	Soil water storage change (mm)
1	25	0.03	0	+ 24.97
7		3.55	0	+ 21.45
8	37.5	3.93	0	+ 33.57
21		8.99	2.3	+ 26.21
22	50	9.34	2.3	+ 38.36
26		12.26	2.3	+ 35.44
27	75	12.65	2.3	+ 60.05
83		23.02	22.32	+ 29.66
84	125	23.14	22.32	+ 79.54
100		32.22	27.85	+ 64.93

With the low initial volumetric water content of 0.04 cm³/cm³, total soil water storage change always was positive. Due to low induced temperatures and relatively high amounts of single irrigations, water losses by evaporation were relatively low. Discharge and evaporation accounted for around one quarter of total irrigation each, whereas highest discharge was measured after the fourth irrigation (Fig. 29). The increase in temperature after the last irrigation yielded increasing evaporation rates.

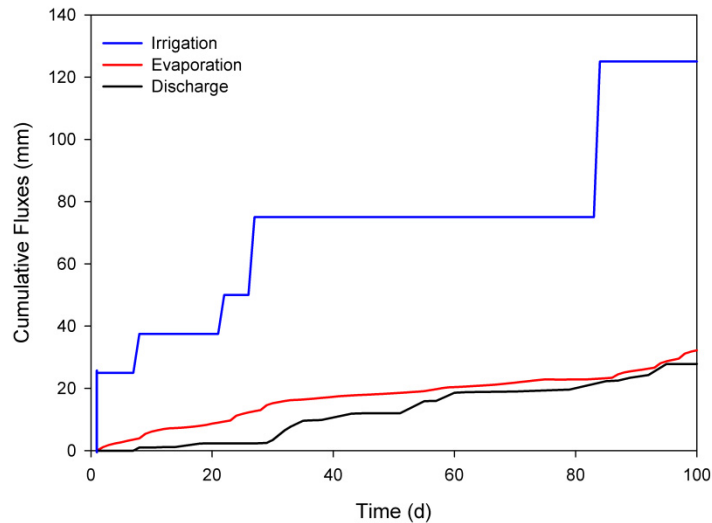


Fig. 29 - Cumulative irrigation, evaporation, and bottom discharge over time for changing boundary conditions applied to the experiments with layered sand filling

The infiltration fronts could clearly be tracked with the TDR cable measurements, especially in the dune sand, where most of the water was retained. Infiltration into and through the uppermost soil layer, which was packed with the silica sand, was relatively fast, whereas the dune sand retained the vertical water flow, forming a distinguishable wetting front (Fig. 30). The finer textured dune sand performed as a capillary barrier. Water flow into the underlying coarser textured silica sand did not occur until, after the second irrigation, water contents reached values high above field capacity. As soon as water infiltrated into the second silica sand layer, faster downward percolation occurred.

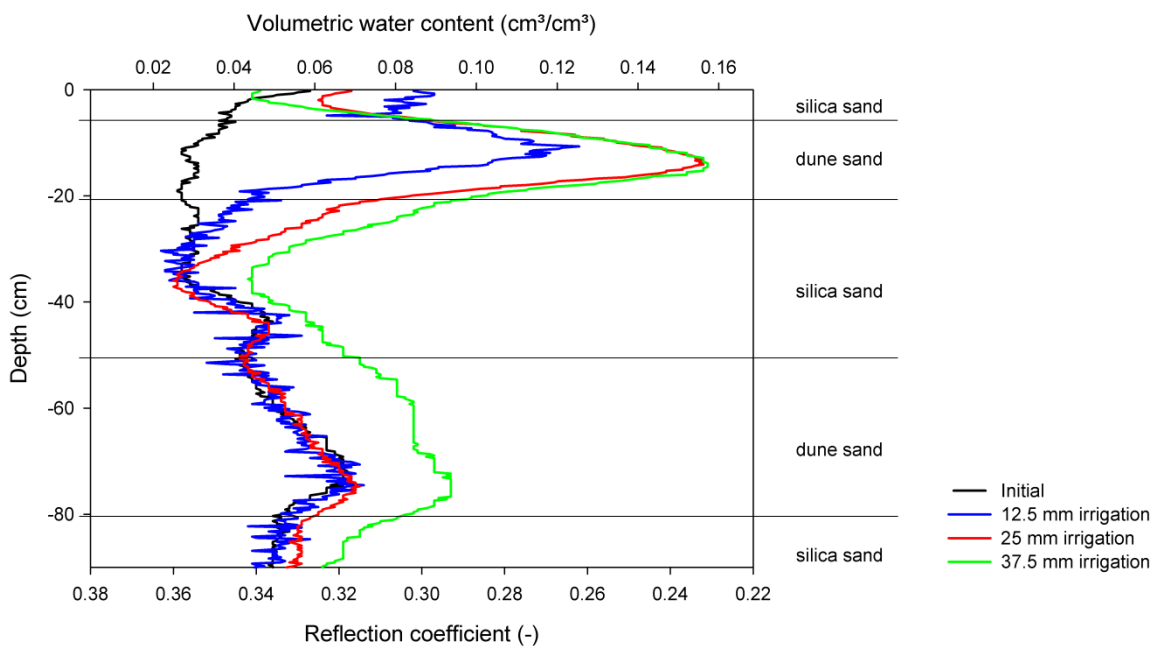


Fig. 30 – TDR cable signals for consecutive irrigation events during experiments with the layered sand packing given as reflection coefficient changes and adapted volumetric water content as calculated from a mixed calibration equation

The water content values, estimated by the mixed calibration equation, were within a reliable range when comparing the first infiltration front with the infiltrated amount of water. Nevertheless, with the uniformly applied conversion equation, the initial measurement still revealed to be heterogeneous, in contrast to the homogenous packing. Possible explanations for this could be either a real downward percolation of water after packing, especially from the silica sand into the dune sand, or signal losses along the silica sand measurements caused by a high amount of air filled pores, leading to an absolute flattening of the curve in depth shown by the lower reflection coefficients.

The 50 mm irrigation infiltration through the upper dune sand layer and percolation through the silica sand layer could also well be traced with the TDR cable measurements. Once again, the wetting front was detained in the lower dune sand layer, at the transition to the silica sand (Fig. 31). Discharge started approximately 28 h after this high irrigation event.

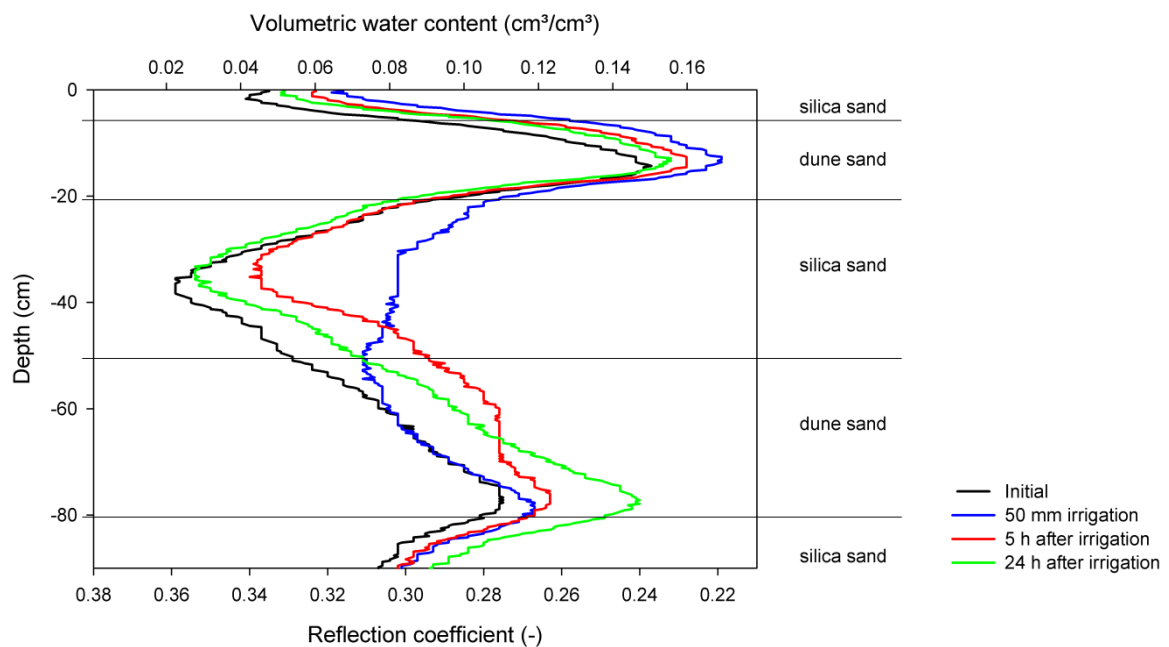


Fig. 31 – TDR cable signals for the 50 mm irrigation during experiments with the layered sand packing given as reflection coefficient changes and adapted volumetric water content as calculated from a mixed calibration equation

The experiments with the layered sand packing showed the high influence of these layers on infiltration and redistribution patterns. The finer grained sand layers acted as capillary barriers and retained much of the infiltrating water. In a 2-dimensional system, probably horizontal water flow would have occurred at the boundaries between the dune sand and the silica sand.

4.4. Numerical Modeling

The numerical modeling included the inverse calibration of the model with experimental data as well as forward modeling with synthetic scenario data to evaluate water, vapor and heat fluxes under transient boundary conditions as they can be expected in arid regions.

4.4.1. Inverse Calibration

For both sands, the PEST instructions had to be modified several times to stabilize the optimization process and obtain a good fit. As the sensitivities of parameters b_1 , b_2 and b_3 , describing thermal conductivity, as well as of the volumetric heat capacity, were up to 10^{15} times lower than those of the other parameters, they were excluded from the optimization process. To account for thermal parameters, and their influence on heat fluxes, a separate calibration, only for temperature distribution was performed. For this, temperature gradient development before irrigation start was inversely calibrated. Fitting was in a reasonable range, whereas especially in the deeper profiles, modeled temperatures did not completely converge with measured temperatures for the dune sand (Fig. 32).

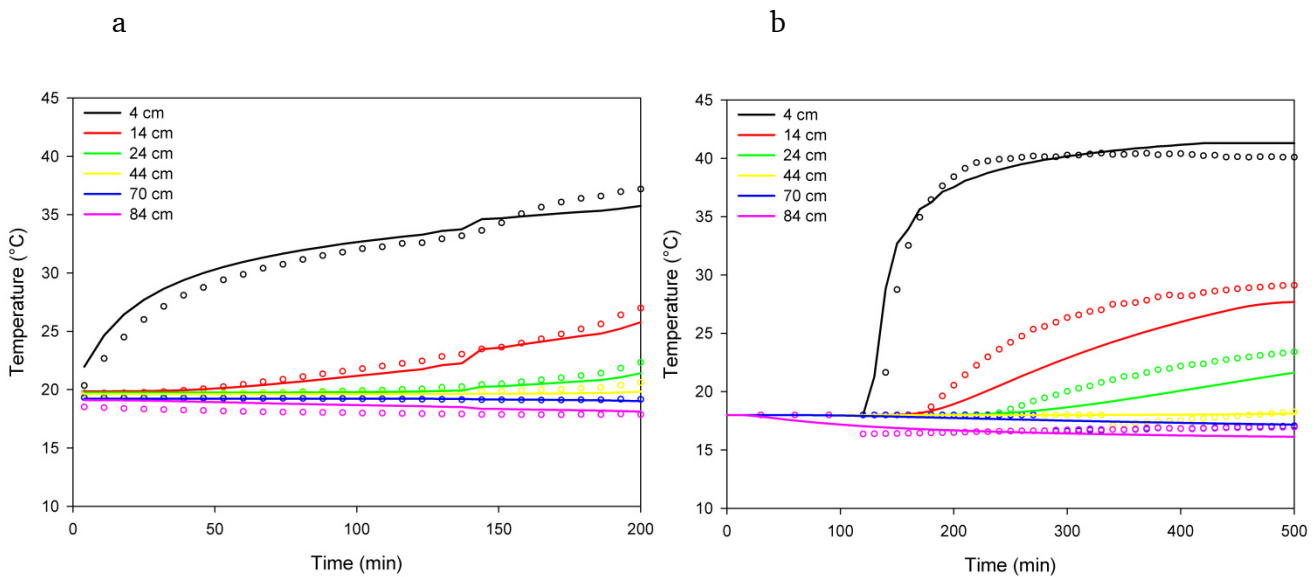


Fig. 32 – Temperature calibration for the silica (a) and the dune sand (b) from steady-state temperature gradient application; measured values are shown in circles, model fit in straight lines

The steeper temperature curves of the dune sand revealed the higher thermal conductivities of the dune sand in the low saturation range. Calibrated values showed that thermal parameters were changed by factors between 0 and 1.8 (Tab. 10). Highest changes were made for the model parameter b_2 during silica sand calibration, which describes the shape of the thermal conductivity curve, resulting in a flatter curve. Reasonable changes in the volumetric heat capacities did not account for better fitting. As the water content was not changed during the calibration of the thermal parameters, the obtained values were handled with care.

Nevertheless, later trials on adjusting temperature measurements under water changing conditions, did not obtain better results.

Tab. 13 - Thermal conductivity parameters according to Chung and Horton optimized for silica and dune sand by inverse calibration

Model parameter	Silica sand		Dune sand	
	Initial	Modeled	Initial	Modeled
b1	0.23	0.23	0.23	0.23
b2	-2.1	-3.7	-5.6	-4.9
b3	5.97	6.28	6.58	6.34

Due to high parameter correlation, some hydraulic parameters had to be excluded from the optimization process. Highest correlations, close to 1 or -1, were found between:

- the saturated water content θ_s and the saturated hydraulic conductivity K_s ,
- the pore size distribution factor n and the tortuosity factor l for the hydraulic models of van Genuchten and Durner,
- the pore size distribution parameter λ and the tortuosity factor l for the hydraulic model of Brooks and Corey, and
- the van Genuchten parameters and the percentage factor w in the hydraulic model of Durner.

The correlation between θ_s and K_s underlined the fact that both are related to the highest saturations within the calibration. The correlation between n and l , and λ and l respectively, accounted for the fact that both parameters are related to the uniformity of the sand material. Following calibration runs were performed with excluding one of the correlated parameters. Thus, final calibrations were performed with maximum 4 parameters, which were α or accordingly h_b , either θ_s or K_s , either n or l , or accordingly λ or l , and θ_r .

When comparing the different initial values obtained from SWRC-Fit for measured and zero residual water content, much better model convergence was obtained for the latter. The high values for n , and respectively λ , increased vertical water fluxes, such that all infiltrated water almost immediately flew through the column, which was not in accordance with measurements. Thus, limiting of value ranges for the parameters that were to be optimized, was oriented along the SWRC-Fit predictions for θ_r equaling zero.

For all tested hydraulic models, the data could best be fitted to the Brooks and Corey model. With the van Genuchten hydraulic model, the whole model run did not converge and no fitting could be obtained for high irrigation amounts, as well as for the dry water content range. The Durner dual domain model also could not be fitted well. Even if it was expected to show good fitting results, especially for the dune sand, the high initial values of the macropore region increased model failure. Additionally, the number of three more parameters to calibrate enlarged the sources of error.

Thus, final calibration runs were only performed for the Brooks and Corey model. For both sands, the silica sand and the dune sand, system behavior for discharge and evaporation could well be simulated. Problems arose mainly for the bottom soil water contents, which were too

high in the model for both sands, accounting for water retention due to the suction plate, respectively the second soil layer in the model.

Figures 33 and 34 show the measured versus modeled results of the silica sand, whereas figures 35 and 36 show the measured versus modeled results of the dune sands. Final results of the calibrated parameters are listed in table 14.

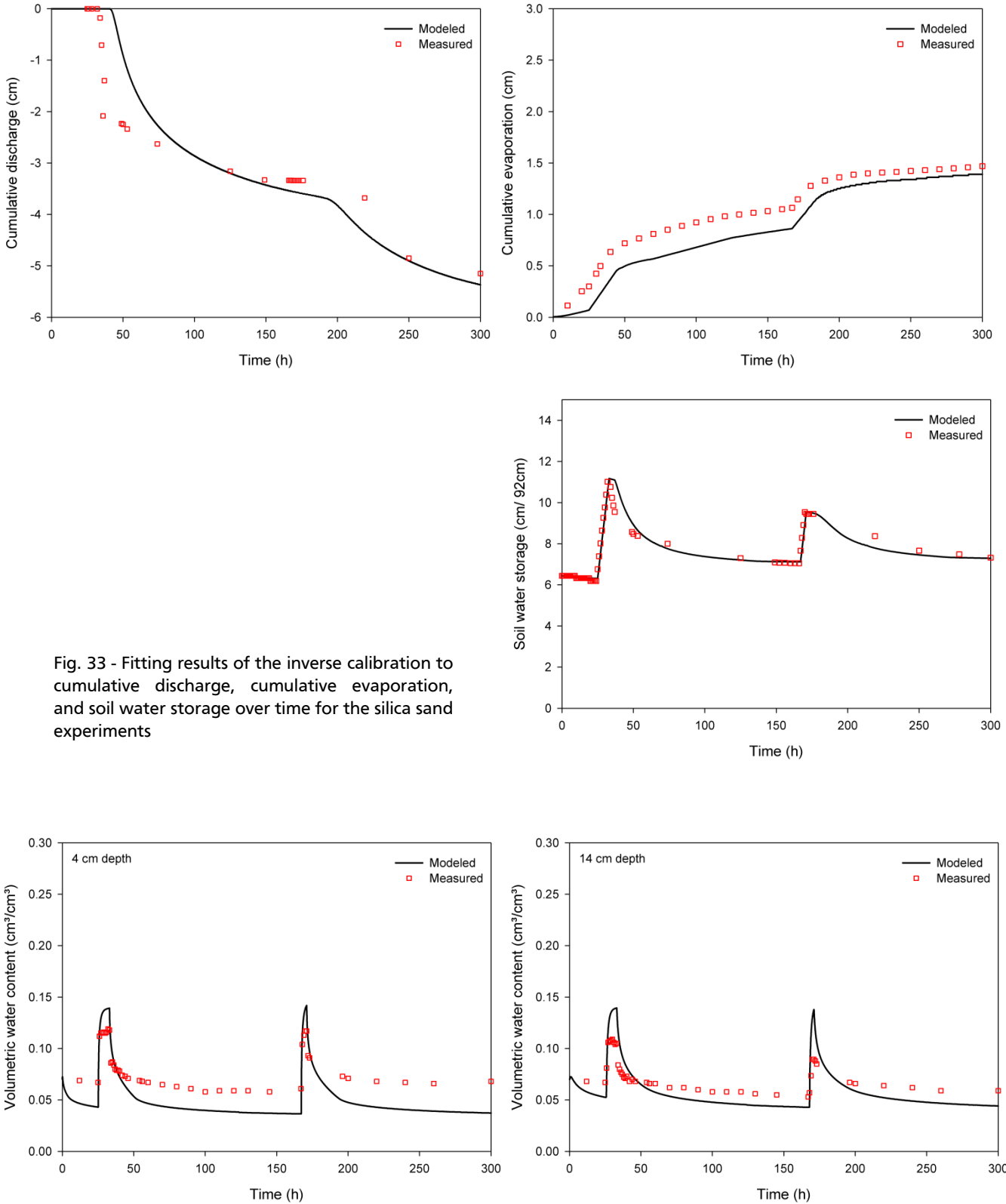


Fig. 33 - Fitting results of the inverse calibration to cumulative discharge, cumulative evaporation, and soil water storage over time for the silica sand experiments

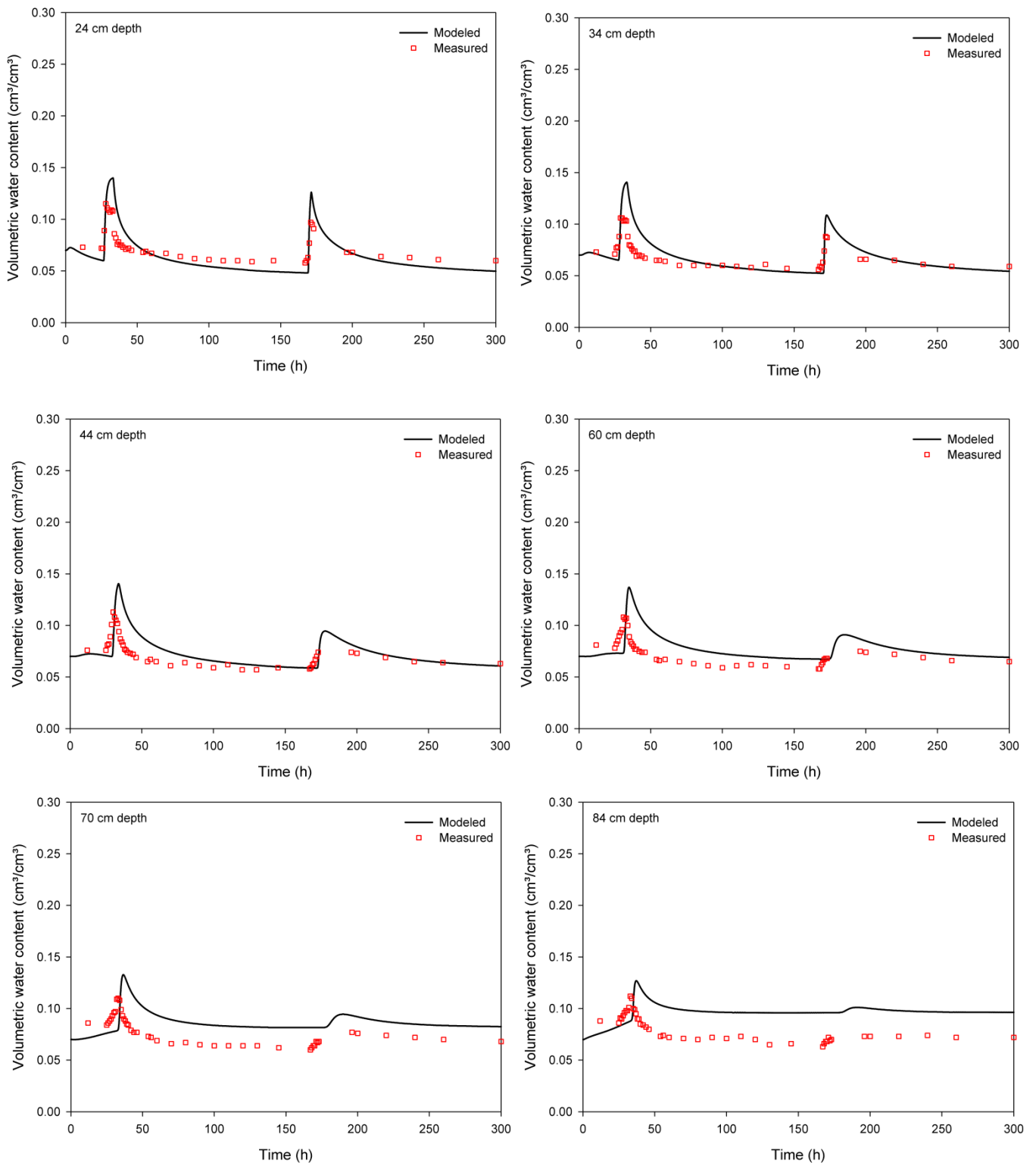


Fig. 34 - Fitting results of the inverse calibration to water content measurements over time in eight different depths for the silica sand experiments

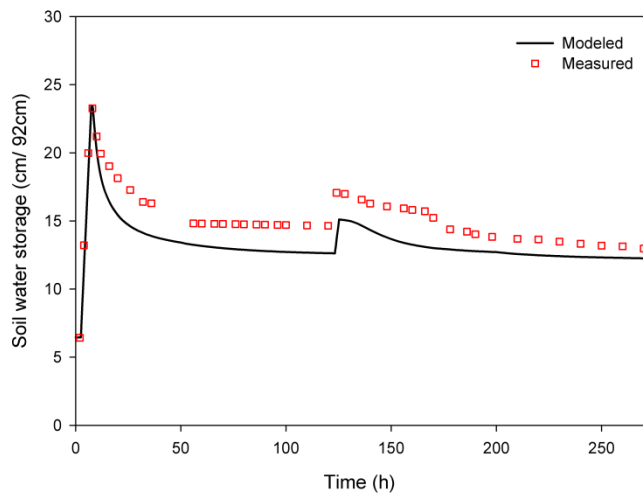
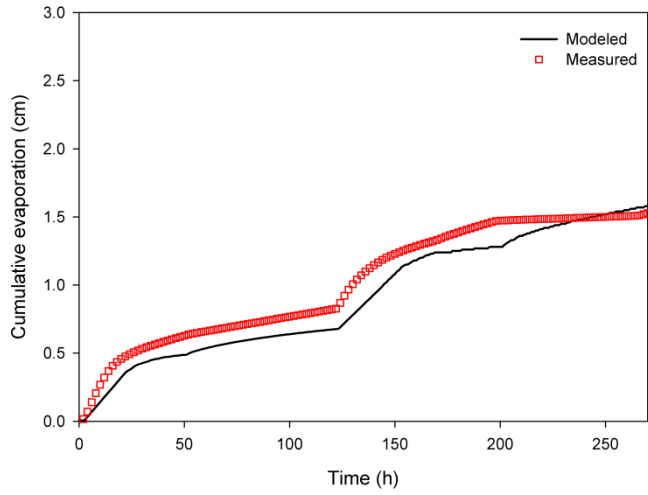
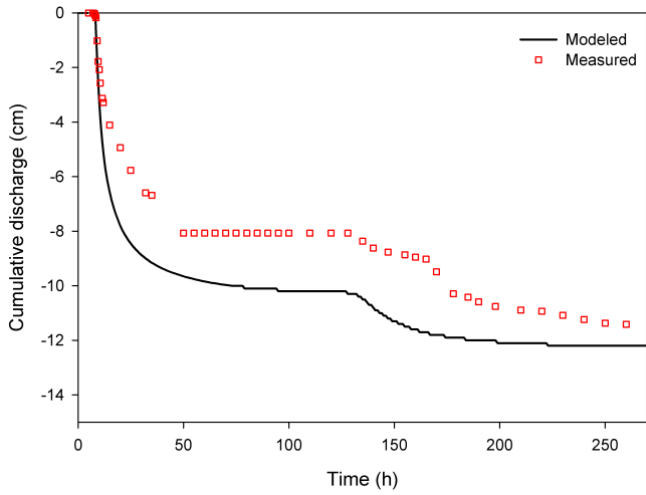
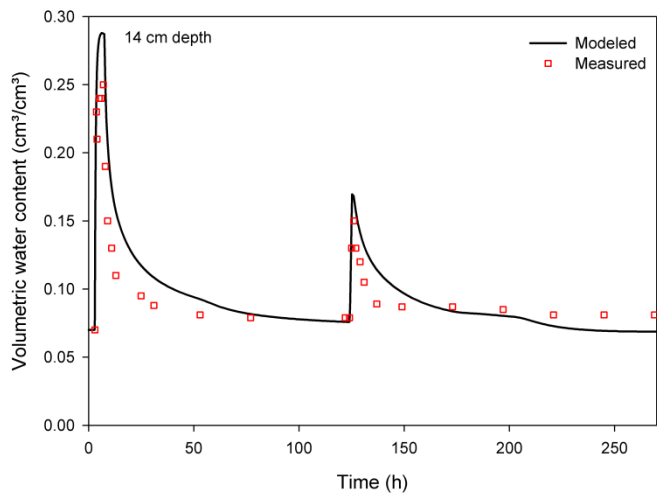
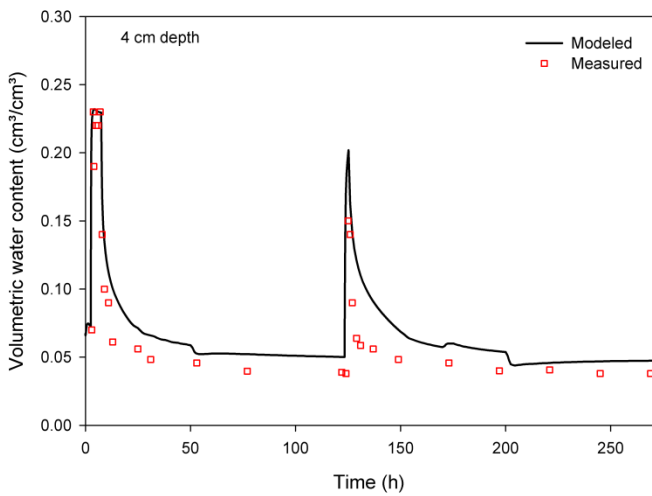


Fig. 35 - Fitting results of the inverse calibration to cumulative discharge, cumulative evaporation, and soil water storage over time for the dune sand experiments



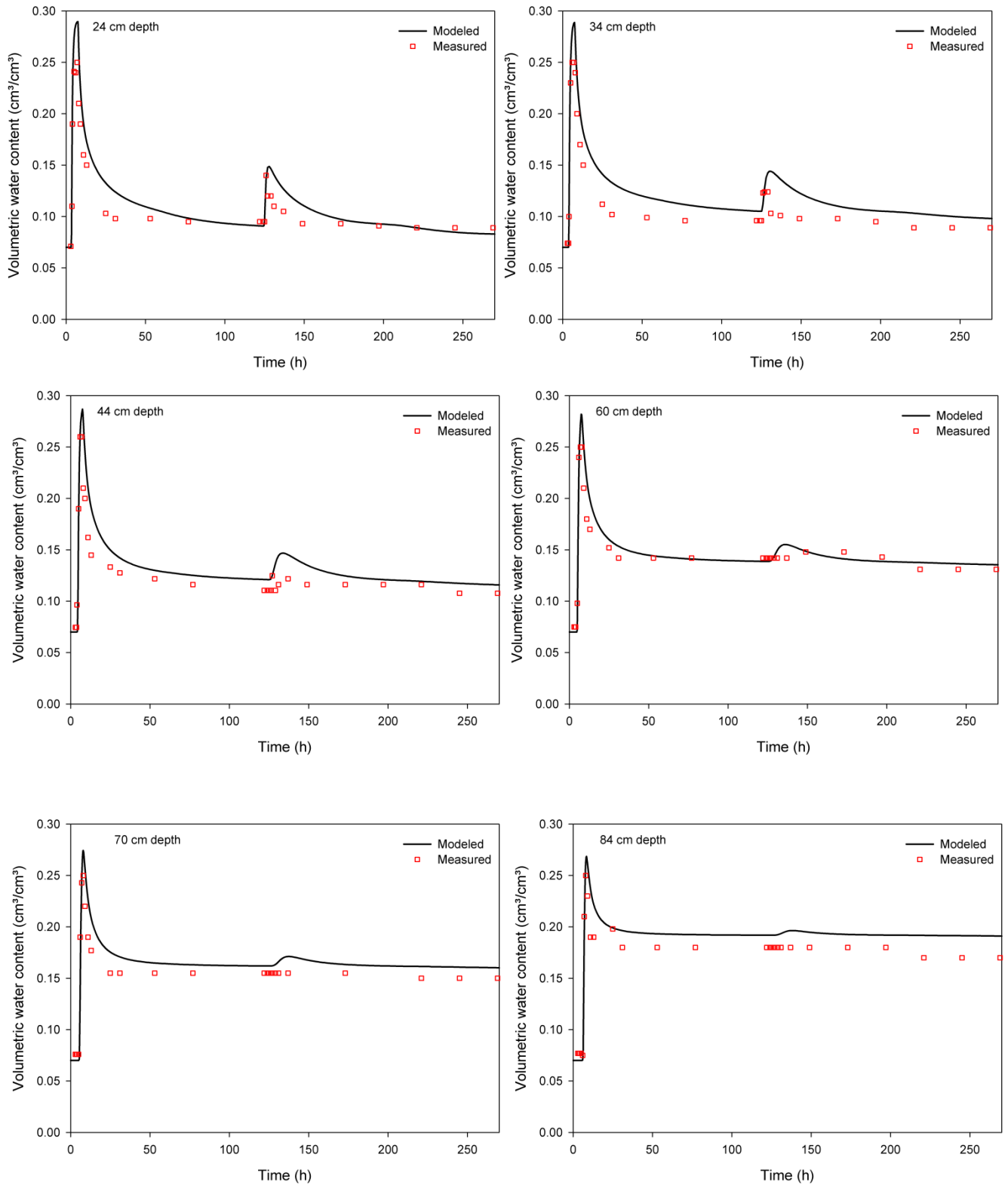


Fig. 36 - Fitting results of the inverse calibration to water content measurements over time in eight different depths for the dune sand experiments

Tab. 14 - Hydraulic parameters from inverse parameter estimation for silica and dune sand – final fitting was performed to the Brooks and Corey model

θ_r = residual water content; θ_s = saturated water content; h_b = air entry pressure; λ = curve shape parameter; ini = initial values obtained from the SWRC-Fit estimation; calib = calibrated values

Sand	Q_r (cm ³ /cm ³)		Q_s (cm ³ /cm ³)		h_b (cm)		λ (-)		K_s (cm/h)		l (-)	
	ini	calib	ini	calib	ini	calib	ini	calib	ini	calib	ini	calib
Silica	0	0.018	0.34	0.35	36.07	32.93	1.20	1.5	46.8	24.5	0.5	0.74
Dune	0	0.009	0.31	0.37	38.22	50	1.27	1.5	26.3	11.9	0.5	1.7

Correlation coefficients R^2 of the final optimization runs were 0.93 for the silica sand fit and 0.97 for the dune sand fit. Evaporation and discharge observations showed good correlations to the model output, especially for the silica sand calibration. The water content observations were generally matched well for the infiltration peaks, regarding breakthrough times as well as highest water contents during infiltration. Drainage velocities were slightly discrepant with increasing depth. For the silica sand, the comparison of measured and modeled soil water storage over time displayed that the measured and modeled water content differences at the soil profile top and bottom counterbalanced, resulting in a consistent water balance. Even if the water content measured and modeled values overall showed better fits for the dune sand calibration, the soil water storage was lower for the modeled than for the measured values during the whole time, resembling the overestimated recharge. Towards the running time end, measured and modeled values converged.

The parameter calibration results of the silica and the dune sand mainly differed in the air entry pressure h_b and the tortuosity factor l . Compared to the measured values, the air entry pressure optimized with a lower value for the silica, and with a higher value for the dune sand. The tortuosity factor l was set significantly higher for the dune sand than for the silica sand. This resulted partly from the smaller and probably more inhomogeneous pores, but could also be an effect of the observed soil aggregation during drying of the dune sand. Physically, setting the tortuosity factor above 1 is incorrect when defining the tortuosity as direct flowing path divided by tortuous path. Nevertheless, as the hydraulic model equations are empirical fitting equations, parameterization does not necessarily rely on physical definitions. The saturated hydraulic conductivity was lowered during optimization, especially for the silica sand, mainly affecting the discharge breakthrough. Within calibration, the saturated hydraulic conductivities of both sands converged, as, for high irrigations, they both showed similar infiltration fronts. With the calibrated saturated hydraulic conductivities, as well as parameters λ and l , the water content - hydraulic conductivity relationship was calculated according to equation 8. The hydraulic conductivity curves are relatively steep, as common for sandy soils, with a high decrease in hydraulic conductivity between a water content of 0.30 cm³/cm³ and 0.10 cm³/cm³ (Fig. 37). Below a volumetric water content of 0.10 cm³/cm³ hydraulic conductivities are close to zero. Overall, the curve of the silica sand is steeper, and hydraulic conductivities are always higher than for the dune sand.

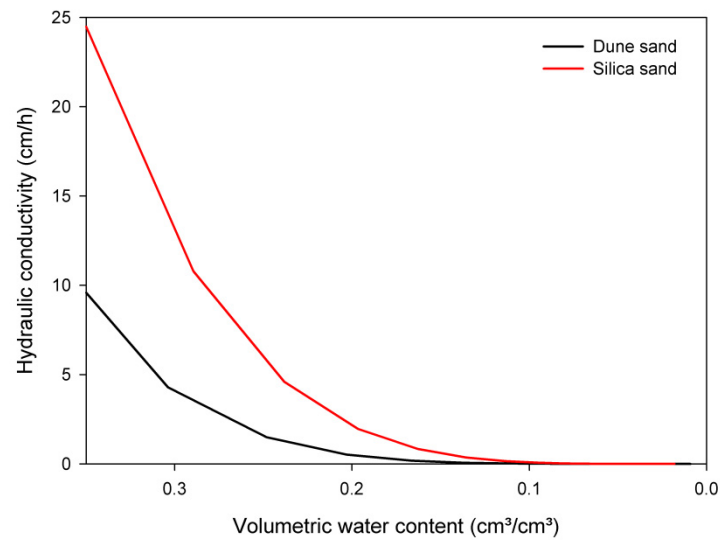


Fig. 37 - Hydraulic conductivity – water content relationship for the silica and the dune sand with values obtained from the inverse model calibration

As the calibration results were in a reasonable range regarding model fit as well as regarding calibrated parameter values, the parameter results were retained for the further predictive modeling.

4.4.2. Sensitivity Analysis

Sensitivity analysis was performed for the calibrated parameters as well as for the observations that were compiled for calibration.

4.4.2.1 Parameter Sensitivities

Within composite parameter sensitivities, the thermal parameters showed lowest sensitivities upon all observations, as well as upon the separately defined observation groups of water content changes in each depth, cumulative evaporation, cumulative evaporation and temperature changes in each depth.

For the hydraulic parameters, sensitivities were generally declining as follows:

$$h_b > \theta_r > \theta_s > \lambda > l > K_s$$

where h_b is the air entry pressure (cm) in the hydraulic Brooks and Corey function, θ_r is the residual water content (cm³/cm³), θ_s is the saturated water content (cm³/cm³), λ is the Brooks-Corey retention curve shape parameter (-), l is the conductivity function tortuosity factor (-), and K_s is the saturated hydraulic conductivity (cm/s).

Figure 38 a-c show the composite parameter sensitivities for each type of observation group (cumulative discharge, cumulative evaporation, water content and temperature) for the dune

sand optimization. The silica sand optimization gave comparable results with the same order of magnitude and h_b as the most sensitive parameter. The sensitivity coefficients were normalized to the observation data values.

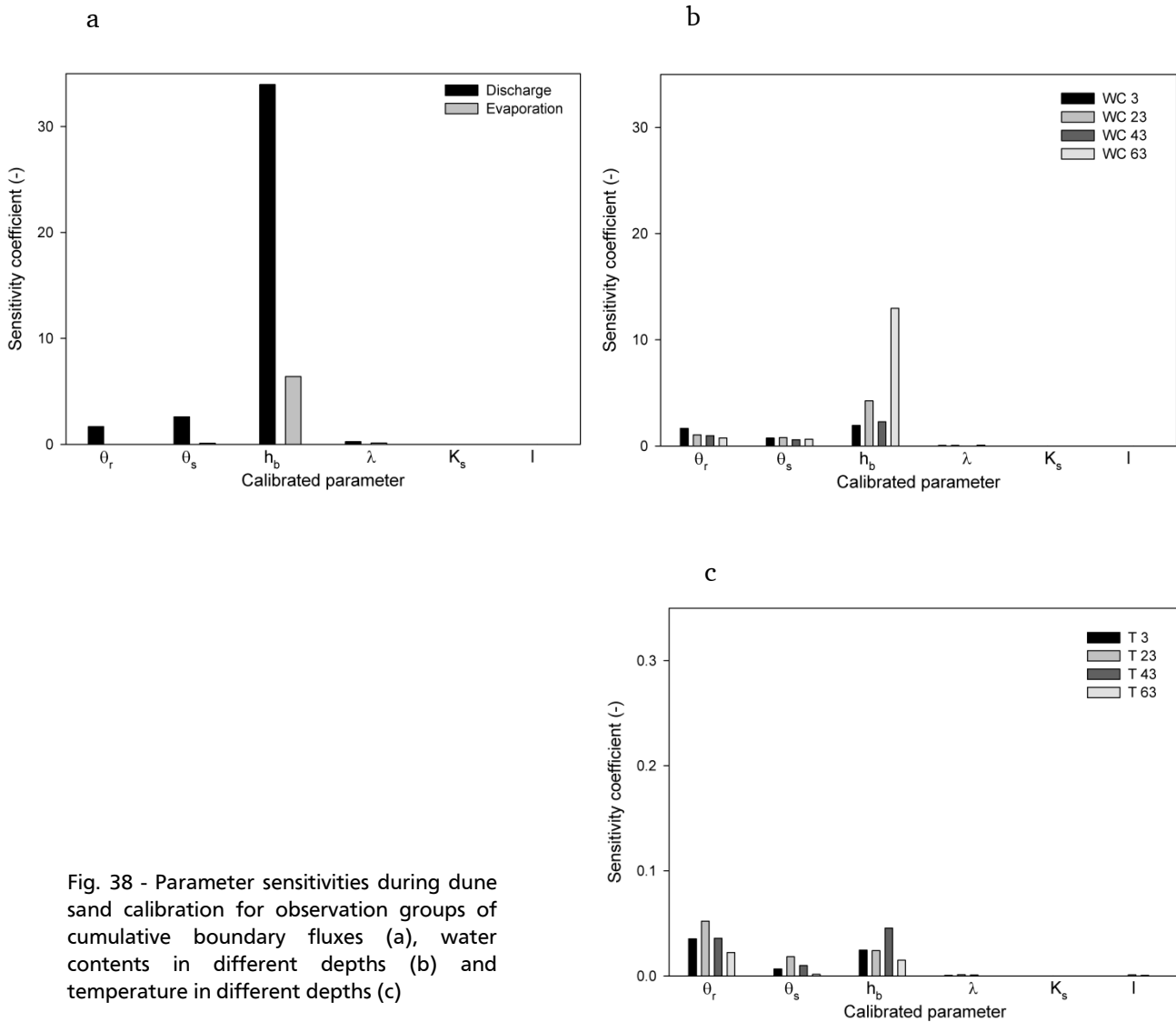


Fig. 38 - Parameter sensitivities during dune sand calibration for observation groups of cumulative boundary fluxes (a), water contents in different depths (b) and temperature in different depths (c)

Parameter sensitivities for the temperature observations were roughly two orders of magnitude lower than for other observations. The discharge observation group had highest parameter sensitivities, displaying the high importance of boundary flux measurements.

For the temperature measurements, residual water contents had a higher sensitivity coefficient than the air entry pressure in some depths, as the thermal conductivity is highly dependent on water content. Overall, the high sensitivities of air entry pressure and residual water content indicated the high importance of parameters that determine evaporation and water fluxes under low water saturations, rather than those determining highly saturated water fluxes, like saturated hydraulic conductivity K_s and the curve shape parameter λ , for the experimental conditions.

The composite sensitivity for all observations, as compiled in figure 39, once again demonstrated the high sensitivity of the air entry pressure. When considering all observation groups, the saturated and the residual water content almost equaled, due to the higher sensitivity of the saturated water content for discharge observations.

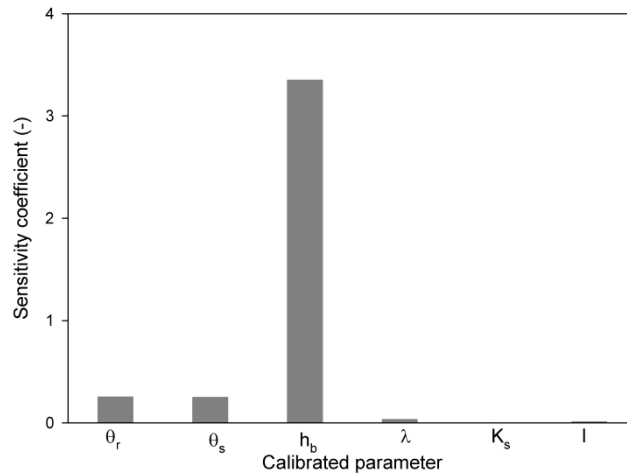


Fig. 39 - Composite parameter sensitivities during dune sand calibration for all observation groups

4.4.2.2 Observation Sensitivities

Observation sensitivities for water content observations all showed similar patterns (Fig. 40). Sensitivities were normalized to the measured water content values. Highest sensitivities were reached as soon as the infiltration front reached the corresponding observation depths. Shortly after, when the soil in the observation depth was sufficiently wetted for gravitational downward water flow, sensitivity dropped down close to zero. As soon as capillary forces were acting on water flow again, sensitivities of the observation points increased, probably until vapor fluxes dominated and overall fluxes were close to zero. Regarding depths, sensitivities increased with depth during gravitational and capillary flow times, whereas they decreased with depth for the infiltration breakthrough as well as during drying, where fluxes were close to zero and vapor fluxes were expected to lead to drying in the upper soil profile.

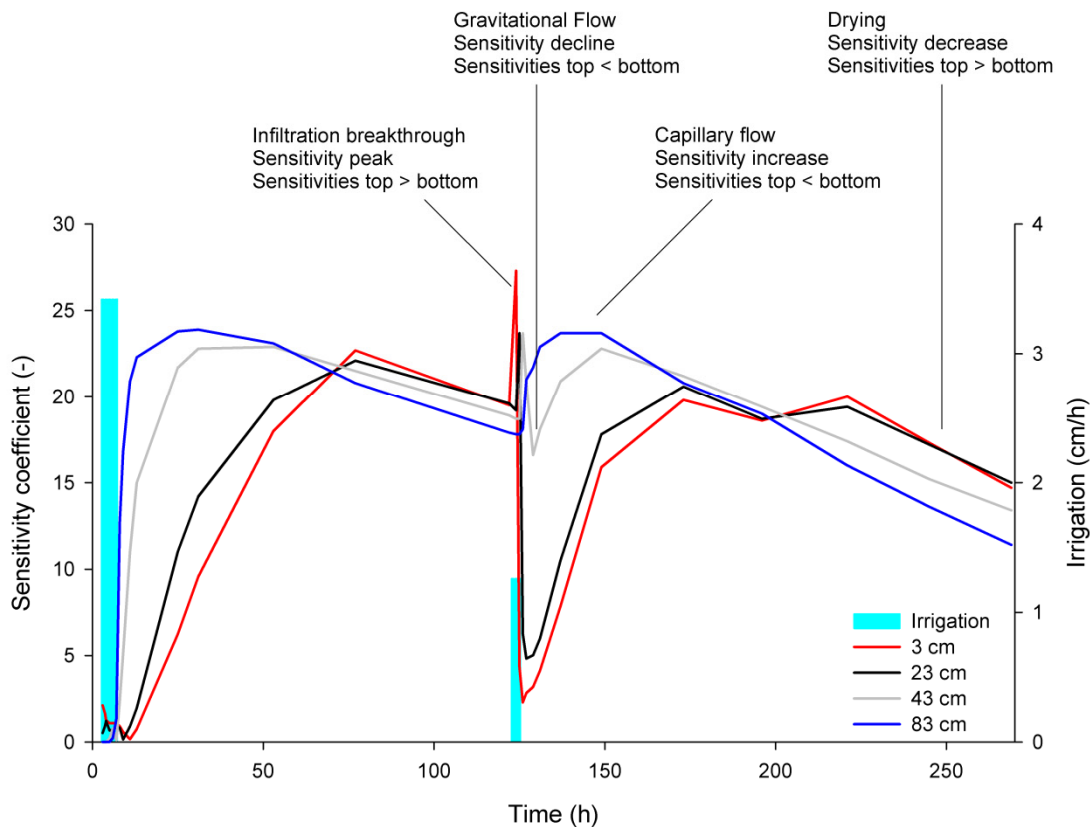


Fig. 40 - Observation sensitivities during dune sand calibration for water content in different depths over time

Temperature observations showed sensitivities similar to those measured for water contents. For evaporation, sensitivities increased simultaneously with the increase in cumulative evaporation. During irrigation, sensitivities dropped, as evaporation during irrigation was constrained by the potential evaporation and not by the hydraulic soil parameters. As soon as water content at the soil surface dropped below water availability for potential evaporation and thus the actual evaporation was constrained by soil parameters, sensitivities increased again (Fig. 41 a). Discharge observations had an extremely high sensitivity for discharge breakthrough from the first irrigation (Fig. 41 b). This one value sensitivity was two orders of magnitude higher than the other discharge sensitivities and the water content and evaporation sensitivities. Discharge breakthrough from the second irrigation had an increased sensitivity as well, but with the same magnitude as the other measured observation sensitivities.

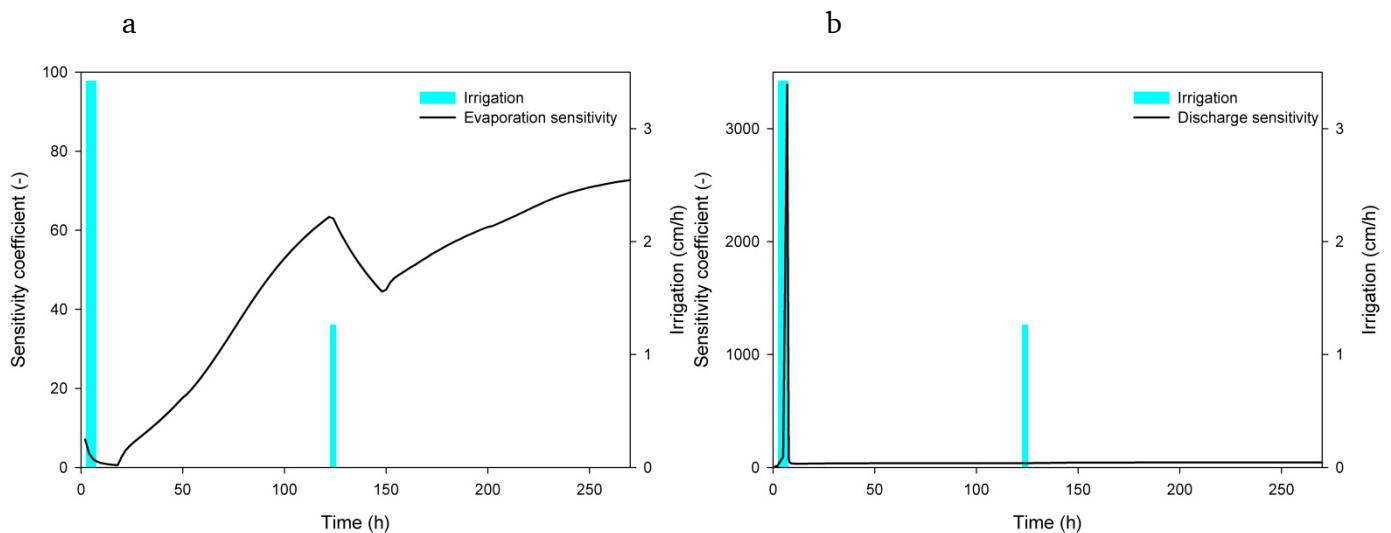


Fig. 41 - Observation sensitivities during dune sand calibration for cumulative evaporation (a) and cumulative discharge (b) over time

The observation sensitivities indicated the importance of measurements during drainage and drying conditions. Measurements during irrigation were only of minor importance regarding model parametrization for displaying the system behavior.

4.4.3. Predictive Modeling

The predictive modeling aimed at analyzing the influence of changing boundary conditions on water infiltration, evaporation and redistribution patterns. The boundary conditions included data of real meteorological data, as measured in arid regions, as well as exaggerated modifications on single parameters to identify driving parameters upon the results. If not indicated elsewhere, the predictive modeling was performed with the hydraulic and thermal parameters obtained from the model calibration for the Brooks and Corey hydraulic model. Most of the scenarios were run with the dune sand calibrated parameter values.

4.4.3.1 Initial and Boundary Conditions

The boundary conditions that were changed for the predictive modeling were tested upon the effect on infiltration, drainage and evaporation for the two stage irrigation model run used for the calibration of the dune sand.

The changed boundary conditions did not change the overall system behavior regarding infiltration fronts and redistribution patterns. Nevertheless, inserting the free flow boundary illustrated the retention behavior of the suction plate within the experiments. Figure 42 a shows the modeled water content profile shortly before discharge breakthrough of the original model run. Curves display the infiltration curve for the model run with experimental boundary conditions, the free drainage boundary condition in the 92 cm model and the enlarged 200 cm model without the suction plate. The infiltration patterns equaled for all

three simulations, whereas at the bottom of the two 92 cm simulations, higher bottom water contents indicated water retention. During redistribution, this effect increased (Fig. 42 b). In the 200 cm model, water homogenously percolated downward. In the 92 cm models, water already discharged at the bottom, but water was retained by the suction plate due to the different flow conditions of the plate material. Thus, with the free flow boundary, bottom water contents were lower than during the experiments and homogenous water contents throughout the whole soil profile were reached after drainage.

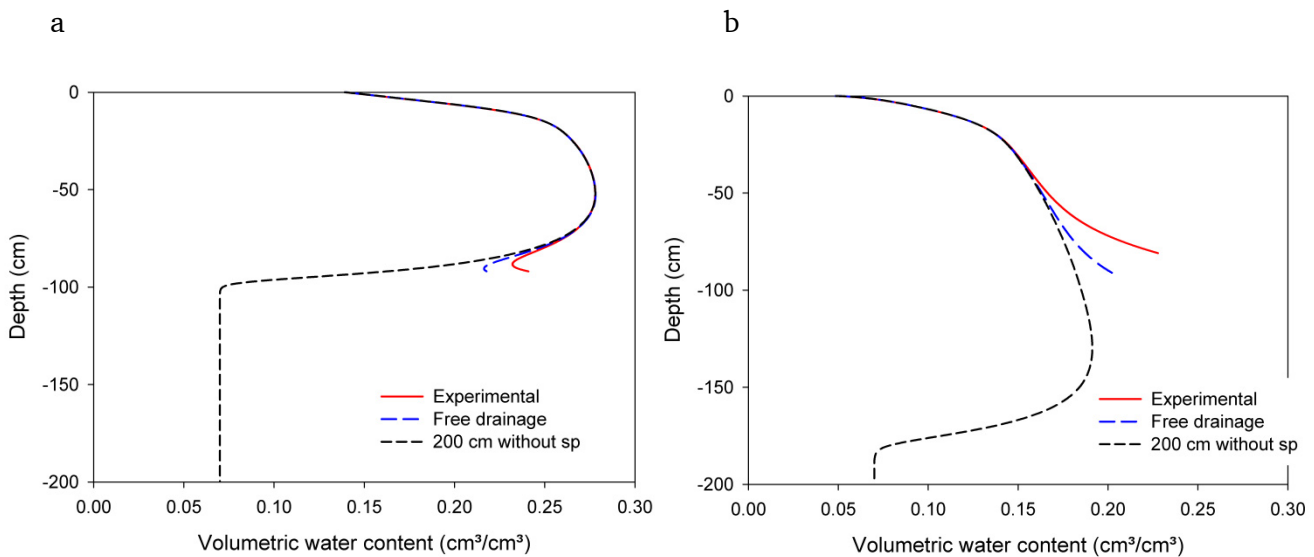


Fig. 42 - Comparison of infiltration fronts for changed scenario boundary conditions – 92 cm with suction plate and seepage face (experimental) versus 92 cm with suction plate and free drainage, versus 200 cm with free drainage without suction plate (sp); water contents were taken after infiltration (a) and 10 h redistribution (b) for the dune sand calibration experiment

As no water retention was obtained with the changed boundaries, overall discharge was slightly higher for the model calibration conditions, even if the profile length was doubled (Fig. 43 a). Evaporation patterns did not change for the changed boundary conditions (Fig. 43 b).

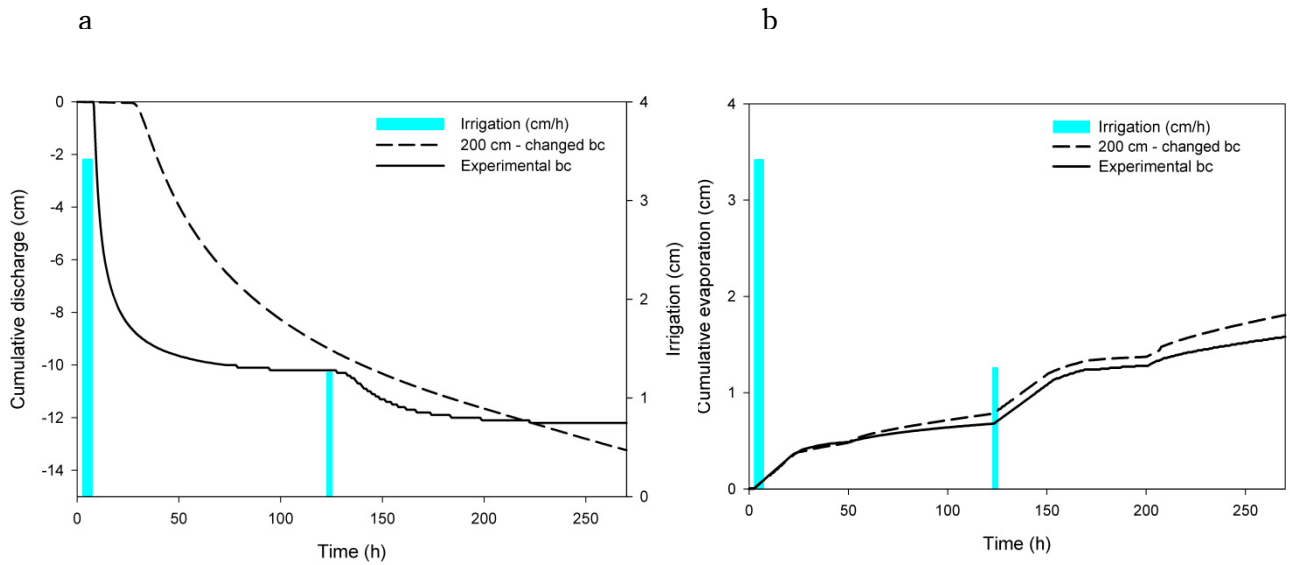


Fig. 43 - Comparison of cumulative discharge (a) and cumulative evaporation (b) for experimental boundary conditions (bc) and changed boundary conditions with a 200 cm profile for predictive modeling

Due to the increased discharge without the suction plate boundary, no discharge disruption occurred during the two modeled irrigation events. Evaporation slightly increased with the 200 cm boundary conditions, which was likely due to a decreased thermal gradient and thus decreased downward thermal vapor fluxes during drying times. Implementing diurnal temperature changes did not change the trend and total evaporation amount, but resulted in higher daily fluctuations. These fluctuations were observed in the upper 10 cm for water content and temperature.

Initial water content and temperature distribution that were used for the predictive modeling, were obtained from a 90 days model pre-run (Fig. 44) with no irrigation and an applied top temperature of 14 °C.

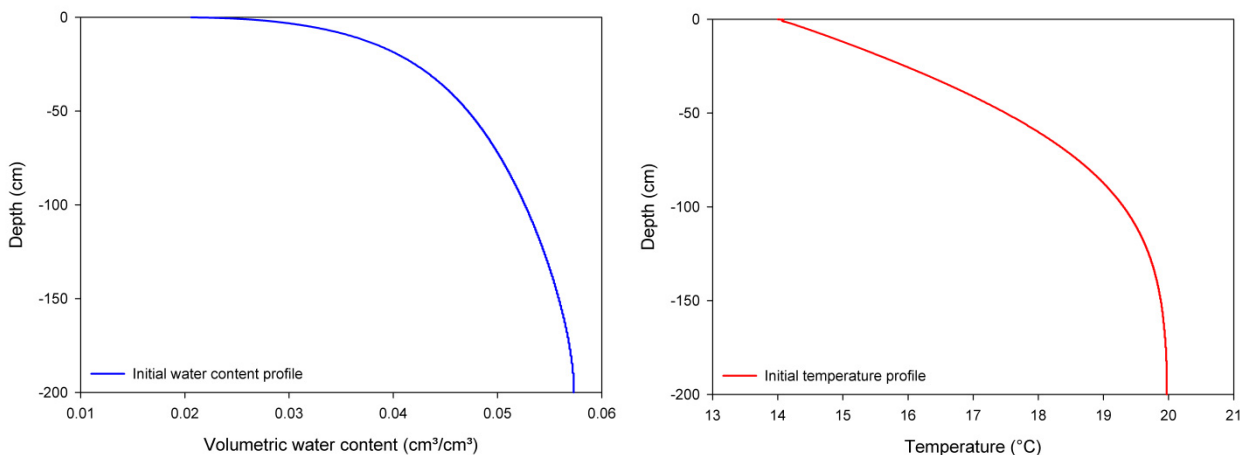


Fig. 44 - Initial water content and temperature distribution conditions for the predictive modeling as obtained from a 90-days steady-state model pre-run

The obtained profiles that were chosen as initial profiles for the annual scenario modeling, only resembled quasi steady-state conditions. Due to a temperature gradient and the calibrated low residual water content as soil property, a continuous discharge at the bottom boundary was identified. This could only be prevented if the model was run without any precipitation for more than 10 years, or by setting the initial water content to $0.01 \text{ cm}^3/\text{cm}^3$. Both conditions were expected to be less realistic than the gradually increasing water content with depths. For the predictive modeling it has to be kept in mind that modeled bottom discharge did not resemble groundwater recharge but downward water percolation beyond the modeled depth of 200 cm.

4.4.3.2 Monthly Scenarios

The monthly scenarios were run prior to the annual scenarios to reflect the effect of extremely differing boundary conditions. Here, initial water contents were homogenous, as the scenarios aimed at water balance differences between the scenarios and not at absolute water balance amounts.

The short time scenarios clearly showed that monthly averaged or cumulated values for precipitation can result in high errors regarding evaporation and recharge calculations. Whereas the single precipitation event of 50 mm resulted in 3.5 mm bottom flux, the 5 x 10 mm irrigation events with 3 days drying in between only resulted in 1 mm bottom flux (Fig. 45 a) due to a much higher loss in evaporation (Fig. 45 b).

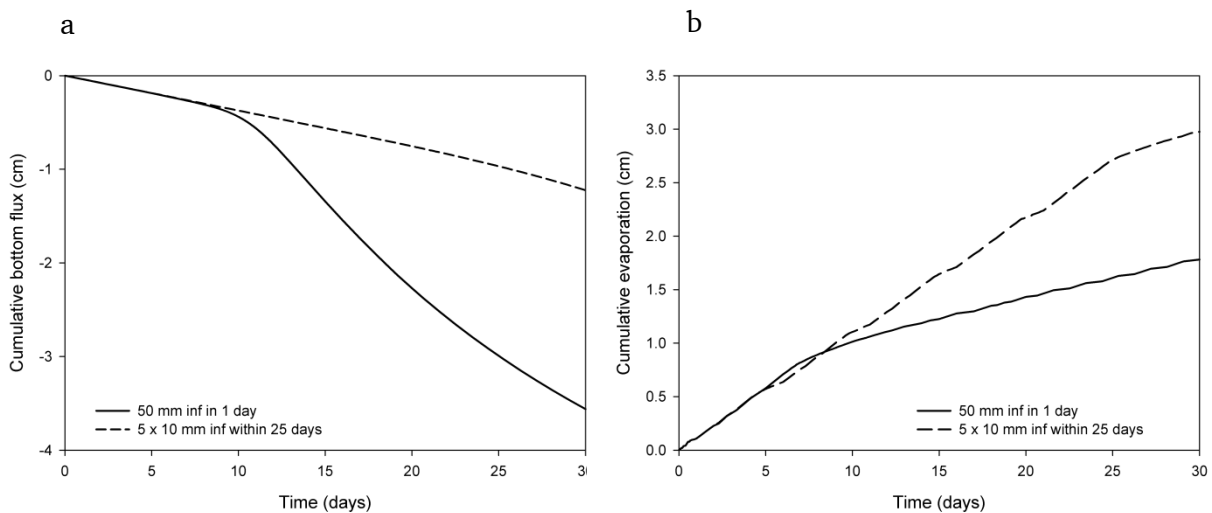


Fig. 45 - Cumulative discharge (a) and cumulative evaporation (b) compared for 50 mm precipitations as of 50 mm within one day and 50 mm within 25 days with 5 times 10 mm precipitation and 5 days drying between each event

Dividing the 50 mm precipitation upon 10 days resulted in bottom fluxes and evaporations between the 1 day and 25 day scenario. No significant differences resulted from the comparison of 10 consecutive days with 5 mm precipitation and 10 days with alternating 1 day of 10 mm/d precipitation and one day without precipitation.

When comparing the different wetting fronts, each taken after the final event and thus after a total of 50 mm precipitation, the single event showed the highest water contents within the wetting fronts whereas the wetting fronts of the two 10 days precipitations were deepest within the profile. The lowest intensity precipitation left a clear wetting front after the last event within the upper 24 cm. Nevertheless, the redistribution and downward movement of the former events resulted in an overall increased water content within the profile down to a depths of around 180 cm (Fig. 46).

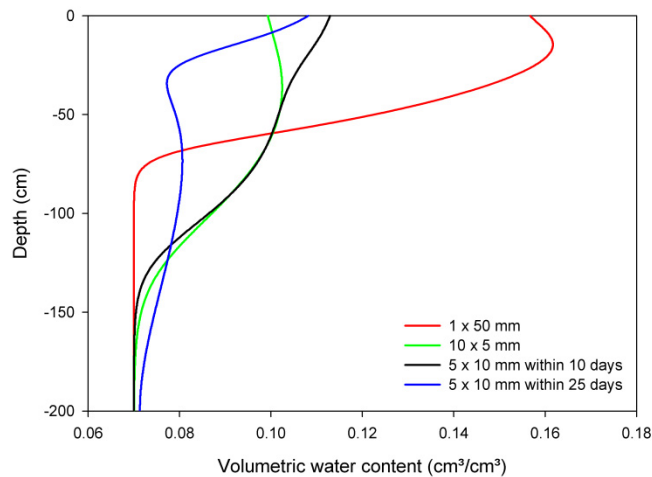


Fig. 46 - Infiltration fronts compared for 50 mm precipitations of different monthly patterns with 50 mm in one day, 50 mm in 10 consecutive days, 50 mm with alternating 1 day of 10 mm precipitation and 1 day drying, and 50 mm with alternating 1 day of 10 mm precipitation and 4 days of drying

These scenarios exaggerated natural precipitation patterns. Nevertheless, when considering monthly or even annual totals of precipitation for groundwater recharge, precipitation intensities highly influence predictions, especially for direct groundwater recharge.

Reversed temperature gradients of 30 °C compared to 8 °C top temperature with both a bottom temperature of 20 °C influenced infiltration and redistribution patterns for the low precipitation of 10 mm. In low saturated conditions, thermal vapor fluxes played an increasing role upon total water fluxes. Thus, infiltrated water moved downward faster with a higher top temperature, whereas upward water movement occurred during the drying phase for the lower top temperature (Fig. 47).

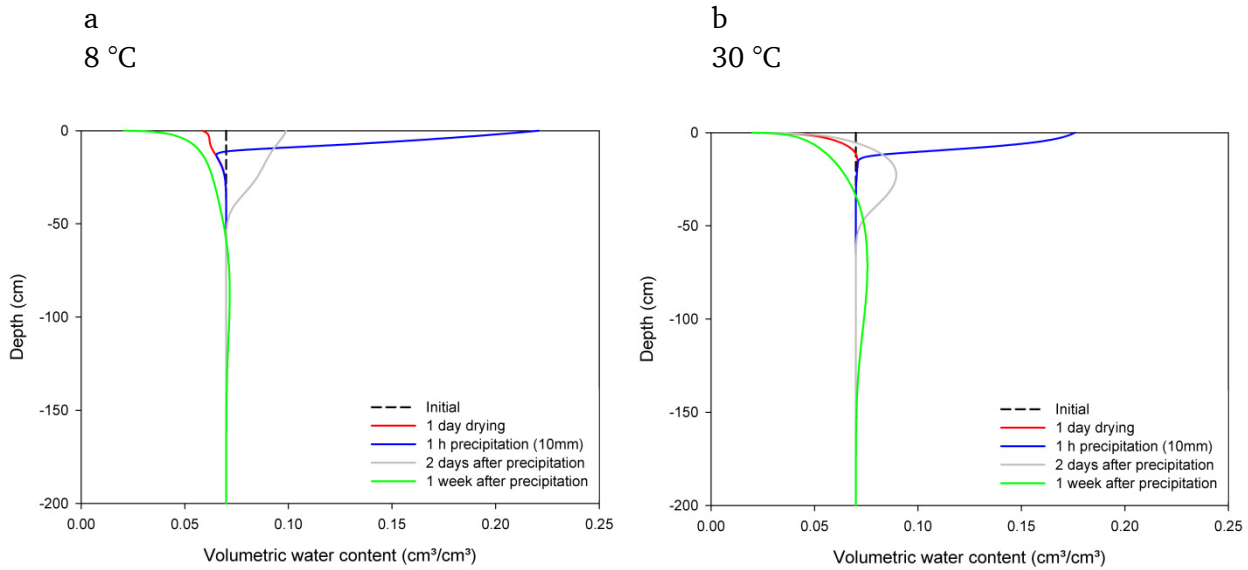


Fig. 47 - Water content profiles with initial homogenous water content for 1 day drying, 10 mm precipitation and drying after precipitation with top temperature of 8 °C (a) and 30 °C (b) and bottom temperature of 20 °C

Regarding evaporation, with an upward thermal water and vapor flux, the evaporative water demand at the soil surface could be served much longer than with the downward thermal water and vapor fluxes when top temperatures were high. With the high top temperature, initial evaporation at the soil surface was higher, but as soon as the upper soil layer was dry, evaporation slowed down and converged to zero. Thus, the soil water storage decreased and was lower for the low top temperature conditions than for the high top temperature conditions (Fig. 48).

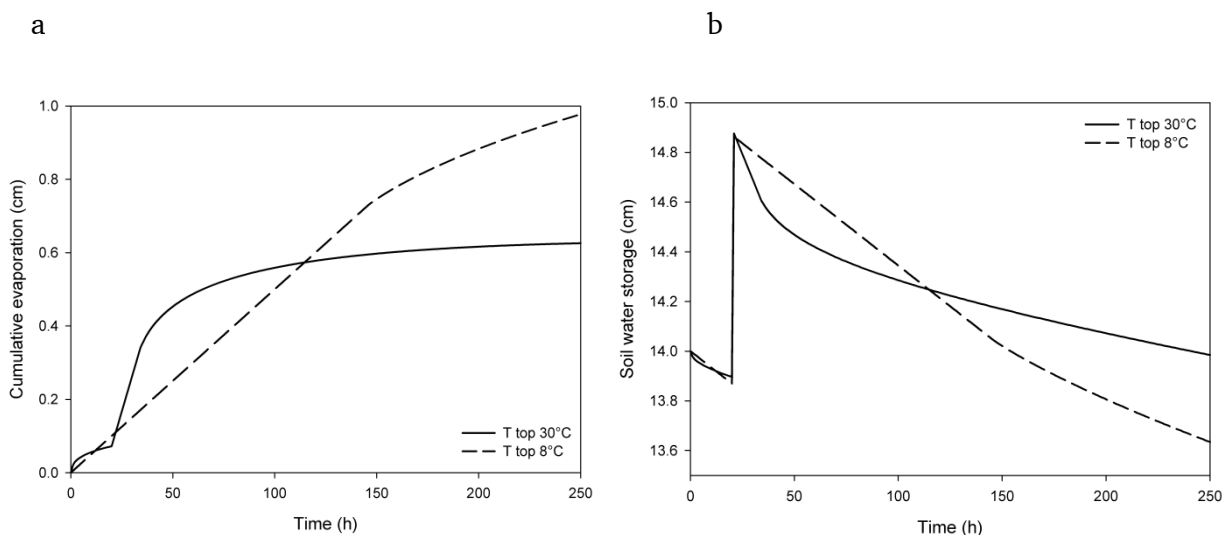


Fig. 48 - Cumulative evaporation (a) and soil water storage (b) for 10 mm precipitation compared for a top temperature of 30 °C and a top temperature of 8 °C with a bottom temperature of 20 °C for both

Here again, conditions were highly exaggerated compared to natural conditions. By not changing the air relative humidity, a continuously high potential evaporation was enforced. Additionally, the temperature gradient with the low top temperature was relatively steep, with a difference of 12 °C within 2 m.

4.4.3.3 Annual Scenarios

Running the annual scenarios with different hydraulic properties as calibrated for the silica and the dune sand and synthetically obtained for 100 % pure sand did show similar patterns for infiltration, evaporation and bottom discharge for the three reference scenarios with high, moderate and low annual precipitation amounts. Nevertheless, as the synthetically derived sand properties had the largest residual water content with 0.02 cm³/cm³ soil water retention was highest in this soil. Thus, whereas in the two calibrated soils, discharge emerged already from the initial water content, water was retained in the soil with hydraulic properties obtained synthetically for pure sand. Continuous bottom discharge could only be prevented with an initial water content close to residual water content. Evaporation was within the same range for the high flux and moderate flux reference scenarios for all the three sand properties. Nevertheless, it was lowest for the silica sand with about 1-5 % lower evaporation, likely due to faster infiltration.

For the high flux scenario, bottom water flux emerged almost instantly after the high precipitation event and total flux accounted for most of the total high precipitation amount of 48 cm, at least for the silica sand and dune sand hydraulic properties (Fig. 49 a). When running the same scenario with calibrated dune sand properties with a dry initial soil profile, bottom flux also started soon after the high precipitation event (Fig. 49 b). Total bottom flux was lower accounting for the wetting of the soil that was needed for continuous water flow.

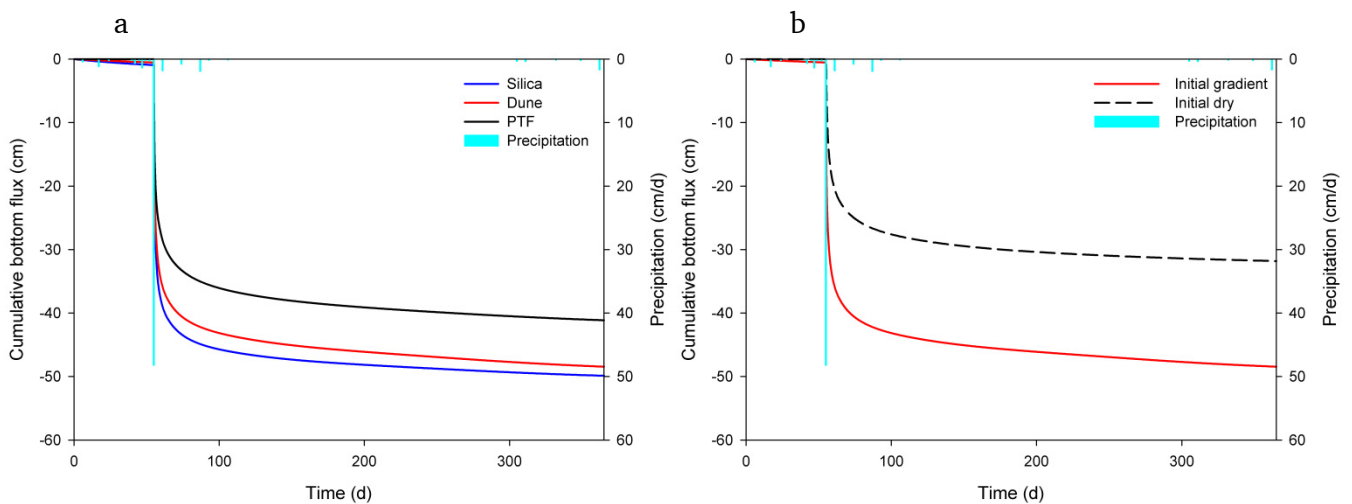


Fig. 49 - Cumulative bottom fluxes and cumulative evaporation fluxes for three tested sand properties for high flux scenarios with initial gradient water content (a), and compared for the dune sand with initial dry water contents (b)

Due to the several factors influencing the discharge, it was not possible to determine one single threshold value. The importance of a specific threshold upon discharge directly caused from one precipitation event already had been pointed out when discussing changed precipitation patterns. With the initially dry conditions, only precipitation amounts of more than 80 mm resulted in bottom flux, resembling the moderate annual precipitation reference scenario (Fig. 50). Water content profiles at the end of the moderate annual precipitation run with initially dry conditions showed a water content gradient comparable to the initial water content after the model pre-run (Fig. 51). Thus, if not having complete dryness over several years, some wetting and deep percolation in the soil profile can be expected continuously.

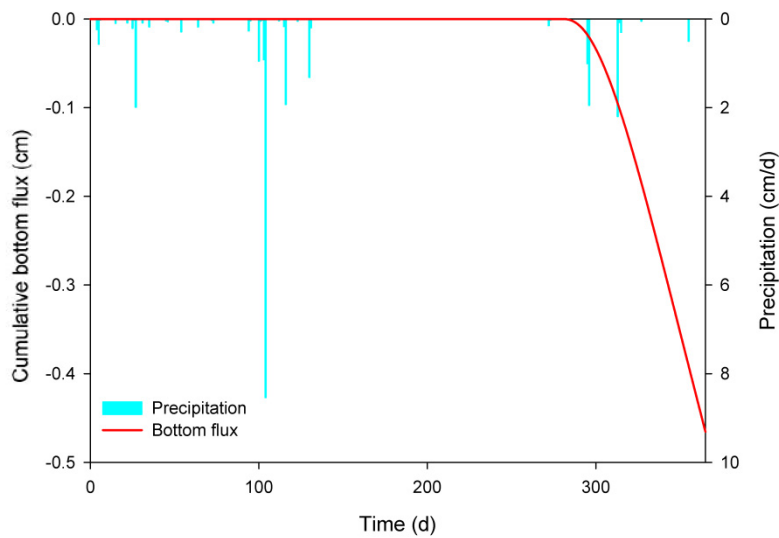


Fig. 50 - Cumulative bottom fluxes for dune sand properties during moderate flux annual reference scenario with dry initial conditions

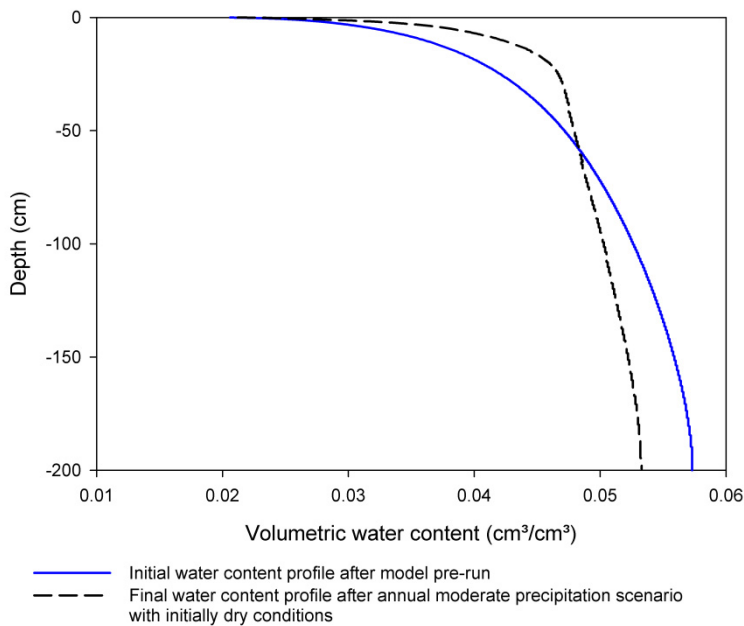


Fig. 51 - Water contents for initial scenario modeling conditions after the 90 days model pre-run and after an annual scenario run with moderate precipitation amounts with initially dry conditions

When running the low precipitation annual scenario with an initially dry water content profile for several years, water contents in the soil profile increased, indicating that not all the infiltrating water evaporated again (Fig. 52). Due to the initial water content equaling residual water contents, the pressure heads in the soil overrated evaporative forces, holding the water back in the soil. Nevertheless, bottom flux was not obtained.

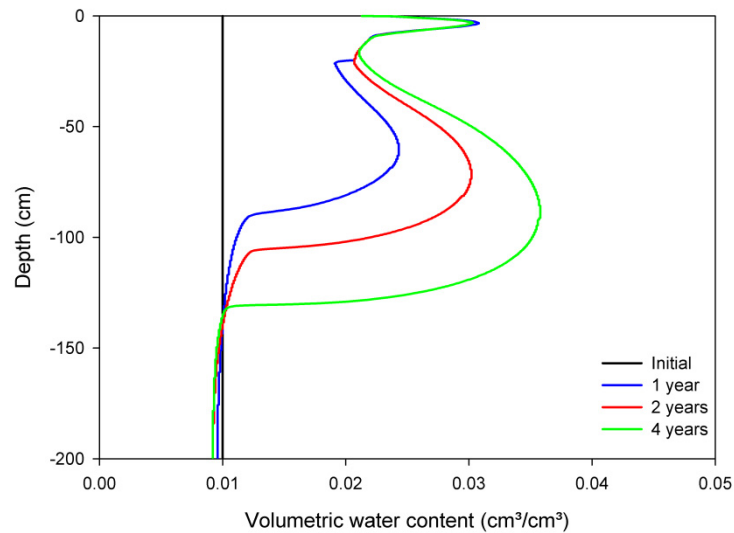


Fig. 52 - Water contents for annual scenario runs with the low precipitation reference scenario (30 mm/a); initial water content was set to residual water content, each following annual run continued with the final water content of the former year

For the pre-wetted initial water content profile, a threshold value for discharge was hard to distinguish, as bottom discharge was measured continuously due to the wetted state, as could be seen for the moderate and the low precipitation annual scenarios (Fig. 53 a and 53 b). Bottom discharge differed for the synthetic sand during the moderate flux simulation. Discharge breakthrough was much faster and lower, probably due to the high predicted saturated water content and higher water storage capacities.

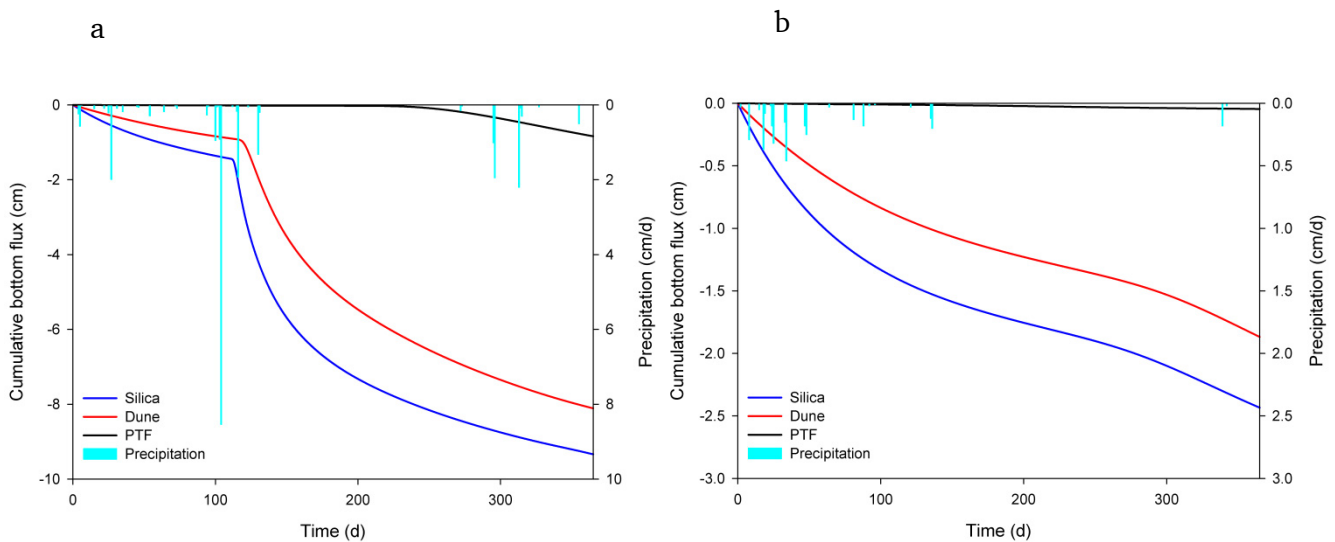


Fig. 53 - Cumulative bottom fluxes for different sand properties during moderate flux annual reference scenario (a) and low flux annual reference scenario (b) with initial gradient water content conditions; sand properties were taken from the silica sand calibration, the dune sand calibration and synthetically derived from pedotransfer functions (PTF) for 100 % sand

Due to the obviously high influence of the initial water content conditions on bottom flux, a sensitivity analysis was performed in PEST, where the sensitivity of initial water content θ_{ini} was calculated against sensitivities of residual water content θ_r , saturated water content θ_s , and the air entry pressure h_b and the retention curve shape parameter λ of the Brooks and Corey hydraulic model on water content profiles at three different times, cumulative bottom flux and cumulative evaporation for the low flux annual scenario. The composite parameter sensitivity analysis showed highest sensitivities, within the single observation groups as well as with all observation groups compiled, for the residual water content, whereas sensitivities for initial water content and air entry pressure were almost similar (Fig. 54).

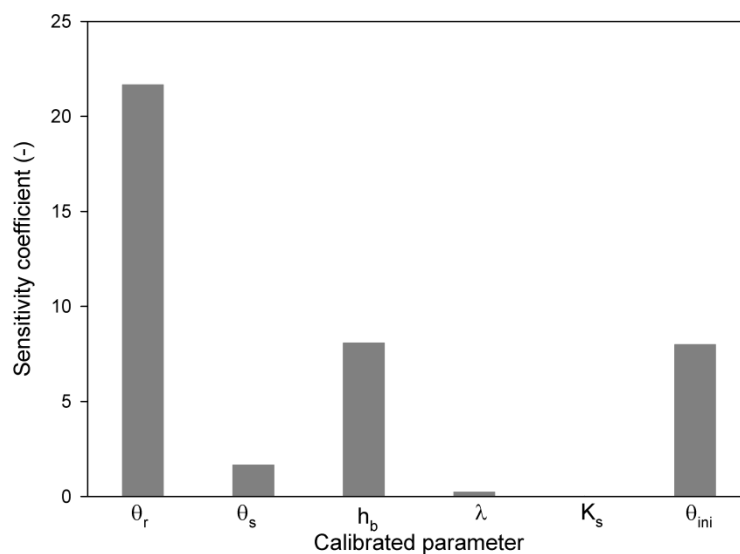


Fig. 54 - Composite parameter sensitivities during annual low precipitation scenario for cumulative bottom flux, cumulative evaporation and water content profiles

Comparable to the calibration sensitivity analysis, the water fluxes and contents were mainly determined by the parameters concerning dry conditions, and especially concerning the capacity for the drying of the soil and the water retention capacity.

Splitting up the high irrigation amount of the high flux annual reference scenario into 10 events within 10 consecutive days did decrease the bottom flux due to higher loss by evaporation. This effect was more pronounced when having two dry days between each precipitation day, comparable to the monthly scenario runs (chapter 4.4.3.2). Bottom flux decreased for the dune sand simulation by almost 7.5 cm, whereas soil water storage was not increased at the end of the simulation time. For the moderate precipitation reference scenario, decreasing precipitation intensity by a factor of 10, decreased bottom discharge to values comparable to the dry reference scenario. The single low amounts of precipitation almost directly evaporated again, as can be seen in the constant soil water storages (Fig. 55).

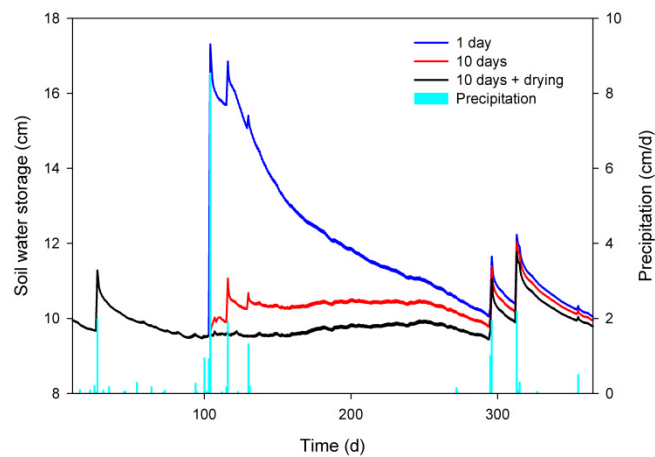


Fig. 55 - Simulated soil water storages for decreasing precipitation intensity (one day, 10 days, 30 days) for the moderate flux reference scenario; precipitation is shown only for the original one day high precipitation event

Evaporative fluxes were, beyond real precipitation input, mainly determined by surface fluxes caused by water vapor adsorption at the soil surface during soil drying periods. Thus, even without precipitation, infiltration fluxes were modeled as soon as the vapor pressure at the soil surface was lower than that of the air, as calculated from the time-variable atmospheric boundary conditions. As, within the model simulation, these infiltrative fluxes caused a positive water vapor pressure at the soil surface, this water uptake almost instantaneously evaporated again, leading to a constant evaporative flux (Fig. 56). For the synthetically derived sand properties these fluxes were significantly lower in the dry conditions than for the calibrated sands.

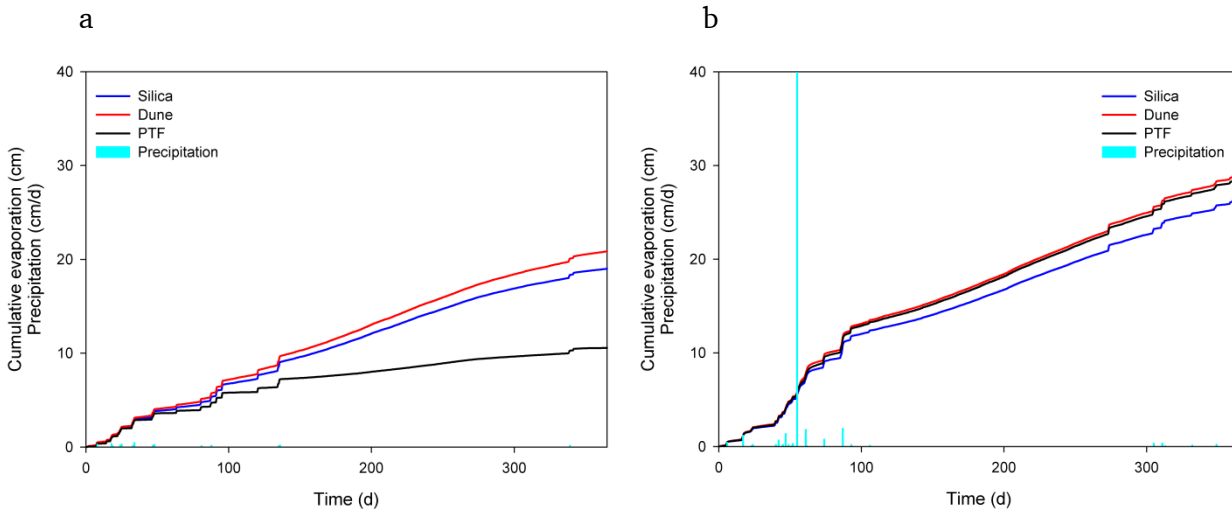


Fig. 56 - Cumulative evaporation during the low (a) and high (b) flux annual scenario with sands of different hydraulic properties; evaporation during dry times was driven by water vapor uptake from the air; sand properties were taken from the silica sand calibration, the dune sand calibration and synthetically derived from pedotransfer functions (PTF) for 100 % sand

The evaporative fluxes were strongly decreased when excluding diurnal temperature changes. The diurnal temperature changes caused continuous changes in the saturated vapor pressure of the air causing eventually high water vapor uptake during the day and water vapor discharge during the night when temperatures decreased (Fig. 57). Only when completely excluding vapor fluxes from the numerical simulations, evaporation close to precipitation amounts could be obtained (Fig. 57).

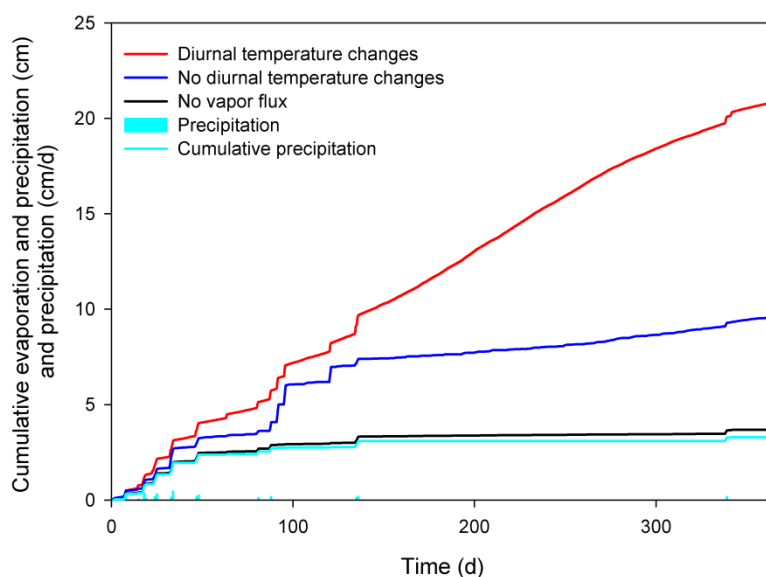


Fig. 57 - Precipitation and cumulative precipitation and evaporation for running the model with diurnal temperature changes, without diurnal temperature changes and without vapor fluxes; evaporation during dry times was driven by water vapor uptake from the air

Changing the air relative humidity did not change the modeling results of the reference scenarios. Even if potential evaporation is influenced by the relative humidity, the actual evaporation within the scenarios was more determined by the soil water states than by the atmospheric conditions. This also applied for changing the solar radiation.

Changing the top temperature mainly influenced the low flux reference scenario. For high infiltration fluxes, no influences of temperature on the infiltration patterns and bottom flux were observed. In the dry saturation range, vapor fluxes, and especially thermal vapor fluxes enhanced. Thus, depending on the temperature, vapor fluxes induced bottom discharge or evaporation. These were significantly enhanced for high top temperatures due to soil water vapor adsorption during dry and hot times, especially shortly after temperature reached the midday maximum.

To better understand the influences and importance of vapor fluxes on overall water fluxes, profiles of the water and vapor fluxes at different times were extracted from the simulation runs. During high precipitation events, vapor fluxes did not influence the total water fluxes at all, as already stated. Figure 58 a shows the total water fluxes within the soil profile directly after the high precipitation event of the high flux scenario. Total water fluxes were only determined by liquid fluxes, whereas negative numbers indicate downward flow. Accordingly, water content profiles did not significantly differ when running the model with or without vapor fluxes (Fig. 58 b). During low flux periods, where surface temperatures were normally lower than deep profile temperatures, and only low water infiltration by precipitation occurred, upward thermal vapor fluxes determined overall water fluxes, whereas gravitational downward liquid movement determined overall water fluxes below a depth of around 50 cm (Fig. 59 a). Water content profiles differed when running the model with or without vapor fluxes, whereas vapor fluxes induced higher water contents in the bottom and lower water contents in the top soil profile (Fig. 59 b). During no flux periods, upper soil total fluxes also were determined by thermal vapor fluxes, whereas they were directed downwards due to the thermal gradient (Fig. 60 a). Below a depth of 100 cm, almost no fluxes were simulated. Simulations with vapor fluxes resulted in higher water contents in the upper 150 cm, whereas differences were only in a range of $0.005 \text{ cm}^3/\text{cm}^3$ (Fig. 60 b).

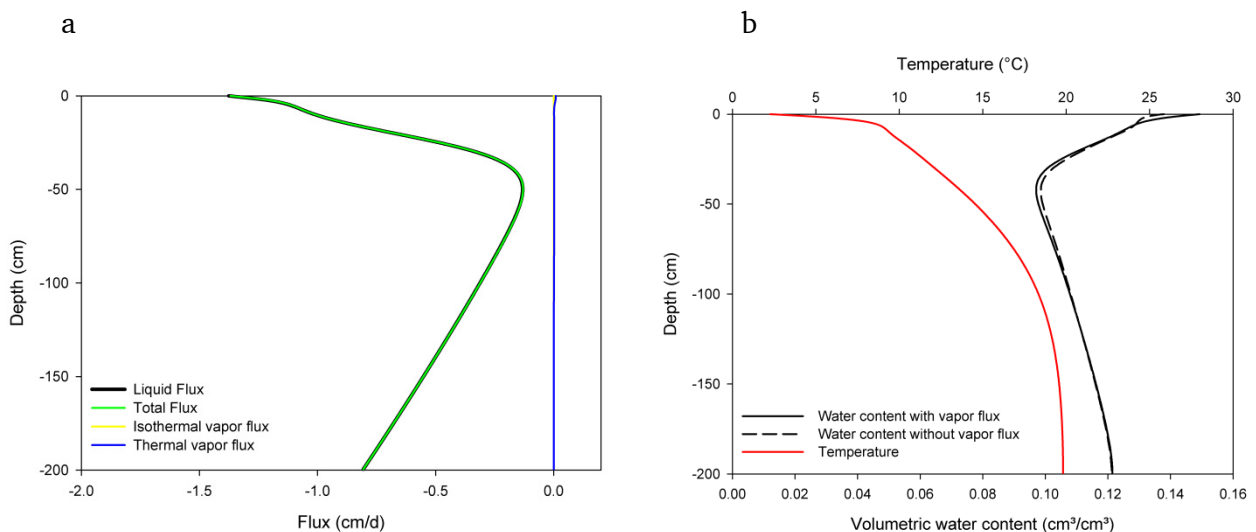


Fig. 58 - Water and vapor fluxes during a high flux period (a) and according temperature and water content profiles, with and without considering vapor fluxes in the model (b)

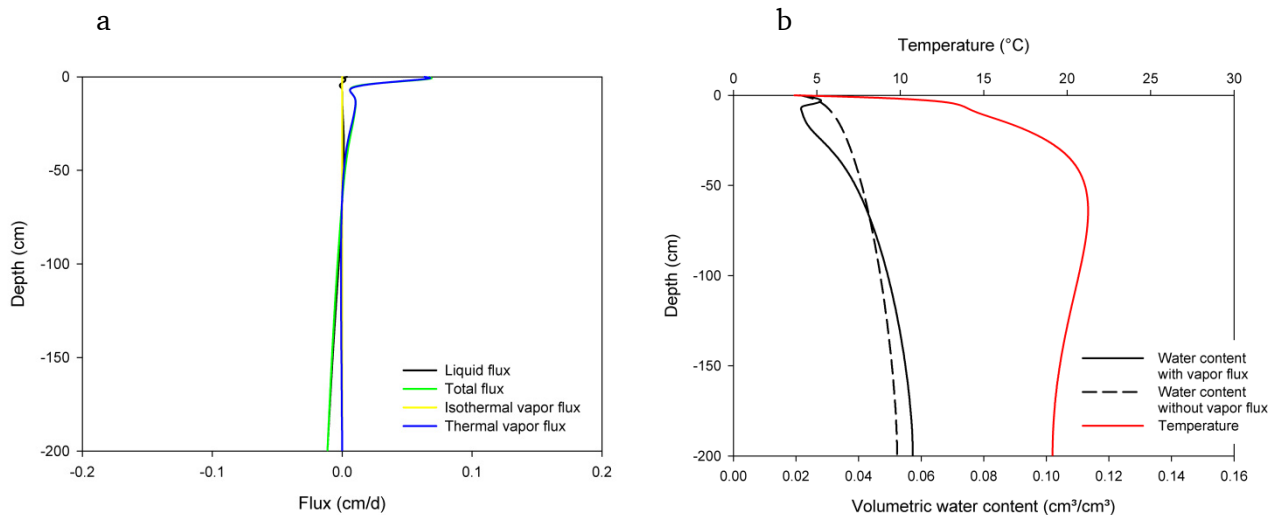


Fig. 59 - Water and vapor fluxes during a low flux period (a) and according to temperature and water content profiles, with and without considering vapor fluxes (b) in the model

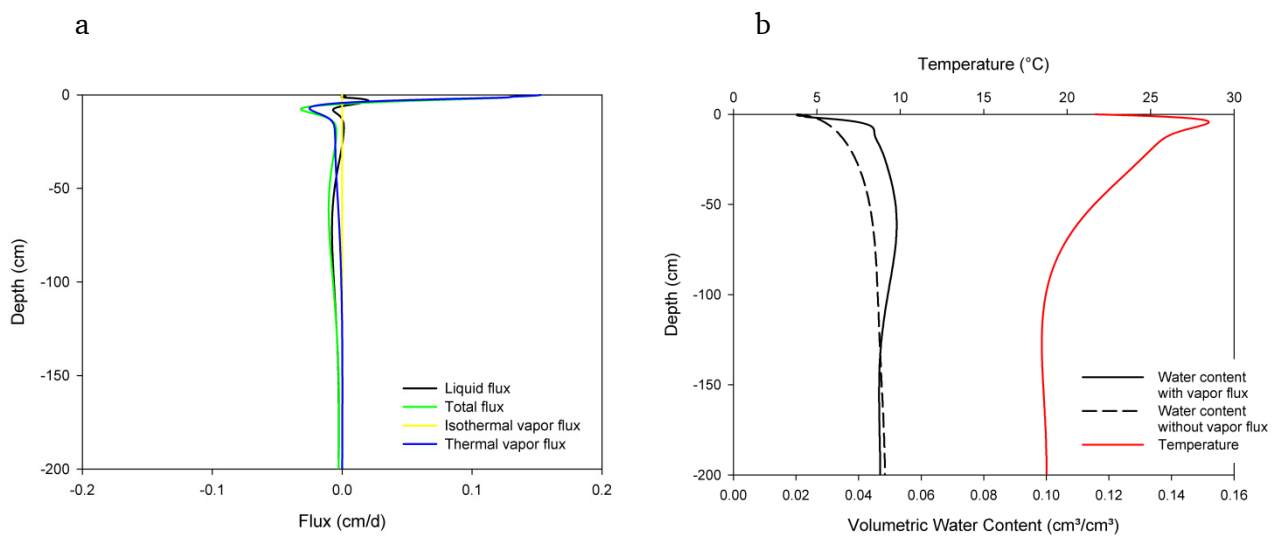


Fig. 60 - Water and vapor fluxes during a no flux period (a) and according to temperature and water content profiles, with and without considering vapor fluxes (b) in the model

During the no flux period, four zones of different flux dominating processes were distinguishable in the soil profile. In the upper 5 cm, the soil dried almost to residual water content. This influenced the temperature, which decreased in this soil zone due to decreased thermal conductivity. Also, temperatures were decreasing due to evaporative cooling at the soil surface. Thus, thermal vapor fluxes in this upper soil region were directed upward, which determined total water fluxes. Below this zone, the thermal gradient was directed downward with a steep gradient between 5 cm and 80 cm depth. Thermal vapor flux was directed downwards, whereas increased fluxes were observed in depths between 5 and 10 cm. Below this depth water contents slightly increased and isothermal downward water fluxes dominated total fluxes. Below a depth of 150 cm fluxes were close to zero.

The extraction of vapor transport within the simulations showed that for vadose zone modeling in arid regions, vapor transport should be considered. Due to the continuous vapor fluxes, even under dry conditions, a clear drying front was not allocable during the modeling runs. Surface drying with water contents down to residual water content only accounted for the upper 5 cm (Fig. 60 a). Nevertheless, dry parts within the soil profile also occurred deeper in the soil profile, whereas this could have been caused by both, upward and downward water movement. Vapor fluxes dominated total water fluxes down to a depth of 100 cm, depending on the drying state of the soil. Liquid water fluxes dominated deeper profile fluxes.

The predictive modeling could not reveal absolute threshold values of meteorological conditions for groundwater discharge, as water flux and heat flux processes are highly coupled. Single precipitation amounts had the highest influence on bottom flux values as well as discharge response times, whereas vapor fluxes during low flux periods were mainly influenced by the ambient temperature gradient and water content. As the hydraulic properties of the modeled sands had high infiltration and low retention capacities, most of the input water either percolated or evaporated and water contents were low during all times. Profile water contents during the predictive modeling were, without precipitation, between 0.02 and 0.06 cm³/cm³. Thus, they were lower than predicted field capacities.



5. Discussion

The discussion includes the experiments, the modeling and the transferability of both to groundwater recharge studies. For the experiments and the modeling, strengths and weaknesses of the specific methods that were used are outlined, whereas the last section of the discussion refers to the study approach.

5.1. Experiments

The experimental setup in general proved to be applicable to study water and temperature fluxes in unsaturated porous media in high temporal and spatial resolution. In the controlled column experiments, homogenous infiltration curves could be obtained using the TDR “Taupe” cable. The TDR cable sensor is therefore a useful tool to obtain continuous profiles upon water content changes, and thus to trace wetting and evaporation fronts. However, its installation, as well as the interpretation of data, needs some care and is especially limited at the sensor transition and thus, in the experimental setup, at the column top. Additionally, for layered soil profiles, the conversion of the cable signal to absolute water contents poses difficulties due to the adaption of different calibration functions. Here, the usage of TDR cable measurements for tracing infiltration fronts and analyzing relative water content changes is much more reliable than the conversion to absolute water content. The TDR cable measurements showed to be very sensitive to electromagnetic disturbances. Especially for field installations, this has to be considered and, prior to installation, possible sources of interference should be identified to avoid erroneous measurements. Also, regarding calibration, one single calibration for each soil has to be considered. The two sands that were used in the experiments had different characteristics regarding grain sizes and mineralogy. This probably determined the highly different calibration function of the TDR cable reflection coefficients to measured water contents. The silica sand seemed to cause higher losses upon the electromagnetic signal, thus also influencing the dune sand when lying below. Nevertheless, regarding calibration of the TDR cable or similar cable sensors in the field, mixing equations for the calibration might be appropriate, which has to be tested. Another aspect of field measurements is the depth of measurements and thus the sensor length. The one meter sensor in the column gave reliable measurement results, whereas the longer the electromagnetic transmission line, and thus the sensor, the higher are the losses of the electromagnetic signal, resulting in decreasing reflections with the sensor length. This especially applies for high electrical conductivities and macroporous material.

Water balances of the experiments showed reliable performance of the experimental setup. By this, the importance of irrigation amounts and intensities as well as on infiltration, evaporation and redistribution could be shown within several experimental runs. Nevertheless, some experimental details are likely to account for errors in measurements or for unwanted system behavior. The packing of the column is a possible source for heterogeneities in the otherwise assumed homogenous conditions. Primarily, the compaction of the 3 cm fillings can cause layers. Moreover, at the sensors and especially at the TDR cable sensor in the middle of the column, possible gaps can promote preferential flow paths. Nevertheless, as the TDR cable signal was controlled for inhomogeneities during packing, effects were assumed to be negligible. The suction plate at the bottom of the column accounted for water flow against air pressure but could not account for free flow conditions as

the pressure had to be held constant for reasons of calibration and comparison. For free flow conditions, the pressure should be transiently adapted according to the ambient pressure within the soil above the suction plate. Another possibility to account for free flow conditions could be a higher column with only considering the upper half of the column for free flow analysis. Another source of irregularities during measurements is the relative humidity of the incoming air stream, which cannot be held constant all the time. As the water of the saturated salt solution is assimilated from the flowing air stream over time, it has to be renewed once in a while resulting in fluctuations of $\pm 10\%$. As relative humidities of both, the incoming and the outflowing air, are measured, calculation errors for evaporation are prevented.

By applying different initial and boundary conditions, the experiments showed the large impact of irrigation amount on column discharge. Only water infiltration amounts above 20 mm resulted in discharge after percolation. Lower single irrigations could only contribute to deep percolation if initial water contents within the soil column were above field capacity and thus if they were applied shortly after a former irrigation. Single irrigations below 5 mm showed very low infiltration rates and no deep percolation was measurable. If not followed by another higher or several consecutive irrigations, these low irrigation amounts completely evaporated again. The two different sands showed similar behavior for continuous irrigation. Layered profiles showed different behavior than homogenous profiles by forming capillary barriers in the fine grained layer. For drying and wetting cycles, the finer dune sand had higher retention capacities. The soil aggregation that was visible after unpacking the column, might have influenced the soil water flux patterns. This was not measurable during the experiments. Hydraulic effects of the observed soil aggregation could have been quantified by unpacking the column after single drying and wetting cycles. For this purpose, smaller experiments would be more appropriate.

The measurement of the soil water retention characteristics prior to the experiments gave information upon expectable infiltration and redistribution patterns. Nevertheless, the different conditions of the retention parameter determination and the transient column experiments proved to result in discrepancies between expected and measured water retention, which could be quantified by the inverse modeling. Thus, the experiments can also function solely for the determination of soil hydraulic properties when considering transient conditions in the dry water content range. The combined simulation of heat and water flux boundaries as well as the enlarged column size and the high resolution measurements can give better estimates for hydraulic properties when studying water fluxes under semi-arid and arid conditions than conventional methods, such as multistep outflow and evaporation methods, as described e.g. by Schelle et al., 2010.

Bench-scale experiments only can give an insight into the complex water and temperature flux processes in the unsaturated zone, and some uncertainties have to be considered. As only the total water content was measured within the column, distinction between pressure induced and temperature induced water fluxes could not be made within the experiments. The experimental scale showed to be manageable in the lab for highly defined initial and boundary conditions, as well as high resolution temporal and spatial measurements. Nevertheless, they can only give an idealized picture of field conditions and thus only supplement field and regional scale studies.

5.2. Modeling

The experimental data were fitted to a numerical model by comparing the hydraulic models van Genuchten-Mualem (1980), Brooks and Corey (1964), and Durner et al. (1994), whereas only the Brooks and Corey model showed good convergence of the measurements and the model calculations. Fitting residuals were not avoidable but the model behavior showed good resemblance with the experimental system behavior. The good fit of the Brooks and Corey model accounts for its applicability to coarse grained material, as stated for example by Schaap et al., 2001. The Durner model was expected to be applicable to the dune sand measurements, especially due to the observed soil aggregation. Nevertheless, the high model complexity, including more calibration parameters than the other two models, enlarged the ill-posedness of the model and convergence could not be achieved. Still, a more complex model, including hysteresis, could have resulted in better fit, but would have been only applicable if some parameters were defined a priori. Generally, hysteresis causes that water content decreases decline with repetitive wetting. In the case of the dune sand calibration experiments, a better fit could have been obtained for water contents in depths between 14 and 24 cm as well as for discharges. As within Hydrus only the van Genuchten model can be supplemented with a hysteresis function, but not the Brooks-Corey model, a trial for including hysteresis was discarded.

The inverse calibration was a good tool for parameter estimation under transient and dual-component boundary conditions, including drying and wetting cycles. Strictly speaking, the complete study was based on two consecutive inverse calibration steps. First, the measured retention data was fitted to hydraulic models, second, the obtained hydraulic model parameters were adjusted to fit data from the described column experiments to the Hydrus model run. Actually, the measurement of retention data aside the column experiments and their fitting to a hydraulic model, would not have been necessary. Nevertheless, they gave an initial guess on parameter values as well as valuable information on the influence of different measurement conditions on parameter estimation by comparing the initially measured and the calibrated parameters. Common methods for retention curve analysis consider the hydraulic function for the whole saturation range. As the experiments focus on the dry end of the hydraulic function, common methods might not be necessarily applicable, which also is true for the application of pedotransfer functions to obtain retention curve parameters.

Using high resolution and reliable water flux as well as water content and temperature measurements for calibration reduced the ill-posedness of the model, which is generally affected by conceptual and measurement errors, as well as unsuitable model parameterization (Bitterlich et al., 2004). Regarding the conceptual model, two constraints had to be made for displaying the experiments. First, the suction plate was inserted as a soil layer and as such was included into the hydraulic gradient in the model. Second, the evaporation had to be induced by specifying the potential evaporation and a pressure head at the soil top constraining this potential evaporation, rather than directly calculating evaporation according to the experimental setup. The observation data generally was assumed to be highly reliable, supporting the well-posedness of the inverse calibration. An upgrade upon calibration regarding observation measurements could have been the additional measurement of pressure heads corresponding to the measured water contents. As up to 9 parameters were calibrated at a time, the calibration results were generally non-unique. This implies that when changing or fixing one of the parameters, the others might have given other calibration results with the same residual fitting. Unique solutions can only be guaranteed with one parameter that is to

be calibrated, and all the others are known in advance. Nevertheless, by reducing the calibrated parameters according to sensitivities and parameter correlations, the overall model parameterization also supported the well-posedness of the inverse model calibration.

Another lack within the inverse modeling is the modeling of vapor fluxes without measured values of vapor fluxes. In the experiments, only total water fluxes and water contents were measured and the calibration to water and vapor fluxes can pose uncertainties regarding model verification, which is the vapor flux calculation implemented in Hydrus. An asset would thus have been to include the measurement of vapor fluxes, respectively vapor contents, into the experiments.

Sensitivities showed that under always unsaturated conditions parameters limiting or influencing evaporation and low saturation fluxes are far more sensitive than those, influencing saturated water flow. Thus, these parameters should be carefully measured and defined for vadose zone water flux modeling for arid conditions, whereas common measurements like the saturated hydraulic conductivity are only of minor importance. Observation sensitivities showed that observations during drying were highly important upon system behavior, whereas measurements during free water flow conditions were of minor importance. Thus, observation schemes should integrate continuous measurements during drying, especially in upper soil profiles.

Forward scenario modeling in Hydrus showed the impact of vapor flow which is not accounted for when using a bucket model or conventional Richards approach that does not include vapor transport calculations. During the predictive forward modeling, water contents within the soil profile decreased clearly below the roughly determined field capacities and converged to the inversely estimated residual water contents. Due to the low residual water content of the modeled sands, bottom discharge for the 200 cm high model was measured continuously. This implies continuous downward percolation even when water input by precipitation is very low. Only after several years of complete dryness, a water content distribution in the 200 cm high model could be established that did not result in downward percolation. For field conditions this implies that downward water percolation is likely to occur in the upper two meter and below, as long as water contents are well above residual water content and no layer that can function as capillary barrier exists. Deep percolation beyond residual water contents was mostly induced by precipitation amounts within one day. Precise threshold values upon precipitation were not definable due to the complex system behavior. Only for initially dry conditions, a threshold of 80 mm resulting in direct model bottom discharge could be defined. Especially for arid regions, this is a fairly high precipitation amount and is likely to occur rarely and only in selected areas. On the other hand, also daily precipitations below this threshold proved to be able to deeply penetrate, depending on the single intensity, the wetting history and the evaporative conditions. Regarding monthly or even annual thresholds, changing timescales also increases the complexity of processes. Clear monthly or annual thresholds are not definable as, again, too many factors are involved, that are the initial water content, the precipitation patterns, and the meteorological conditions. Nevertheless, even for monthly and annual precipitation thresholds, daily precipitation patterns and amounts play a significant role, as daily potential evaporation rates have to be exceeded by precipitation, according to the abundant meteorological and soil surface conditions, to account for soil water storage. Thus, calculating recharge from annual or monthly precipitation sums can be very misleading.

Model output for evaporation appeared to be highly overestimated, as even during drying times, continuous evaporation was simulated. The simulated water vapor adsorption from the atmosphere, causing this continuous evaporation, is an effect that was noted and stated by several authors especially in semi-arid regions (e.g. Agam and Berliner, 2006; Kosmas et al., 2001). Nevertheless, the high fluctuations during the predictive modeling could not be verified within this work due to the absence of corresponding data for the given conditions.

5.3. Groundwater Recharge Studies

The bench-scale experiments and 1-dimensional modeling cannot directly be transferred to field- or large-scale groundwater recharge studies, due to the non-linearity of vadose zone processes, additional unknowns, and the idealized experimental and model conditions. Nevertheless, obtained results can be implemented into groundwater recharge studies by considering them for measurement and observation schemes. The strengths of the study approach are within the high reliability of results due to the controllable and adjustable initial and boundary conditions. Regarding the experimental setup, experiments with undisturbed field soils are also feasible. As such, it can supplement water hydraulic and thermal property measurements for model calibration even for field conditions.

Direct groundwater recharge is limited to precipitation amounts as well as the soil infiltration capacity and stratigraphy. Whenever precipitation amounts are not sufficiently high to induce direct recharge, other seasonal patterns effect the direction of fluxes and dispositions of the water in the vadose zone. These fluxes generally are very low but considerably influence the water content distribution within a soil profile. The study showed that within the given setup and boundaries the main driver for groundwater recharge is the daily precipitation amount, whereas monthly or annual sums of precipitation can be largely misleading. Thus, aside other meteorological conditions, special focus for observation data should be made upon daily precipitation rates. The soil properties, at least when talking about sandy soils, are only important when looking at soil water retention in terms of residual water content and the air entry pressure. As under arid conditions the soil is hardly ever saturated, the saturated hydraulic conductivity is only of minor importance. The dune sand used in the experiments and for model calibration promoted fast infiltration, and high infiltration capacities are outnumbered by saturated conditions. Thus, when investigating soils in arid regions for groundwater recharge capacities, focus of measuring hydraulic properties should not only be on infiltration capacities, but on unsaturated hydraulic properties, and especially the air entry pressure and the residual water content. As shown in the observation sensitivities of the model calibration, observation schemes should not only focus on high infiltration times but also on the drying period. During the drying period especially the upper soil layers should be monitored to trace drying fronts as well as to quantify vapor adsorption at the soil surface from the air. For the modeling of groundwater recharge in arid regions, the vadose zone model compartment should consider vapor flow, as it proved to have influences on total water contents, especially under dry conditions.



6. Conclusions

Soil column experiments and subsequent numerical modeling for quantifying water fluxes and temperature transport in unsaturated porous media under boundary conditions that can be expected in arid regions were performed. The experiments and the model were applicable to bench-scale, 1-dimensional vertical vadose zone water flux studies under simplified hypothesized conditions.

The column experiments proved to reliably measure water content and temperature distribution in the soil profile, as well as water fluxes amongst the column boundaries under transient non-isothermal conditions, which could be shown in the tracking of infiltration and drying fronts as well as by overall water balances. One feature of the experiments was the testing of a TDR cable sensor for measuring continuous water content profiles. The TDR cable proved to be a good tool for water flux tracking and can be recommended for field studies as well. Nevertheless, the analysis of the cable measurements is still very laborious and more effective in determining relative changes in water content rather than quantify absolute water contents. For the usage of cable measurements in the field this implies that valuable information on infiltration depths and water redistribution patterns can be obtained. For the conversion of the TDR signal to absolute water contents within depths, more studies have to be complemented to include environmental site-specific influences into conversion algorithms.

Experiments were performed for different sand fillings and boundary water flux as well as temperature conditions. The depths and water content of infiltration fronts were mainly influenced by irrigation amounts and intensities, respectively. Losses of irrigation water by evaporation increased with decreasing intensity. Discharge at the bottom of the column could only be reached for irrigation amounts of more than 20 mm.

According to the experiments, a numerical model was set up in Hydrus-1D and calibrated with PEST by using experimental data for inversely optimizing hydraulic and thermal model parameter. A good fit could be obtained with the hydraulic model of Brooks and Corey (1964). The calibration revealed the high sensitivity of air entry pressure and residual water content upon modeling unsaturated water fluxes in porous media under isothermal conditions and low saturations. Predictive scenario modeling showed that for meteorological data, the temporal resolution is highly important for predictions, especially when averaging or summing up precipitation values. Thus, for the definition of threshold values of precipitation for the influence to groundwater recharge, not annual or monthly, but daily values have to be considered. Additionally, vadose zone water fluxes under arid conditions showed to be highly determined by vapor fluxes, which are mainly induced by temperature gradients under low saturation conditions. Measuring and modeling vadose zone water fluxes under arid conditions should thus include temperature observations within depth, as well as consider vapor flow for overall water flow calculations.

Based on the calibrated model, further predictive modeling studies can be performed by considering field measurements of water contents and temperature gradients, or predicted climate changes. Additionally, further experimental studies can be conducted with the developed experimental setup to determine hydraulic and thermal properties of field samples under conditions that can be expected in arid regions. By this, it can supplement field-scale and regional-scale studies on vadose zone water fluxes under non-isothermal conditions and accordingly groundwater recharge studies.



Literature

- Aba-Husayn M.M., Sayegh A.H. (1977) Mineralogy of Al-Hasa desert soils (Saudi Arabia). *Clays and Clay Minerals* 25(2):138-147. DOI: 10.1346/CCMN.1977.0250211.
- Abu-Hamdeh N.H. (2001) SW – soil and water: measurement of the thermal conductivity of sandy loam and clay loam soils using single and dual probes. *Journal of Agricultural Engineering Research* 80(2):209-216. DOI: 10.1006/jaer.2001.0730.
- Agam N., Berliner P.R. (2006) Dew formation and water vapor adsorption in semi-arid environments – A review. *Journal of Arid Environments* 65(4):572-590. DOI: 10.1016/j.jaridenv.2005.09.004.
- Allen R.G., Pereira L.S., Raes D., Smith M. (1998) Crop evapotranspiration: guidelines for computing crop water requirements. FAO Irrigation and drainage paper. FAO - Food and Agriculture Organization of the United Nations. Rome. pp. 300.
- Balba A.M. (1995) Management of problem soils in arid ecosystems. CRC Lewis Publishers, Florida. pp. 250.
- Bazuhair A.S., Wood W.W. (1996) Chloride mass-balance method for estimating groundwater recharge in arid areas: examples from western Saudi Arabia. *Journal of Hydrology* 186(1-4):153-159. DOI: 10.1016/S0022-1694(96)03028-4.
- Benson C.H. (2007) Modeling unsaturated flow and atmospheric interactions. In: Schanz T. (Ed.) *Theoretical and numerical unsaturated soil mechanics*. Springer Berlin. pp. 187-201.
- Bitterlich S., Durner W., Iden S.C., Knabner P. (2004) Inverse estimation of the unsaturated soil hydraulic properties from column outflow experiments using free-form parameterizations. *Vadose Zone Journal* 3(3):971-981. DOI: 10.2113/3.3.971.
- Brandelik A., Huebner C., Schuhmann R. (1998) Moisture sensor for large area layers. (German patent no. 4432687, European patent no. 0804724, US patent no. 5942904), 16 June 1998.
- Brooks R.H., Corey A.T. (1964) Hydraulic properties of porous media. *Hydrology Papers* 3(3). pp. 27.
- Brooks R.H., Corey A.T. (1966) Properties of porous media affecting fluid flow. *J Irrig and Drainage* 92(2):61-88.
- BSL (2009) Berkeley Seismological Laboratory Annual Report. July 2008 - June 2009. In: B. S. Laboratory (Ed.) *Annual Report*. Berkeley Seismological Laboratory, Berkeley, California. http://seismo.berkeley.edu/annual_report/ar08_09/. As of March 10th, 2009.
- Cary J.W. (1965) Soil moisture transport due to thermal gradients: Practical aspects. *Soil Sci. Soc. Am. Proceedings* 30(4):428-433.
- Cass A., Campbell G.S., Jones T.L. (1984) Enhancement of thermal water vapor diffusion in soil. *Soil Sci. Soc. Am. J.* 48(1):25-32. DOI: 10.2136/sssaj1984.03615995004800010005x.
- Chung S.O., Horton R. (1987) Soil heat and water flow with a partial surface mulch. *Water Resour. Res.* 23(12):2175-2186. DOI: 10.1029/WR023i012p02175.

-
- Constantz J., Tyler S.W., Kwicklis E. (2003) Temperature-profile methods for estimating percolation rates in arid environments. *Vadose Zone Journal* 2(1):12-24. DOI: 10.2113/2.1.12.
- Cooke R., Warren A., Goudie A. (1993) *Desert geomorphology*. UCL Press Limited, London. pp. 534.
- Dahan O., McDonald E.V., Young M.H. (2003) Flexible time domain reflectometry probe for deep vadose zone monitoring. *Vadose Zone Journal* 2(2):270-275. DOI: 10.2113/2.2.270.
- de Vries J.J., Simmers I. (2002) Groundwater recharge: an overview of processes and challenges. *Hydrogeology Journal* 10(1):5-17. DOI: 10.1007/s10040-001-0171-7.
- Dincer T., Al-Mugrin A., Zimmermann U. (1974) Study of the infiltration and recharge through the sand dunes in arid zones with special reference to the stable isotopes and thermonuclear Tritium. *Journal of Hydrology* 23(1-2):79-109. DOI: 10.1016/0022-1694(74)90025-0.
- Doherty J. (2010) *PEST surface water utilities user's manual*. Watermark Numerical Computing. 5th edition. Brisbane, Australia, and University of Idaho, Idaho Falls, Idaho. pp. 336.
- Doherty J.E., Hunt R.J. (2010) Approaches to highly parameterized inversion: A guide to using PEST for groundwater-model calibration. In: U. S. D. o. t. Interior and U. S. G. Survey (Eds.) *Scientific Investigations Report*. USGS, Reston, Virginia. pp. 59.
- Dong W., Yu Z., Weber D. (2003) Simulations on soil water variation in arid regions. *Journal of Hydrology* 275(3-4):162-181. DOI: 10.1016/S0022-1694(03)00041-6.
- Dregne H.E. (1976) *Soils of arid regions*. Elsevier Scientific Publishing Company, Amsterdam. pp. 237.
- Durner W. (1994) Hydraulic conductivity estimation for soils with heterogeneous pore structure. *Water Resources Research* 30(2):211-224. DOI: 10.1029/93WR02676.
- Energy Research Institute (1998) *Solar radiation atlas for the Kingdom of Saudi Arabia*. - National Renewable Energy Lab (NREL). Nov 1998.
- Engelhardt I., Finsterle S., Hofstee C. (2003) Experimental and numerical investigation of flow phenomena in nonisothermal, variably saturated bentonite-crushed rock mixtures. *Vadose Zone Journal* 2(2):239-246. DOI: 10.2113/2.2.239.
- FAO (2003) *Groundwater Management - The Search for Practical Approaches*. Water Reports. No. 25. Food and Agriculture Organization of the United Nations. Rome. pp. 55.
- Finsterle S. (2004) Multiphase Inverse Modeling: Review and iTOUGH2 applications. *Vadose Zone Journal* 3(3):747-762. DOI: 10.2113/3.3.747.
- Gee G.W., Hillel D. (1988) Groundwater recharge in arid regions: review and critique of estimation methods. *Hydrological Processes* 2(3):255-266. DOI: 10.1002/hyp.3360020306.

-
- Gong Y., Cao Q., Sun Z. (2003) The effects of soil bulk density, clay content and temperature on soil water content measurement using time-domain reflectometry. *Hydrological Processes* 17(18):3601–3614. DOI: 10.1002/hyp.1358.
- Grifoll J., Gastó J.M., Cohen Y. (2005) Non-isothermal soil water transport and evaporation. *Advances in Water Resources* 28(11):1254-1266. DOI: 10.1016/j.advwatres.2005.04.008.
- Heimovaara T.J., Freijer J.I., Bouten W. (1993) The application of TDR in laboratory column experiments. *Soil Technology* 6(3):261-272. DOI: 10.1016/0933-3630(93)90015-7.
- Hendrickx J.M.H., Flury M. (2001) Uniform and preferential flow mechanisms in the vadose zone. In: CGER (Ed.) *Conceptual models of flow and transport in the fractured vadose zone*. National Academy Press. Washington. pp. 149-187.
- Hill M.C. (1998) *Methods and guidelines for effective model calibration*. U. S. Geological Survey Water-Resources Investigations Report 98-4005. Denver, Colorado. pp. 97.
- Hillel D. (2004) *Introduction to environmental soil physics*. Elsevier Academic Press. Massachusetts. pp. 511.
- Hopmans J.W., Schoups G. (2006) Soil water flow at different spatial scales. *Encyclopedia of Hydrological Sciences*. 66. DOI: 10.1002/0470848944.hsa070.
- Huebner C., Schlaeger S., Becker R., Scheuermann A., Brandelik A., Schaedel W., Schuhmann R. (2005) Advanced measurement methods in time domain reflectometry for soil moisture determination. In: Kupfer K. (Ed.) *Electromagnetic Aquametry*. Springer Berlin. pp. 317-347.
- Huebner C., Kupfer K. (2007) Modelling of electromagnetic wave propagation along transmission lines in inhomogeneous media. *Measurement Science and Technology* 18(4):1147-1154. DOI: 10.1088/0957-0233/18/4/023.
- IWAS (2011) International Water Research Alliance Saxony. www.iwas-initiative.de. As of Oct 20th, 2011.
- Jarvis N.J. (2007) A review of non-equilibrium water flow and solute transport in soil macropores: Principles, controlling factors and consequences for water quality. *European Journal of Soil Science* 58(3):523-546. DOI: 10.1111/j.1365-2389.2007.00915.x.
- Jones S.B., Mace R.W., Or D. (2005) A time domain reflectometry coaxial cell for manipulation and monitoring of water content and electrical conductivity in variably saturated porous media. *Vadose Zone Journal* 4(4):977-982. DOI: 10.2136/vzj2005.0048.
- Jury W.A., Horton R. (2004) *Soil Physics*. 6th ed. John Wiley and Sons. Hoboken. New Jersey. pp. 370.
- Koeniger F., Nueesch R., Rabl-Lasar W., Roth J., Ruppert P., Schuhmann R. (2005) Alternative surface covering of landfill using the TAUPE sealing monitoring system, 6th Conference on electromagnetic wave interaction with water an moist substances, ISEMA. Weimar, Deutschland. May 29th – June 01st. pp. 422-428.

-
- Kosmas C., Marathianou M., Gerontidis St., Detsis V., Tsara M., Poesen J. (2001) Parameters affecting water vapor adsorption by the soil under semi-arid climatic conditions. *Agricultural Water Management* 48(1):61-78. DOI: 10.1016/S0378-3774(00)00113-X.
- Lerner D.N., Issar A.S., Simmers I. (1990) Groundwater recharge. A guide to understanding and estimating natural recharge. *International Contributions to Hydrogeology*. Volume 8. Heinz Heise, Hannover. pp. 42.
- Letey J., Carrillo M.L.K., Pang X.P. (2000) Approaches to characterize the degree of water repellency. *Journal of Hydrology* 231-232:61-65. DOI: 10.1016/S0022-1694(00)00183-9.
- Littmann T., Berkowicz S.M. (2008) The regional climate setting. In: Breckle S.W., Yair A., Veste M. (Eds.) *Arid Dune Ecosystems. The Nizzana Sands in the Negev Desert*. Ecological Studies. Vol. 200. Springer Berlin. pp. 49-62.
- Lu S., Ren T., Yu Z., Horton R. (2011) A method to estimate the water vapour enhancement factor in soil. *European Journal of Soil Science* 62(4):498-504. DOI: 10.1111/j.1365-2389.2011.01359.x.
- Marquardt D. (1963) An Algorithm for Least-Squares Estimation of Nonlinear Parameters. *SIAM J. Appl. Math.* 11(2):431-441. DOI: 10.1137/0111030.
- Mattson E.D., Magnuson S.O., Ansley S.L. (2004) Interpreting INEEL vadose zone water movement on the basis of large-scale field tests and long-term vadose zone monitoring results. *Vadose Zone Journal* 3(1):35-46. DOI: 10.2113/3.1.35.
- Mattson E.D., Baker K.E., Palmer C.D., Breckenridge C.R., Svoboda J.M., Smith R.W. (2006) A flexible water content probe for unsaturated soil column experiments. *Vadose Zone Journal* 5(2):805-808. DOI: 10.2136/vzj2006.0139.
- McNamara J.P., Chandler D., Seyfried M., Achet S. (2005) Soil moisture states, lateral flow and streamflow generation in a semi-arid, snowmelt-driven catchment. *Hydrological Processes* 19(20):4023-4038. DOI: 10.1002/hyp.5869.
- Monteith J.L., Unsworth M.H. (1990) *Principles of environmental physics*. 2nd Edn. Edward Arnold, New York. pp 291.
- Mooney S.J., Morris C. (2004) Quantification of preferential flow in undisturbed soil columns using dye tracers and image analysis, SuperSoil 2004: 3rd Australian New Zealand Soils Conference. 5 – 9 December 2004. University of Sydney, Australia.
- Mori Y., Hopmans J.W., Mortensen A.P., Kluitenberg G.J. (2005) Estimation of vadose zone water flux from multi-functional heat pulse probe measurements. *Soil Sci. Soc. Am. J.* 69(3):599-606. DOI: 10.2136/sssaj2004.0174.
- Mualem Y. (1976) A new model for predicting the hydraulic conductivity of unsaturated porous media. *Water Resour. Res.* 12(3):513-522. DOI: 10.1029/WR012i003p00513.
- Nassar I.N., Horton R. (1989) Water transport in unsaturated nonisothermal salty soil: I. Experimental results. *Soil Sci. Soc. Am. J.* 53(5):1323-1329. DOI: 10.2136/sssaj1989.03615995005300050004x.

-
- Nimmo J.R., Miller E.E. (1986) The temperature dependence of isothermal moisture vs. potential characteristics of soils. *Soil Sci. Soc. Am. J.* 50(5):1105-1113. DOI: 10.2136/sssaj1986.03615995005000050004x.
- NOAA (2010): NNDC climate data online. Global summary of the day. Country Saudi Arabia. <http://www7.ncdc.noaa.gov/CDO/cdoselect.cmd?datasetabbv=GSOD&countryabbv=SA&georegionabbv=&resolution=40>. As of Sept 28th, 2010.
- Noborio K. (2001) Measurement of soil water content and electrical conductivity by time domain reflectometry: a review. *Computers and Electronics in Agriculture* 31(3):213–237. DOI: 10.1016/S0168-1699(00)00184-8.
- Noy-Meir I. (1973) Desert ecosystems: environment and producers. *Annual Review of Ecology and Systematics* 4(1):25-51. DOI: 10.1146/annurev.es.04.110173.000325.
- Oostrom M., Dane J.H., Wietsma T.W. (2007) A review of multidimensional, multifluid, intermediate-scale experiments: flow behavior, saturation imaging, and tracer detection and quantification. *Vadose Zone Journal* 6(3):610-637. DOI: 10.2136/vzj2006.0178.
- Or D., Wraith J.M. (1999) Temperature effects on soil bulk dielectric permittivity measured by time domain reflectometry: A physical model. *Water Resour. Res.* 35(2):371-383. DOI: 10.1029/1998wr900008.
- Pan H.L., Mahrt L. (1987) Interaction between soil hydrology and boundary-layer development. *Boundary-Layer Meteorology* 38(1-2):185-202. DOI: 10.1007/bf00121563.
- Parlange M.B., Cahill A.T., Nielsen D.R., Hopmans J.W., Wendroth O. (1998) Review of heat and water movement in field soils. *Soil and Tillage Research* 47(1):5-10. DOI: 10.1016/S0167-1987(98)00066-X.
- Pfletschinger H., Engelhardt I., Piepenbrink M., Königer F., Schuhmann R., Kallioras A., Schüth C. (2012) Soil column experiments to quantify vadose zone water fluxes in arid settings. *Environ Earth Sci.* 65(5):1523-1533. DOI: 10.1007/s12665-011-1257-8.
- Philip J., de Vries D. (1957) Moisture movement in porous materials under temperature gradients. *Trans. Am. Geophys. Union* 38(2):222-232.
- Qiu G.Y., Ben-Asher J. (2010) Experimental determination of soil evaporation stages with soil surface temperature. *Soil Sci. Soc. Am. J.* 74(1):13-22. DOI: 10.2136/sssaj2008.0135.
- Rawls W.J., Brakensiek D.L., Saxton K.E. (1982) Estimation of soil water properties. *Transactions of the ASAE* 25(5):1316-1320 and 1328.
- Richards L.A. (1931) Capillary conduction of liquids through porous media. *Physics* 1:318-333. DOI: 10.1063/1.1745010.
- Robinson D.A., Jones S.B., Wraith J.M., Or D., Friedman S.P. (2003) A review of advances in dielectric and electrical conductivity measurement in soils using time domain reflectometry. *Vadose Zone Journal* 2(4):444-475. DOI: 10.2113/2.4.444.
- Saito H., Simunek J., Mohanty B.P. (2006) Numerical analysis of coupled water, vapor, and heat transport in the vadose zone. *Vadose Zone Journal* 5(2):784-800. DOI: 10.2136/vzj2006.0007.

-
- Sakai M., Toride N., Šimůnek J. (2009) Water and vapor movement with condensation and evaporation in a sandy column. *Soil Sci. Soc. Am. J.* 73(3):707-717. DOI: 10.2136/sssaj2008.0094.
- Scanlon B.R., Milly P.C.D. (1994) Water and heat fluxes in desert soils 2. Numerical simulations. *Water Resour. Res.* 30(3):721-733. DOI: 10.1029/93WR03252.
- Scanlon B.R., Tyler S.W., Wierenga P.J. (1997) Hydrologic issues in arid, unsaturated systems and implications for contaminant transport. *Rev. Geophys.* 35(4):461-490. DOI: 10.1029/97rg01172.
- Scanlon B.R., Healy R.W., Cook P.G. (2002a) Choosing appropriate techniques for quantifying groundwater recharge. *Hydrogeology Journal* 10(2):347-347. DOI: 10.1007/s10040-002-0200-1.
- Scanlon B.R., Christman M., Reedy R.C., Porro I., Simunek J., Flerchinger G.N. (2002b) Intercode comparisons for simulating water balance of surficial sediments in semiarid regions. *Water Resour. Res.* 38(12):1323-1339. DOI: 10.1029/2001wr001233.
- Scanlon B.R., Keese K., Reedy R.C., Simunek J., Andraski B.J. (2003) Variations in flow and transport in thick desert vadose zones in response to paleoclimatic forcing (0–90 kyr): Field measurements, modeling, and uncertainties. *Water Resour. Res.* 39(7):1179-1186. DOI: 10.1029/2002WR001604.
- Scanlon B.R., Keese K.E., Flint A.L., Flint L.E., Gaye C.B., Edmunds W.M., Simmers I. (2006) Global synthesis of groundwater recharge in semiarid and arid regions. *Hydrological Processes* 20(15):3335-3370. DOI: 10.1002/hyp.6335.
- Schaap M.G., Leij F.J., van Genuchten M.T. (2001) Rosetta: a computer program for estimating soil hydraulic parameters with hierarchical pedotransfer functions. *Journal of Hydrology* 251(3-4):163-176. DOI: 10.1016/S0022-1694(01)00466-8.
- Schelle H., Iden S.C., Peters A., Durner W. (2010) Analysis of the agreement of soil hydraulic properties obtained from multistep-outflow and evaporation methods. *Vadose Zone Journal* 9(4): 1080-1091. DOI: 10.2136/vzj2010.0050.
- Scheuermann A., Schlaeger S., Becker R., Schädel W., Schuhmann R. (2002) Nutzen der TDR-Meßtechnik zur Beurteilung ungesättigter Böden in der Geotechnik. BAW-Kolloquium: Der Einfluß von Luft einschüssen auf die Strömungs- und Druckdynamik in Erdbauwerken. Karlsruhe. pp. 24.
- Schlaeger S. (2005) A fast TDR-inversion technique for the reconstruction of spatial soil moisture content. *Hydrology and Earth System Sciences* 9(5):481-492. DOI: 10.5194/hess-14-1843-2010.
- Schlaeger S., Becker R., Schadel W., Scheuermann A., Worsching H. (2006) Improvements of spatial-TDR for hydrological and geotechnical applications. TDR 2006. Purdue University. West Lafayette. USA. Sept. 2006. Paper ID 31. pp 19.
- Seki K. (2007) SWRC fit - a nonlinear fitting program with a water retention curve for soils having unimodal and bimodal pore structure. *Hydrol. Earth Syst. Sci. Discuss.* 4(1):407-437. DOI: 10.5194/hessd-4-407-2007.

-
- Seyfried M.S., Schwinning S., Walvoord M.A., Pockman W.T., Newman B.D., Jackson R.B., Phillips F.M. (2005) Ecohydrological control of deep drainage in arid and semiarid regions. *Ecology* 86(2):277-287. DOI: 10.1890/03-0568.
- Silio O.T.N., Tellam J.H. (2000) Fingering in unsaturated zone flow: a qualitative review with laboratory experiments on heterogeneous systems. *Ground Water* 38(6):864-871. DOI: 10.1111/j.1745-6584.2000.tb00685.x.
- Šimůnek J., Šejna M., Saito H., Sakai M., van Genuchten M.T. (2009) The Hydrus-1D software package for simulating the movement of water, heat, and multiple solutes in variably saturated media. Version 4.08. HYDRUS Software Series 3. Department of Environmental Sciences. University of California. Riverside. USA. pp. 330.
- Singer A. (1995) The mineral composition of hot and cold desert soils. *Advances in GeoEcology* 28:13-28.
- Sorman A.U., Abdulrazzak M.J. (1995) Estimation of actual evaporation using precipitation and soil moisture records in arid climates. *Hydrological Processes* 9(7):729-741. DOI: 10.1002/hyp.3360090702.
- Stacheder M., Koeniger F., Schuhmann R. (2009) New dielectric sensors and sensing techniques for soil and snow moisture measurements. *Sensors* 9(4):2951-2967. DOI: 10.3390/s90402951.
- Suleiman A.A., Ritchie J.T. (2003) Modeling soil water redistribution during second-stage evaporation. *Soil Sci. Soc. Am. J.* 67(2):377-386. DOI: 10.2136/sssaj2003.3770.
- Todoroff P., Luk J.-D.L.S. (2001) Calculation of in situ soil water content profiles from TDR signal traces. *Measurement Science and Technology* 12(1):27-36. DOI: 10.1088/0957-0233/12/1/304.
- Topp G.C., Davis J.L., Annan A.P. (1980) Electromagnetic determination of soil water content: Measurements in coaxial transmission lines. *Water Resources Research* 16(3):574-582. DOI: 10.1029/WR016i003p00574.
- Twarakavi N., Šimunek J., Seo S. (2008) Evaluating interactions between groundwater and vadose zone using the HYDRUS-based flow package for MODFLOW. *Vadose Zone Journal* 7(2):757-768. DOI: 10.2136/vzj2007.0082.
- UNEP (1992) World atlas of desertification. Edward Arnold. Sevenoaks. UK. pp. 70.
- Valiantzas J.D. (2011) Combined Brooks-Corey/Burdine and van Genuchten/Mualem closed-form model for improving prediction of unsaturated conductivity. *J. Irrig. Drain Eng.* 137(4):223-234. DOI: 10.1061/(ASCE)IR.1943-4774.0000284.
- van Genuchten M.T. (1980) A closed-form equation for predicting the hydraulic conductivity of unsaturated soils. *Soil Sci. Soc. Am. J.* 44(5):892-898. DOI: 10.2136/sssaj1980.03615995004400050002x.
- Venkanna B.K. (2010) Fundamentals of heat and mass transfer. PHI Learning Private Limited. New Delhi. pp. 493.

-
- Walvoord M.A., Plummer M.A., Phillips F.M., Wolfsberg A.V. (2002) Deep arid system hydrodynamics. 1. Equilibrium states and response times in thick desert vadose zones. *Water Resour. Res.* 38(12):1308-1323. DOI: 10.1029/2001wr000824.
- Wernecke R. (2005) Feuchtemessung unter Laborbedingungen. *Industrielle Feuchtemessung*. Wiley-VCH Verlag. Weinheim. pp. 447-483.
- Wietsma T.W., Oostrom M., Covert M.A., Queen T.E., Fayer M.J. (2009) An automated tool for three types of saturated hydraulic conductivity laboratory measurements. *Soil Science Society of America Journal* 73(2):466-470. DOI: 10.2136/sssaj2008.0154.
- Wildenschild D., Hopmans J.W., Simunek J. (2001) Flow rate dependence of soil hydraulic characteristics. *Soil Sci. Soc. Am. J.* 65(1):35-48. DOI: 10.2136/sssaj2001.65135x.
- Worsching H., Becker R., Schlaeger S., Bieberstein A., Kudella P. (2006) Spatial-TDR moisture measurement in a large scale levee model made of loamy soil material. *Proc. TDR 2006*, Purdue University, West Lafayette, USA. pp. 15.
- Yang H., Rahardjo H., Wibawa B., Leong E.-C. (2004) A soil column apparatus for laboratory infiltration study. *Geotechnical Testing Journal* 27(4):347-355. DOI: 10.1520/GTJ11549.
- Zeng Y., Su Z., Wan L., Wen J. (2011) A simulation analysis of the advective effect on evaporation using a two-phase heat and mass flow model. *Water Resour. Res.* 47(10). DOI: W10529. DOI: 10.1029/2011wr010701.
- Zeng Y., Su Z., Wan L., Yang Z., Zhang T., Tian H., Shi X., Wang X., Cao W. (2009) Diurnal pattern of the drying front in desert and its application for determining the effective infiltration. *Hydrology and Earth System Sciences* 13(6):703-714. DOI: 10.5194/hess-13-703-2009.

Acknowledgements

I gratefully acknowledge my supervisor Prof. Dr. Christoph Schüth for his support, his helpful comments, advice, and his encouragement during all the stages of this research studies. I also thank him for making this research possible by always assuring financial support for the experiments, the modeling, as well as for visiting conferences and cooperation partners for presenting and discussing my work. A special thank goes to Dr. Irina Engelhardt, who always supported my work, especially by intensive discussions and valuable comments which highly improved the scientific quality of my work. I would also like to thank Dr. Matthias Piepenbrink for his help, support, and his unique ideas during the development of the column experiments.

This work was only possible through the financial support of the Federal German Ministry of Education and Research (BMBF). I deeply thank the International Postgraduate Studies in Water and Technologies (IPSWaT) team for the scholarship and all the benefits I could gain from this great program. I also thank all partners of the International Water Research Alliance Saxony (IWAS) for the good cooperation and the commitment to support integrated water resources management strategies in hydrological sensitive regions. Big thanks go to the Competence Center for Material Moisture at the KIT, and especially to Franz Königler for his time, support, ideas and very fruitful discussions upon the TDR measurement technique. During my research I had the opportunity to visit the Environmental Molecular Sciences Laboratory (EMSL) in Richland, WA, USA. I thank the whole team of the Subsurface Flow and Transport Research group, and especially Dr. Mart Oostrom and Thomas Wietsma for a great, informative, and successful stay, and the opportunity for soil physical measurements in their laboratory facilities.

Many thanks go to my co-supervisor Prof. Dr. Matthias Hinderer, as well as to Prof. Dr. Ingo Sass, and Prof. Dr.-Ing. Matthias Becker for their interest in my work and their support.

I furthermore thank the hydrogeology and sedimentary geology group, and especially Michaela Laxander, Dr. Andreas Kallioras, Abidur Khan, Nils Michelsen, Mustefa Yasin Reshid, Dr. Thomas Schiedek, Sybille Siebert, Rainer Brannolte, Daniel Franke, and Dr. Jens Hornung for discussions, laughter and support. Additionally, I thank Rainer Seehaus and Jürgen Krumm for their efficient and inevitable help for the experimental construction, Gabriela Schubert for support in the soil-mechanical laboratory, Petra Kraft for helping upon all kinds of literature search, the EDV-team for their IT-support, Holger Scheibner for his help, and Kirsten Herrmann and Angela Bretzel for their always helping hand regarding administrative questions and problems.

Last but not least I thank my partner Florian for his patience and understanding, my sister Anke for always cheering me up, my father Götz for always supporting me, and all of them and my friends for their trust in me.



Curriculum Vitae

Heike Pfletschinger

Education

- 12/2008 – 01/2012 PhD student, Technische Universität Darmstadt
IPSWaT Scholarship (01/2009 – 12/2011)
- 10/2005 – 12/2007 Master postgraduate studies “Environmental Management”, MSc
Christian-Albrechts-University Kiel, Ecology Center
- 10/1997 – 12/2002 Undergraduate studies “International Studies in Environmental
Engineering”, Dipl.-Ing. (FH)
Hochschule Bremen, Faculty of Architecture, Civil and Environmental
Engineering

International Experience

- 04/2010 – 05/2010 Research Visit
Subsurface Flow and Transport Laboratory, EMSL, PNNL, Richland,
WA, USA
- 01/2001 – 05/2001 Internship
Soil and Water Conservation Society of Metro Halifax, Canada
- 09/2000 – 12/2000 Visiting Student
Dalhousie University, Department of Biological Engineering, Halifax,
Canada

Work Experience

- 04/2008 – 09/2008 Research Assistance, Geoarchaeology
Christian-Albrechts-University Kiel, Ecology Center
- 07/2003 – 06-2005 Technical Staff, Non-Destructive Core Analysis
University Bremen, Marum, Research Center for Ocean Margins
- 05/2003 – 06/2003 Project Management Assistance, Wind Energy Sector
NEGMicon, Husum-Ostenfeld



Publications and Conference Contributions

2012

Pfletschinger H., Engelhardt I., Piepenbrink M., Königer F., Schuhmann R., Kallioras A., Schüth C. (2011) Soil column experiments to quantify vadose zone water fluxes in arid settings. *Environ Earth Sci.* 65(5):1523-1533.

2011

Pfletschinger H., Engelhardt I., Schüth C. (2011) Vadose zone water fluxes under arid conditions – Bench-scale soil column experiments and 1D-modeling. EGU General Assembly. April 04-08, 2011. Vienna, Austria.

Schüth C., Kallioras A., Piepenbrink M., Pfletschinger H., Al-Ajmi, H., Engelhardt I., Rausch R., Al-Saud M. (2011) New approaches to quantify groundwater recharge in arid areas. *International Journal of Water Resources and Arid Environments* 1(1):33-37.

2010

Pfletschinger H., Engelhardt I., Piepenbrink M., Königer F., Schüth C. (2010) Vadose zone water fluxes under arid conditions – Bench-scale soil column experiments. *GeoDarmstadt2010*. October 10-13, 2010. Darmstadt, Germany.

Pfletschinger H., Engelhardt I., Königer F., Piepenbrink M., Kallioras A., Schüth C. (2010) Vadose zone processes in arid regions - Small-scale soil column experiments for the determination of water fluxes. *Tagung der FH-DGG*. May 12-16, 2010. Tübingen, Germany.

2009

Engelhardt I., Pfletschinger H., Schüth C., Rausch R. (2009) Estimation of groundwater recharge in arid settings using large-scale numerical modelling and soil column experiments. 4. CMM Workshop. September 30 – October 01., 2009. Bad Herrenalb, Germany.



Erklärung der Urheberschaft

Ich erkläre hiermit an Eides statt, dass ich die vorliegende Arbeit selbständig und ohne Benutzung anderer als der angegebenen Hilfsmittel angefertigt habe.

Alle Stellen, die wörtlich oder sinngemäß aus anderen Schriften entnommen sind, sind als solche kenntlich gemacht.

Die Arbeit ist in gleicher oder ähnlicher Form noch nicht als Prüfungsarbeit eingereicht worden.

Darmstadt, den

Heike Pfletschinger



Appendix

A1 Pictures of the experiments

A1-a Column packing during experimental development and testing phase

A1-b Final experimental setup before packing

A1-c Final experimental setup during packing

A1-d Final experimental setup during experiments (1)

A1-e Final experimental setup during experiments (2)

A2 TDR data

A2-a TDR raw data explanation

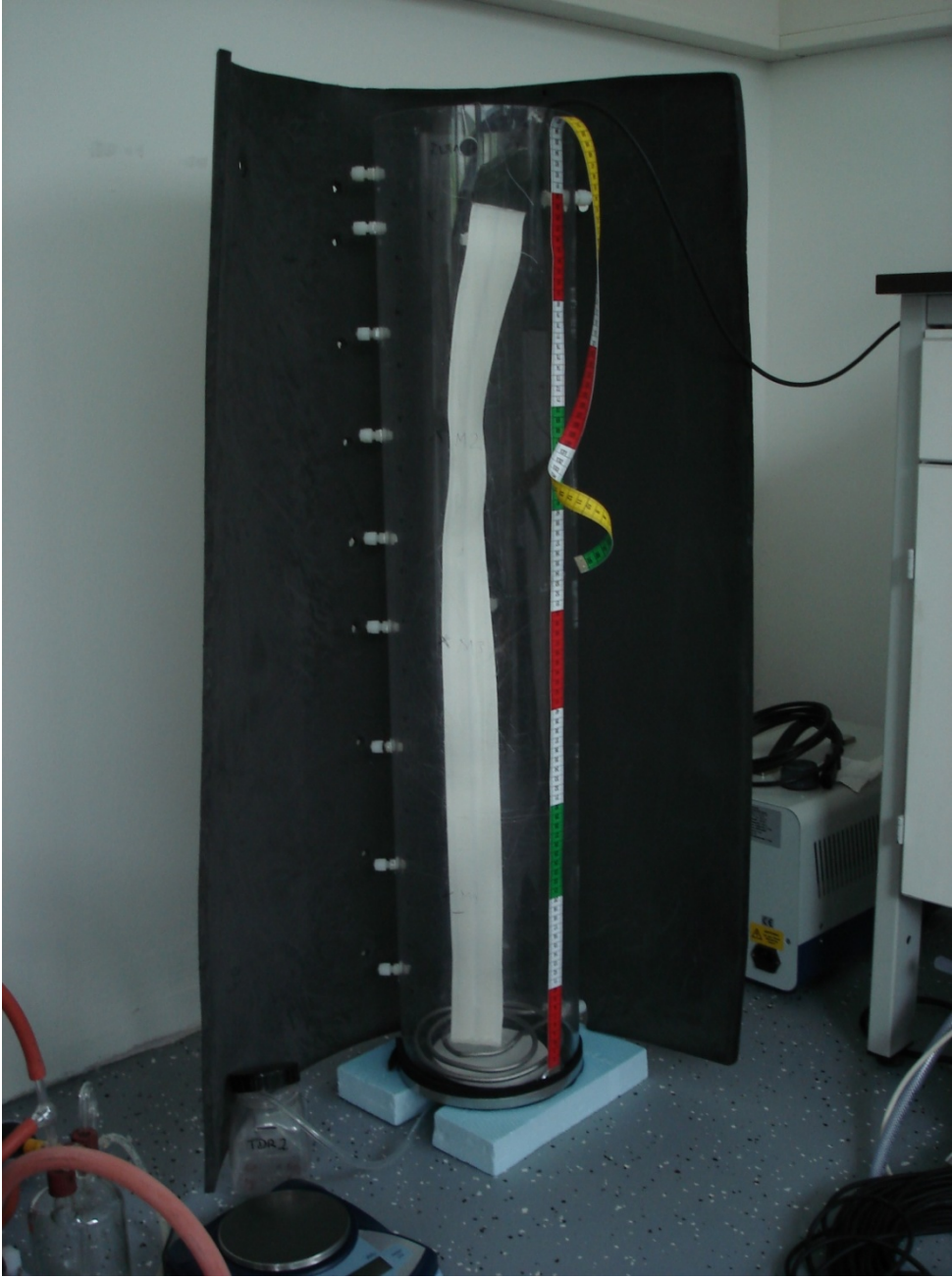
A2-b TDR infiltration curves before processing for the silica sand steady state irrigation

A2-c TDR infiltration curves before processing for the dune sand irrigation breakthrough

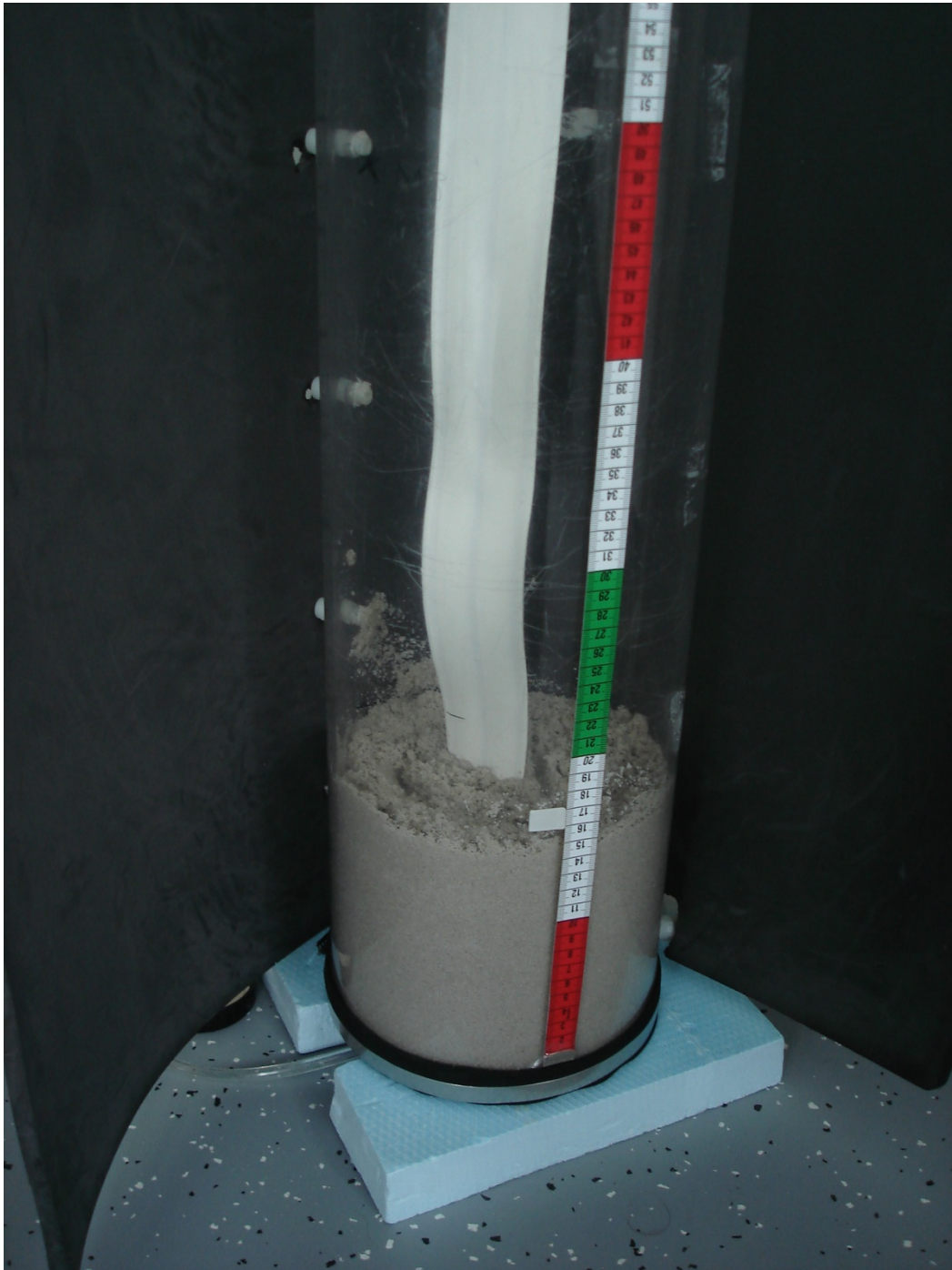
A1-a Column packing during experimental development and testing phase



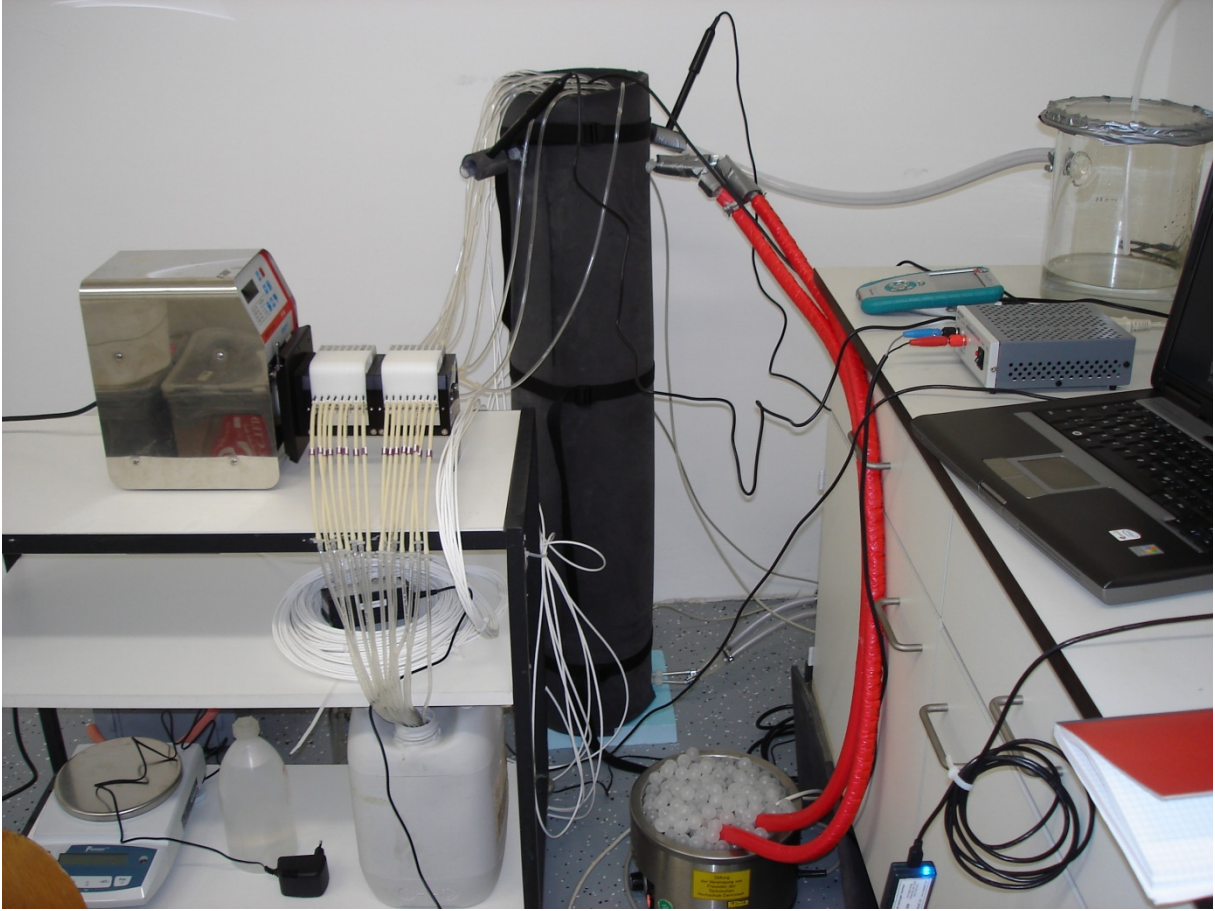
A1-b Final experimental setup before packing



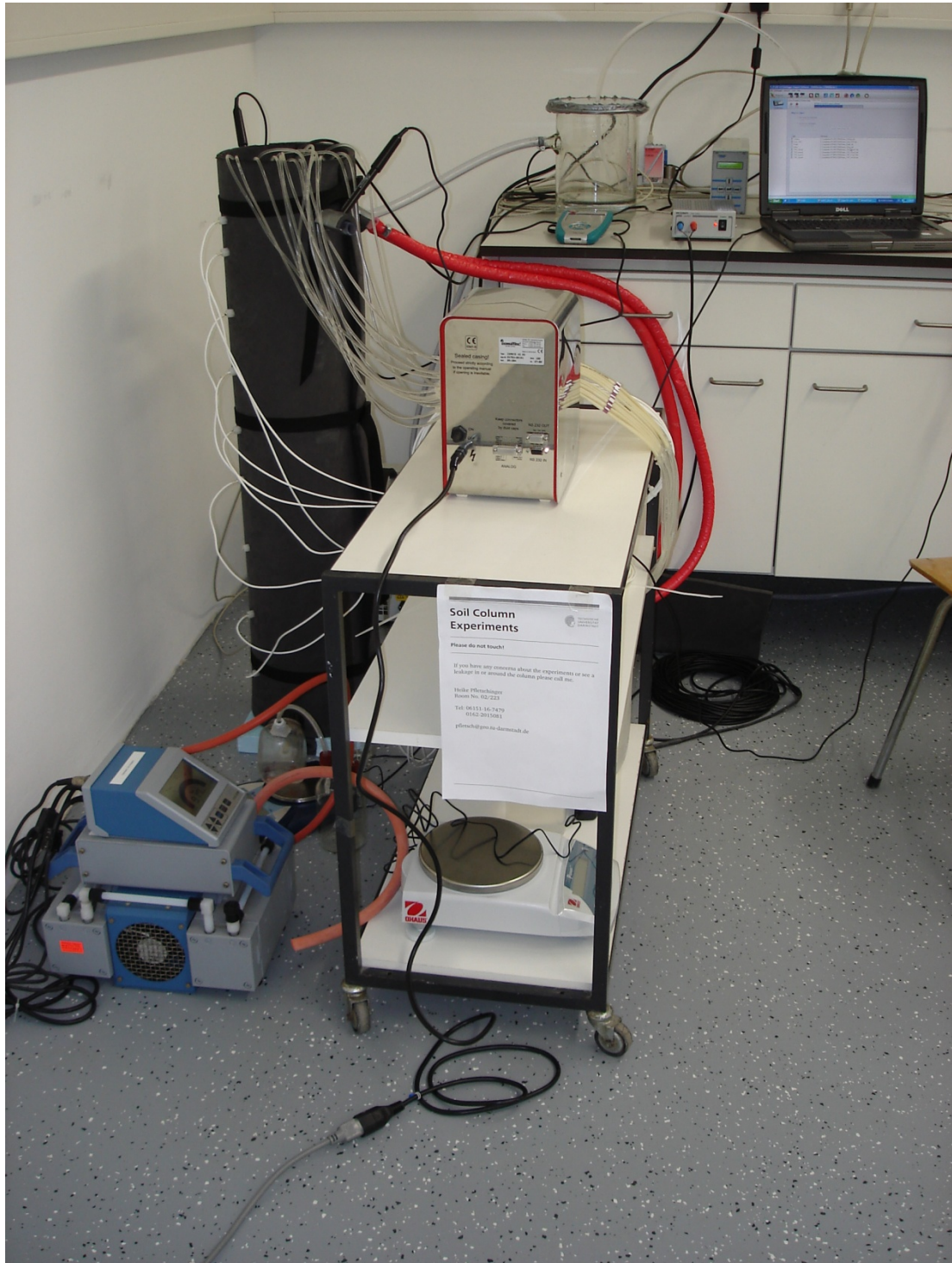
A1-c Final experimental setup during packing



A1-d Final experimental setup during experiments (1)



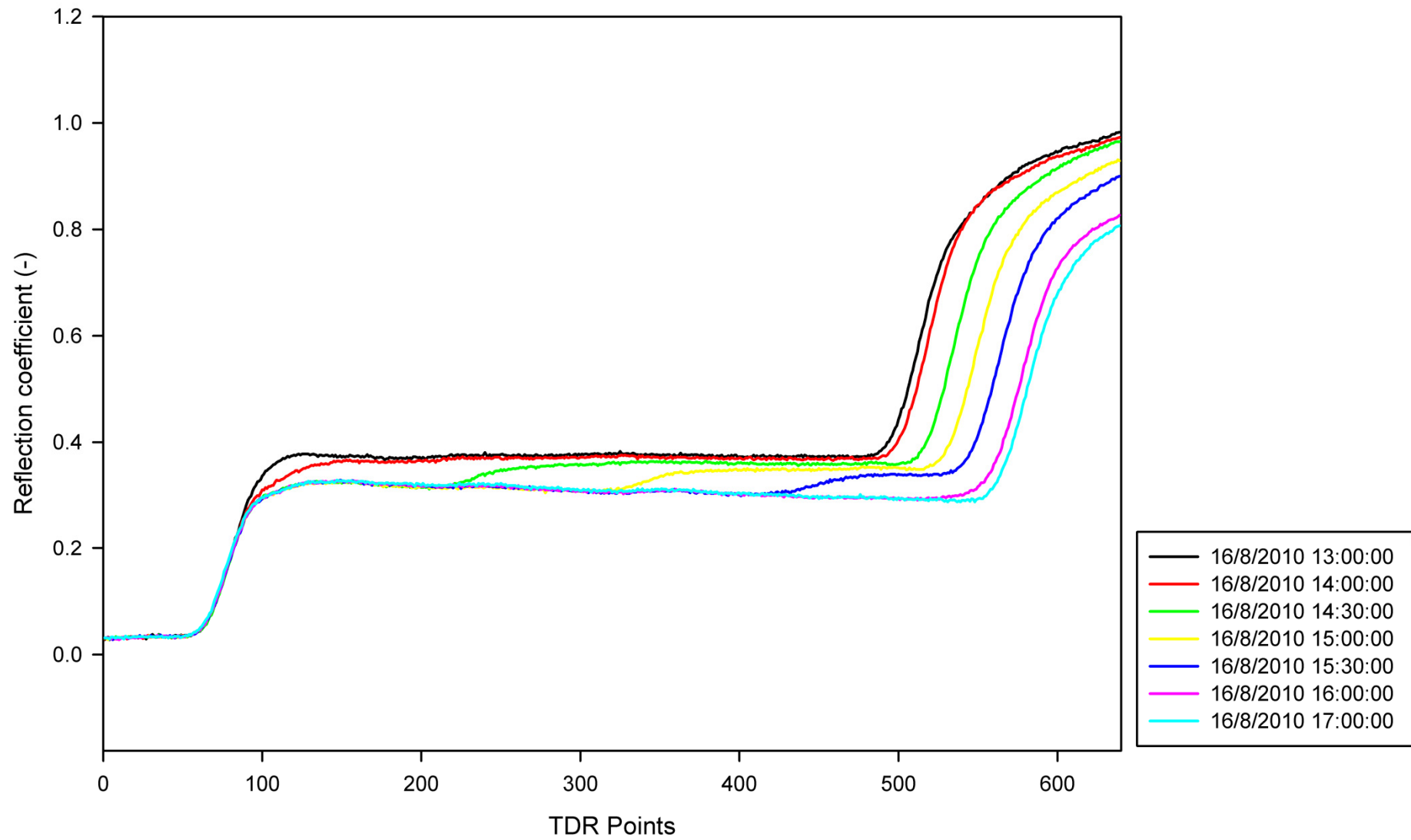
A1-e Final experimental setup during experiments (2)



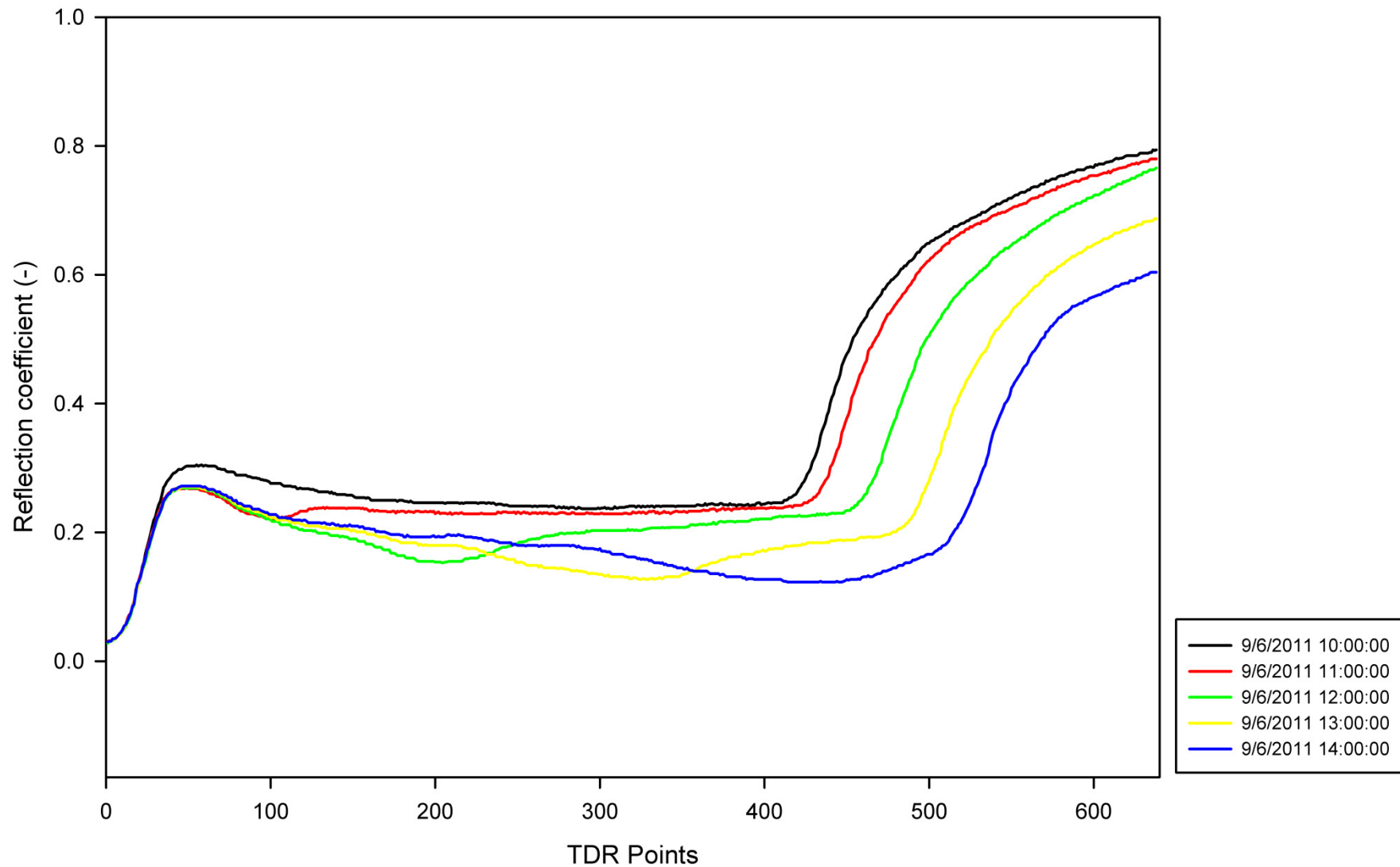
A2-a TDR raw data explanation

The Campbell Scientific raw data is given according to the measurement instruction files that are programmed by the user in CRBasic Editor. Definitions for the output file header are as follows (Campbell Scientific, Inc. 2000-2007 – CRBasic Editor 2.9):

CR Basic Code	Explanation	File Setting
MuxProbe	Multiplexer setting of the probe	1001 (defines the probe to be set on position 1 in the first multiplexer level)
WaveAvg	Number of waveform reflections averaged for the final single result (high values are necessary under high noise conditions)	10
TDRVp	Propagation velocity of the coaxial cable connecting the TDR reflectometer and the probe (material specific, has to be determined in advance)	0.63
TDRPoints	Number of points in the collected waveform	651
CableLength	Length of the coaxial cable; defines the starting point of waveform collection	6 m
WindowLength	Length of the waveform to be collected; must be chosen to collect the whole probe reflection in fully saturated conditions	2.5 m
ProbeLength	Length of the probe (only important for direct conversion of the waveform length to water content)	0.9 m
ProbeOffset	Length of the probe offset (only important for direct conversion of the waveform length to water content)	0.06 m
TDROption	Determination of output	1 (defines to collect the waveform values)
SDMAddress	Address for the communication with the TDR100 reflectometer	0 (defined by the TDR100 settings)



A2-b TDR infiltration curves before processing for the silica sand steady state irrigation - Irrigation start: 16/8/2010 13:30



A2-c TDR infiltration curves before processing for the dune sand irrigation breakthrough - Irrigation start 9/6/2011 10:00

